

# Stochastic Energy Management of Electric Vehicles in Smart Grid

by

Yuan Liu

A thesis submitted in partial fulfillment of the requirements for the degree of

Doctor of Philosophy  
in  
Energy Systems

Department of Electrical and Computer Engineering  
University of Alberta

©Yuan Liu, 2020

# Abstract

Along with the growing environmental concerns, it is envisioned that electric vehicles (EVs) will play a significant role in transportation systems in the near future. Due to the ever-increasing penetration rate of EVs, new opportunities and challenges come one after another. On one hand, the increasing concentrated charging load of EVs potentially affect the power quality in the distribution systems. On the other hand, based on the vehicle-to-grid (V2G) mechanism, EVs can also provide ancillary services by optimizing the charging/discharging schedules according to the requirement of the distribution systems. Furthermore, by involving the EV aggregators (AGGs) to manage all the EVs' charging/discharging processes in a certain region, the EVs' ancillary service capacity can be boosted. In order to optimize EV energy management, the randomness of individual EV mobility, electricity market, and power systems should be taken into account.

As a special category of EVs, the electric buses (EBs) also attract extensive attention in recent years because of their significance in the future public transportation systems. Compared with general EVs, EBs have large charging demand, considerable battery size, regular operation schedule, and high controllability in charging schedule. Thus, the impact of increasing EBs' charging load on the distribution system should be evaluated. On the other hand, by effectively managing the energy flows in the EB transit center (EBTC) in coordination with the distribution system operator (DSO), the EBTC can become a valuable source of ancillary services.

In this thesis, stochastic energy management of EVs and EBs in smart grid is investigated to mitigate the negative impact on power distribution systems and provide ancillary services. Four main research topics have been investigated. Firstly, the stochastic EV charging station operation in the smart grid is investigated. To achieve peak-load shaving, the DSO needs to guide the charging process of individual EVs indirectly through adjusting the real-time price (RTP) while EV owners need to minimize the charging cost by optimizing the charging schedule. Queuing theory is applied to model the random arrival and departure processes of EVs. Based on the operation model of the charging station, we

proposed a repeated Stackelberg game approach to analyze the interaction among the individual EVs. The revenue of individual EV is optimized through Markov decision process (MDP). In order to obtain the Nash-equilibrium solution, a backward iteration algorithm is developed. Then, the impact of RTP on the EV charging power and duration is analyzed, and the DSO's pricing scheme is optimized to minimize the cost for achieving peak load shaving. In the case study, the performance of the proposed approach is evaluated based on the IEEE 123-bus test feeder with real vehicle mobility data. The results indicate that our approach not only reduces the peak load, but also minimizes the charging cost of EVs.

Secondly, the voltage regulation (VR) auction mechanism in the distribution system involving EV AGGs is studied. The DSO aims at minimizing the VR cost while satisfying the VR requirement through VR auction, integrated with an AGG selection and scoring mechanism. To participate in the VR market, AGGs require VR capacity estimation approaches and optimal auction strategies. Accordingly, the impact of distribution network topology on the VR efficiency is analyzed. Also, a VR auction model with performance scoring mechanism is developed. Then, we investigate AGG's VR capacity estimation method, the impact of auction strategy on the performance score, and the interaction among AGGs. Then, a discounted stochastic multiplayer game (DSMG) approach is developed to optimize the AGG's auction strategy. The existence proof for the stationary Markov equilibrium solution is derived and the corresponding algorithms are developed. In the case study, the performance of the proposed DSMG approach is evaluated and compared with other game approaches. The results indicate that the proposed approach can achieve better revenue for the EV AGGs while satisfying the VR requirement of the DSO.

Thirdly, a data-driven approach for EB energy consumption estimation is proposed. In particular, an Android application is developed to collect the motion data of buses so that any general Android smartphone can be used for data collection. Then, a detailed physical model of EB is constructed to model its energy consumption considering the randomness in EB operation, including speed, acceleration and passenger count. In order to improve the estimation accuracy, the conventional Kalman filter (KF) is modified to involve EB mass estimation by considering stochastic real-time passenger count, motion data dimension reduction based on EB operation route, and EB acceleration estimation based on extended random decision forest algorithm. In the case study, the performance of the proposed approach is evaluated based on real-world EB operation data collected from St. Albert Transit, AB, Canada, and the IEEE 33-bus test feeder. Compared with the existing approaches, the proposed approach achieves more accurate real-time energy consumption

estimation of EBs, which in turn, provides better characterization of power system loading and voltage variation.

Fourthly, a three-layer stochastic energy management approach is proposed for EBTCs to reduce the operation cost while maintaining local voltage quality. In the first layer, a modified robust optimization over time (ROOT) approach is developed to obtain the charging/discharging margin with minimum EBTC operation cost. In the second layer, the voltage regulation impact on the local voltage quality is estimated through power flow analysis considering voltage fluctuation and line loss minimization. In the third layer, the charging/discharging strategy is optimized with dynamic programming based on a modified greedy algorithm. The performance of the proposed approach is evaluated in a case study based on the IEEE 123-bus test feeder and the real operation data obtained from St. Albert Transit in Alberta, Canada. The results indicate that the proposed approach can not only minimize the EBTC operation cost but also well maintain the local voltage quality, in comparison with existing energy management approaches.

# Preface

The material presented in this thesis is based on original work by Yuan Liu. As detailed in the following, material from some chapters of this thesis has been published in transactions under the supervision of Dr. Hao Liang in concept formation and by providing comments and corrections to the article manuscript.

Chapter 2 includes the results published in the following paper:

- Y. Liu, R. Deng, and H. Liang, "A stochastic game approach for PEV charging station operation in smart grid," *IEEE Transactions on Industrial Informatics*, vol. 14, no. 3, pp. 969-979, Mar. 2018.

Chapter 3 includes the results published in the following paper:

- Y. Liu and H. Liang, "A discounted stochastic multiplayer game approach for vehicle-to-grid voltage regulation," *IEEE Transactions on Vehicular Technology*, vol. 68, no. 10, pp. 9647-9659, Oct. 2019.

Chapter 4 includes the results in following paper that has been submitted:

- Y. Liu and H. Liang, "A data-driven approach for electric bus energy consumption estimation," submitted to *IEEE Transactions on Intelligent Transportation Systems*, 2020, under 2<sup>nd</sup> round review. (1<sup>st</sup> Round Decision: Accept as Regular Paper after Minor Revision)

Chapter 5 includes the results published in the following paper:

- Y. Liu and H. Liang, "A three-layer stochastic energy management approach for electric bus transit centers with PV and energy storage systems," *IEEE Transactions on Smart Grid*, 2020, in press.

# Acknowledgements

First, I would like to express my sincere gratitude to my supervisor *Prof. Hao Liang* for the continuous support of my Ph.D. study and related research. All his patience, motivation, and immense knowledge have helped me so much in all the time of research and writing of this thesis.

In addition, it is an honor for me to extend my gratitude to all my Ph.D. committee members for reviewing my thesis and providing thoughtful comments to improve it. I also thank all my colleagues in my lab and friends I met at the University of Alberta during my Ph.D. program, especially Dr. Ruilong Deng, who helped me so much when I started my first research.

Finally, I would like to thank my parents for their unconditional love and support. Though we are thousands of miles apart, they are always there to encourage me to move forward.

# Table of Contents

<b>1</b>	<b>Introduction</b>	<b>1</b>
1.1	Background . . . . .	1
1.2	General Terms and Definitions . . . . .	4
1.2.1	G2V and V2G . . . . .	4
1.2.2	Markov Decision Process . . . . .	5
1.2.3	Stackelberg Game . . . . .	5
1.2.4	Network Topology in VR Market . . . . .	6
1.2.5	Stochastic Multi-Player Game . . . . .	6
1.2.6	Random Decision Forest . . . . .	6
1.2.7	Robust Optimization Over Time . . . . .	7
1.2.8	RTP Scheme . . . . .	7
1.3	Research Definition and Literature Review . . . . .	8
1.3.1	In-Station EV Charging Optimization . . . . .	8
1.3.2	EV AGG Energy Management in the Voltage Regulation Market . . . . .	9
1.3.3	EB Energy Consumption Estimation . . . . .	11
1.3.4	Stochastic EBTC Energy Management . . . . .	12
1.4	Thesis Motivation and Contribution . . . . .	14
1.4.1	A Stochastic Game Approach for EV Charging Station Operation in Smart Grid . . . . .	15
1.4.2	A Discounted Stochastic Multiplayer Game Approach for V2G Voltage Regulation . . . . .	15
1.4.3	A Data-Driven Approach for Electric Bus Energy Consumption Estimation . . . . .	16
1.4.4	A Three-Layer Stochastic Energy Management Approach for Electric Bus Transit Centers with PV and Energy Storage Systems . . . . .	16
1.5	Thesis Outline . . . . .	17
<b>2</b>	<b>A Stochastic Game Approach for EV Charging Station Operation in Smart Grid</b>	<b>20</b>
2.1	System Model . . . . .	20
2.1.1	Charging Station Model . . . . .	21
2.1.2	EV Charging Model . . . . .	22
2.2	Stochastic Game Formulation . . . . .	23

2.2.1	Repeated Inverse Stackelberg Game . . . . .	24
2.2.2	MDP for Charging Decision Making . . . . .	25
2.2.3	Nash Equilibrium Solution . . . . .	27
2.3	Optimal Real Time Pricing Scheme . . . . .	28
2.3.1	Impact of RTP on EV Charging Demand . . . . .	29
2.3.2	Optimal RTP Scheme . . . . .	30
2.4	Simulation Results . . . . .	31
2.5	Summary . . . . .	35
<b>3</b>	<b>A Discounted Stochastic Multiplayer Game Approach for V2G Voltage Regulation</b>	<b>36</b>
3.1	System Model . . . . .	36
3.1.1	Impact of Network Topology on VR . . . . .	38
3.1.2	Auction Process and Selection Mechanism . . . . .	39
3.1.3	Controllability-based EV Queue Model . . . . .	41
3.2	Topology-Aware VR Auction Formulation . . . . .	42
3.2.1	Topology-aware VR Efficiency . . . . .	42
3.2.2	Scoring Mechanism Based on VR Performance . . . . .	43
3.2.3	Stochastic VR Capacity Evaluation and Score Estimation . . . . .	44
3.3	Discounted Stochastic Multiplayer Game . . . . .	45
3.3.1	Game Formulation . . . . .	45
3.3.2	State-based Feasible Action Space . . . . .	46
3.3.3	Existence of Stationary Markov Perfect Equilibrium . . . . .	47
3.4	Case Study . . . . .	48
3.5	Summary . . . . .	55
<b>4</b>	<b>A Data-Driven Approach for Electric Bus Energy Consumption Estimation</b>	<b>56</b>
4.1	System Model . . . . .	56
4.1.1	Bus Operation Parameters . . . . .	57
4.1.2	Physical Model of EB Energy Consumption . . . . .	57
4.2	Data-Driven EB Energy Consumption Estimation Based on Modified Kalman Filter . . . . .	59
4.2.1	Real-time Dynamic Passenger Count Estimation . . . . .	59
4.2.2	EB Motion State Dimension Deduction . . . . .	61
4.2.3	The Modified One-Dimension KF for EB Motion Tracing . . . . .	62
4.2.4	Real-time EB Acceleration Estimation Based on Modified Decision Forest Algorithm . . . . .	63
4.3	Case Study . . . . .	66
4.3.1	Data Collection . . . . .	66
4.3.2	Performance Comparison and Impacts Analysis . . . . .	70

4.4	Summary . . . . .	75
<b>5</b>	<b>A Three-Layer Stochastic Energy Management Approach for Electric Bus Transit Centers with PV and Energy Storage Systems</b>	<b>76</b>
5.1	System Model . . . . .	76
5.1.1	EBTC Operation Cost . . . . .	77
5.1.2	Energy Flow in the EBTC . . . . .	78
5.1.3	EB Energy Consumption Model . . . . .	78
5.1.4	Battery Degradation Cost Model . . . . .	80
5.2	Problem Formulation . . . . .	80
5.3	A Three-Layer Stochastic Energy Management Approach . . . . .	82
5.3.1	Stochastic EB Energy Consumption Estimation Based on Synthetic Driving Profile . . . . .	82
5.3.2	Stochastic EBTC Energy Management Based on Modified Robust Optimization Over Time . . . . .	86
5.3.3	Impact Analysis of EBTC Load on the Tap Selection in Voltage Regulation Process . . . . .	87
5.3.4	Local Voltage Quality Optimization . . . . .	88
5.4	Case Study . . . . .	90
5.5	Summary . . . . .	95
<b>6</b>	<b>Conclusions and Future Works</b>	<b>96</b>
6.1	Contributions of Thesis . . . . .	97
6.2	Directions for Future Work . . . . .	97
	<b>References</b>	<b>100</b>

# List of Tables

2.1	STATE TRANSITION PROBABILITIES. . . . .	23
2.2	RESULTS OF THE FOUR APPROACHES WITH DIFFERENT $\eta$ AND AVERAGE CHARGING DEMAND. . . . .	31
2.3	AVERAGE UNIT PRICE OF THE FOUR APPROACHES. . . . .	33
3.1	REVENUE AND SELECTION RATE OF AGG 2 . . . . .	50
4.1	CONSTANT PARAMETERS IN THE SIMULATION. . . . .	69
4.2	PERFORMANCE OF DECISION FORESTS WITH DIFFERENT FEATURE NUMBERS. . . . .	71
4.3	POWER FLOW ANALYSIS RESULTS. . . . .	74
5.1	CONSTANT PARAMETERS IN SIMULATION. . . . .	91
5.2	IMPACT OF CONSIDERING VOLTAGE REGULATION ON THE LOCAL VOLTAGE QUALITY. . . . .	93
5.3	PERFORMANCE COMPARISON AMONG SEMA, RSEMA, AND TSEMA. . . . .	94

# List of Figures

1.1	An illustration of the smart grid with EV integration. . . . .	3
1.2	Structure of this thesis. . . . .	18
2.1	An illustration of charging station operation in distribution system. . . . .	23
2.2	A diagram of EV charging leader-follower relationship. . . . .	24
2.3	An illustration of system state transitions. . . . .	26
2.4	Modified IEEE 123-bus test feeder [112]. . . . .	32
2.5	The reduction of average unit price versus average charging demand and $\eta$ . . . . .	33
2.6	Load of charging station on bus 20. . . . .	34
2.7	Load of charging station on bus 40. . . . .	35
3.1	An illustration of the distribution system. . . . .	37
3.2	An illustration of the VR process of for DSO and AGG. . . . .	40
3.3	An illustration of the IEEE 33-bus test feeder [131]. . . . .	49
3.4	The real-time total VR capacity for satisfying the DSO's requirement. . . . .	50
3.5	The real-time minimum voltage magnitude. . . . .	50
3.6	The real-time maximum voltage magnitude. . . . .	51
3.7	An illustration of the modified IEEE 123-bus test feeder [112]. . . . .	52
3.8	The real-time available VR capacities. . . . .	52
3.9	The convergence process for solving the stationary Markov perfect equilibrium. . . . .	53
3.10	The real-time minimum voltage magnitude. . . . .	53
3.11	The real-time total VR capacity. . . . .	54
3.12	The accumulated revenue of AGGs. . . . .	54
4.1	Force analysis illustration of EB. . . . .	58
4.2	An illustration of the data-driven approach for EB energy consumption estimation. . . . .	60
4.3	An illustration of the smartphone installation on EB. . . . .	67
4.4	Android APP for collecting motion data. . . . .	67
4.5	St. Albert Transit: A1 EB route. . . . .	68
4.6	Google Elevation API: A1 EB route elevation. . . . .	69
4.7	An illustration of the data preprocessing process. . . . .	70

4.8	Feature selection/discarding process. . . . .	71
4.9	A comparison of the driving mileages. . . . .	72
4.10	A comparison of the driving speed estimation. . . . .	73
4.11	A comparison of the estimated energy consumption. . . . .	73
4.12	A comparison of proposed approach and other EB energy consumption estimation approaches. . . . .	74
4.13	An illustration of the IEEE 33-bus test feeder. . . . .	74
5.1	An illustration of EBTC energy management. . . . .	77
5.2	Flowchart of the three-layer EBTC energy management approach. . . . .	83
5.3	An illustration of greedy algorithm proof. . . . .	88
5.4	An illustration of the IEEE 123-bus test feeder with an EBTC. . . . .	91
5.5	EB data collection APP and bus operation routes. . . . .	92
5.6	Comparison between the estimated energy consumption and the actual statistics. . . . .	92
5.7	EBTC load profile comparison among different strategies. . . . .	93
5.8	Performance comparison among SEMA, RSEMA, and TSEMA over time. . .	94

## List of Acronyms

<b>AGG</b>	Aggregator
<b>AKF</b>	Acceleration estimated Kalman filter
<b>CART</b>	Classification and regression tree
<b>CSP</b>	Charging service providers
<b>DSMG</b>	Discounted stochastic multiplayer game
<b>DSO</b>	Distribution system operator
<b>EB</b>	Electric buses
<b>EBTC</b>	EB transit center
<b>EEEC</b>	Estimated EB energy consumption
<b>ESS</b>	Energy storage system
<b>EV</b>	Electric vehicles
<b>FHO</b>	Finite horizon optimization
<b>ICCT</b>	International Council on Clean Transportation
<b>ITS</b>	Intelligent transportation systems
<b>KF</b>	Kalman filter
<b>MAPL-OPF</b>	Minimum active power losses-optimal power flow
<b>MMSE</b>	Minimum mean-square error
<b>NHTS</b>	National Household Travel Survey
<b>NNG</b>	Noncooperative N-player game
<b>NTS</b>	National Travel Survey
<b>OCL</b>	Original charging load
<b>PAR</b>	Peak-to-average ratio
<b>PDF</b>	Probability density function
<b>PV</b>	Photovoltaic
<b>REEC</b>	Real EB energy consumption
<b>RKF</b>	Route based KF
<b>ROOT</b>	Robust optimization over time
<b>RR</b>	Rejection rate
<b>RTP</b>	Real-time price
<b>SG</b>	Stochastic game
<b>SOC</b>	State of charge
<b>V2G</b>	Vehicle-to-grid
<b>VR</b>	Voltage regulation

# Nomenclature

## Chapter 2

$\delta_t$	EV maintaining probability
$\Delta t$	Time slot duration
$\Gamma$	Game strategy space
$\kappa$	Bus index
$\lambda^{a_i}$	EV arrival probability of charging station $i$
$\mu^{a_i}$	EV departure probability of charging station $i$
$\omega_t^k$	Weight of bus $k$ in time slot $t$
$\pi_t$	Nash equilibrium solution in time slot $t$
$\lambda$	Set of arrival probability of EVs
$\Psi_{g,t}^{a_i}$	Charging power selection probability
$a_i$	Charging station $i$
$\mathcal{B}$	Set of distribution system base load
$\mathbf{B}$	Set of time-variant load data
$\mathbf{B}_t$	Set of load data in time slot $t$
$B_t^k$	Base load of bus $k$ in time slot $t$
$\mathcal{C}$	Vector of charging cost
$c$	Per-slot charging cost
$C_t^V$	Original cost of DSO
$c_T$	Charging cost
$D$	Charging duration

$E_C$	Charging demand
$G$	Total charging power level
$g$	Charging power level index
$I$	Charging station number
$i$	Charging station index
$\mathbf{K}$	Set of buses in the distribution system
$\mathbf{K}_c$	Set of buses connected with charging stations
$K$	Number of buses in the distribution system
$k$	Bus index
$L^{a_i}$	Charging station load
$\mathcal{N}$	Set of all EV owners
$n$	EV index
$n_g^{a_i}$	EV number with charging power $g$ in station $i$
$\mathbf{Pr}$	Transition matrix
$\mathbf{P}$	Set of charging powers
$\vec{Pr}$	Vector in the transition matrix
$P$	Charging power
$P_g$	Charging power level
$p_{a_i,t}$	RTP of bus $a_i$
$p_{k,t}$	RTP of bus $k$ in time slot $t$
$Pr$	Transition probability
$\mathbf{q}$	Vector of state of all the charging stations
$Q$	Set of all the system states
$Q$	System state number
$q$	System state index
$R_{P,D}$	Charging reservation

<b>S</b>	Set of all the charging station states
$\mathbf{s}^{a_i}$	Vector of charging station state
$S$	Charging station state number
<b>t</b>	Time period
$T$	Total time slots number
$t$	Time slot index
$t_0$	EV arrival time
$t_f$	Final time slot
$\mathbf{U}$	Vector of per-slot charging utility
$U$	EV charging utility

### Chapter 3

$\beta$	Discount factor
$\Delta P_k$	Maximum adjustable power on bus $k$
$\Delta v_D$	Maximum voltage regulation down range
$\Delta v_e$	Maximum adjustable voltage range
$\Delta v_U$	Maximum voltage regulation up range
$\Gamma$	Discounted stochastic game
$\theta$	Voltage angle vector
$\omega_i$	Auction result
$\pi, \pi_i, \pi_{i^-}$	Strategy profile
$\theta_{i,h}$	Hourly bus voltage angle
<b>a</b>	Set of specific AGGs' action vectors
$\mathbf{A}_i$	Action space of AGG on bus $i$
$\mathcal{A}$	Set of buses with AGGs
$\mathcal{A}_s^+$	Set of AGGs winning the auction in state $s$
$\mathcal{A}_s^-$	Set of AGGs losing the auction in state $s$

$A_i$	Feasible action space of AGG on bus $i$
$a_i$	Action vector
$\bar{c}_i^A$	Equivalent offer VR price of AGG on bus $i$
$\bar{c}_i^T$	Expected AGG stage cost
$C_i^A$	DSO payment for AGGs on bus $i$
$C^D$	DSO total VR cost
$c^T$	Traditional VR source price
$C_i^T$	DSO payment for traditional VR sources
$c_i^A$	Offer VR price of AGG on bus $i$
$c_i^D$	Regulation down price
$c_i^T$	AGG stage cost
$c_i^U$	Regulation up price
<b>E</b>	Set of possible subsequent states
$\mathcal{G}$	Sub- $\sigma$ -algebra of $\mathcal{S}$
$H$	Total number of time intervals
$h$	Hourly time index
$\mathcal{I}$	Set of buses
$I$	Total bus number
$i, k, l$	Bus index
<b>L</b> <sub><math>h</math></sub>	Set of base load
$L_{i,h}$	Hourly base load
<b>M</b>	Intermediate matrices
$\hat{P}_i^D$	Real-time regulation down capacity of AGG on bus $i$
$\hat{P}_i^U$	Real-time regulation up capacity of AGG on bus $i$
<b>P</b>	Active power vector
$\vec{P}_k$	Equivalent active power

$P_i^T$	Booked VR capacity
$P_i^A$	Offer VR capacity of AGG on bus $i$
$P_i^a$	Real-time VR capacity of AGG on bus $i$
$P_i^D$	Offer regulation down capacity of AGG on bus $i$
$P_i^U$	Offer regulation up capacity of AGG on bus $i$
$P_{i,h}, P_i, P_k$	Active power
$\mathbf{Q}$	Reactive power vector
$q$	Radon-Nikodym derivative
$Q_{i,h}, Q_i$	Hourly reactive power
$\bar{r}_i$	Expected AGG stage payoff
$\mathbb{R}^*$	Set of non-negative real numbers
$r_i$	AGG stage revenue
$r_i^D$	AGG stage payoff
$\mathbf{S}$	State space
$\mathbf{s}$	State vector
$\mathcal{S}$	Borel- $\sigma$ -algebra
$s_i, s_i^P$	Performance score of AGG on bus $i$
$\mathcal{T}$	Set of buses with traditional VR sources
$T$	Time interval number in one stage
$\mathbf{v}$	Voltage magnitude vector
$\mathbf{V}_h$	Set of voltages
$\mathcal{V}_{i,h}, V_i$	Hourly bus voltage
$V^R$	Total VR capacity requirement
$V_{\max}$	Maximum bus voltage
$V_{\min}$	Minimum bus voltage
$v_{i,h}, v_i$	Hourly bus voltage magnitude

$z_{ik}, r_{ik}, x_{ik}$  Impedance, resistance, reactance

## Chapter 4

$\beta_1, \beta_2, \beta_3, \beta_4$  Constant values

$\Delta t$  Sampling interval

$\eta^D$  Driver efficiency

$\eta^E$  Engine efficiency

$\eta^G$  Gravity acceleration

$\gamma^\xi$  Normalized decision tree

$\kappa$  Threshold value for node splitting weight

$\lambda_s$  Passenger frequency getting on EB at stop  $s$

$\mu_{s,s'}$  Passenger frequency in  $\lambda_s$  getting off EB at stop  $s'$

$\rho_s$  Passenger count in the bus between stop  $s$  and  $s'$

$\theta$  Road slope

$\varsigma$  Air density

$\xi$  Decision tree index

$A$  Frontal area of EB

$a$  Real-time EB acceleration

$alt_n$  Altitude of  $n^{th}$  road segment

$B_t$  Control input matrix

$C$  Accumulated energy consumption of EB

$C^A$  Aerodynamic dragging coefficient

$C^F$  Friction coefficient

$C^R$  Road friction coefficient

$D1, D2$  Data subset after node splitting

$d_s$  Passenger count taking off at stop

$E$  Real-time EB energy consumption

$F$	Real-time total force
$F_a$	Real-time aerodynamic drag force
$F_f$	Real-time friction force
$F_r$	Real-time resultant force
$F_s$	Real-time decomposed gravity
$F_t$	State transition matrix
$G$	Driving distance to departure station
$G^r$	Gear ratio
$g_{s,s'}$	Passenger count traveling from stop $s$ to $s'$
$h_s$	Passenger count getting on EB at stop $s$
$H_t$	Observation matrix
$\mathcal{I}$	Important feature set
$I$	Road intersection number
$I^M$	Identity matrix
$K_t$	Kalman gain
$l$	Horizontal distance
$Lat$	Latitude of EB in time slot $t$
$Lon$	Longitude of EB in time slot $t$
$m^a$	Average adult weight
$m^B$	Real-time EB mass
$m^b$	Pure EB mass
$\mathbf{N}$	Set of road segments
$N$	Road segment number
$Pow$	Real-time EB engine power
$Q$	Splitting feature quality
$Q_t$	Process noise covariance

$r$	Tire radius
$S$	Bus stop number
$s$	Bus stop index
$t$	Time slot index
$Tq$	Real-time EB engine torque
$\mathcal{U}$	Unimportant feature set
$U$	Splitting node number
$u$	Splitting node index
$u_t$	Control input
$v$	Real-time EB speed
$v^E$	Real-time engine angular speed
$w$	Global feature weight
$w^\xi$	Local feature weight
$x_t$	EB motion state
$z$	Node splitting feature

## Chapter 5

$\alpha$	Road gradient
$\Delta h$	Altitude difference
$\Delta t$	Time slot duration
$\delta_1, \delta_2, \dots$	Stage price thresholds
$\eta$	Constant efficiency coefficient
$\Gamma$	Monotone interval number
$\gamma$	Monotone interval index
$\lambda$	OLTC tap position
$\phi$	Drivetrain impact coefficient
$\pi$	EB and ESS charging/discharging strategy

$\alpha_{n,j,i}$	Road slope set
$\pi$	EB and ESS charging/discharging strategy set
$\rho$	Air density
$\tau, \kappa, t$	Time slot index
$\varphi_k, \epsilon_k, \mathcal{Z}_{kk'}$	Power flow analysis parameters
$\zeta$	Rolling friction coefficient
$\hat{P}$	EBTC daily peak load
$\mathcal{T}^+$	Periods that EB is on the way
$\mathcal{T}^-$	Periods that EB is in EBTC
$A$	EB front area
$a, a^+, a^-$	EB acceleration
$C^a$	Aerodynamic drag coefficient
$c^e$	Energy consumption cost
$c^r$	Power generation revenue
$c^s$	Service charge for capacity cost
$D$	Driving distance
$E, E_{i,j}, \dots$	EB power consumption
$F^a$	EB aerodynamic drag force
$F^f$	EB friction force
$F^r$	EB resultant force
$F^s$	EB decomposed gravity
$F^{tr}$	EB tractive force
$g$	Gravitational acceleration
$i$	Road segment index
$I_{n,j}$	Road segment number
$j$	Journey index

$J_n$	Journey number
$K$	Bus node index
$K$	Bus node number
$m$	EB mass
$m^c$	EB curb mass
$m^p$	Average passenger mass
$N$	Total EB count
$n$	EB index
$\hat{P}_t$	EBTC peak load expected currently
$\hat{P}_{t+}$	EBTC peak load in the future
$\hat{P}_{t-}$	EBTC peak load in the past
$p^c$	Service charge for capacity price
$p^e$	Energy consumption price
$p^r$	Power generation reward price
$P_{dis/ch}^S$	Maximum EB discharging/charging power
$P_{dis/ch}^S$	Maximum ESS discharging/charging power
$P^E$	EBs charging/discharging load
$P_n^E$	EB $n$ charging/discharging load
$P^O$	Office load
$P^S$	ESS charging/discharging load
$P^{TC}$	EBTC total active power
$P^V$	PV load
$PSVF$	Percentage steady-state voltage fluctuation
$Q^{TC}$	EBTC total reactive power
$T$	Total time slots
$Tr_{n,j,i}$	EB trip time

$v$	EB speed
$V^{ref}$	Reference voltage
$V_k$	Bus node $k$ voltage
$X$	EB charging power level number
$x$	EB charging power level index

# 1

## Introduction

### 1.1 Background

In the recent years, the increasing concerns on environmental and energy issues have promoted the development of alternatives for private travel and public transportation. Specifically, the electric vehicles (EVs) have attracted significant attention due to the environment-friendly feature and the government policy support. According to the report from International Energy Agency [1], the EV stock has been growing since 2010 and surpassed the 2 million threshold in 2016. In 2019 nearly 2.2 million EVs have been sold globally and in 2020, Tesla, BYD, BAIC Motor, and other international EV manufactures are expected to launch 66 EV models [2]. By 2040, the increased electricity demand from EVs will be 1964 TWh according to [3], in which 216 TWh will be consumed by electric buses (EBs). Obviously, the ever-increasing EV charging load can potentially affect the power quality in the distribution system. The charging load can be twice as much as the current basic load, and the charging activity usually happens when home appliances are used so that the peak load can be aggravated. Thus, there is an urgent need to develop feasible solutions to mitigate the negative impact of the increasing charging load in the distribution system [4–6].

Among the various feasible solutions, the EV charging power management has attracted a lot of attention due to its flexibility, reliability, and economy. At present, the EV chargers can enable bidirectional charging with adjustable charging power. The integrated servomechanism makes the charging power and duration controllable during the charging process, which guarantees the flexibility of EV charging power management in the aspect of hardware. Besides, due to the high penetration, large charging/discharging power, ever-increasing battery size, and short reaction time of EVs, the total charging load

in a specific distribution system can be adjusted effectively and accurately according to the real-time power grid condition. Through proper coordination approach and charging control strategy, such EV charging power management can be a reliable solution to address the enormous charging load. Considering the acceptance of the EV owners, the pricing intensive can encourage more EV owners to participate in the energy management. Through specific pricing scheme, the distribution system operator (DSO) adjusts the charging price in different period according to the power grid condition. Such real-time price (RTP) mechanism can guide the EV owners' charging activities and decrease the peak charging load. Accordingly, the DSO's reliance on the ancillary service providers is reduced. In this way, the EV owners can decrease the charging cost and the DSO can maintain the power quality with lower cost.

In addition, when the charging demands of EVs are satisfied, the idle EVs are able to discharge and provide energy to the distribution system. In the traditional grid to vehicle (G2V) scenario, the EV owners usually make the charging decisions according to their own charging demand and cost. Involving the vehicle-to-grid (V2G) mechanism, the EVs can communicate with the DSO and selectively adjust charging schedule or inject power to the distribution system according to its real-time requirement. Also, these EV owners will be paid accordingly for providing the ancillary service. Compared with traditional ancillary service providers, EVs can reduce the cost and achieve a fast demand response. To effectively coordinate the individual EV's charging activity and integrate the EV ancillary service resources, the concept of EV aggregator (AGG) has been proposed, which aggregates the EVs in a specific area and optimize their charging process simultaneously. Through signing contracts with the EV owners, the AGGs can obtain all the charging/discharging controllability of the EVs in the plug-in state. Also, the AGGs need to satisfy the EVs' charging demand before departure. In this way, the integrated EV fleets can be regarded as an independent reliable ancillary service provider in the distribution system. However, the randomness of the charging demand, charging time, and charging location of individual EVs make it difficult to estimate the charging demand and optimize the charging process. Thus, how to analyze the interaction among DSO, AGGs, and EV owners considering the aforementioned randomness is still an open issue. Further, as a special category of EVs, EBs have many particular features such as larger charging/discharging power, higher battery capacity, known operation schedule and route, and higher controllability. To replace the existing diesel buses with EBs, the research to analyze the impact on the distribution system power quality is needed. Also, integrating the ever-increasing EBs into the current distribution system demands special optimization approaches and energy management strategies.

An illustration of the smart grid with EV integration is shown in Fig. 1.1. In this thesis, for in-station charging EVs, the relation between EV owners' charging process and the RTP is investigated, along with the interaction among individual EV owners' charg-

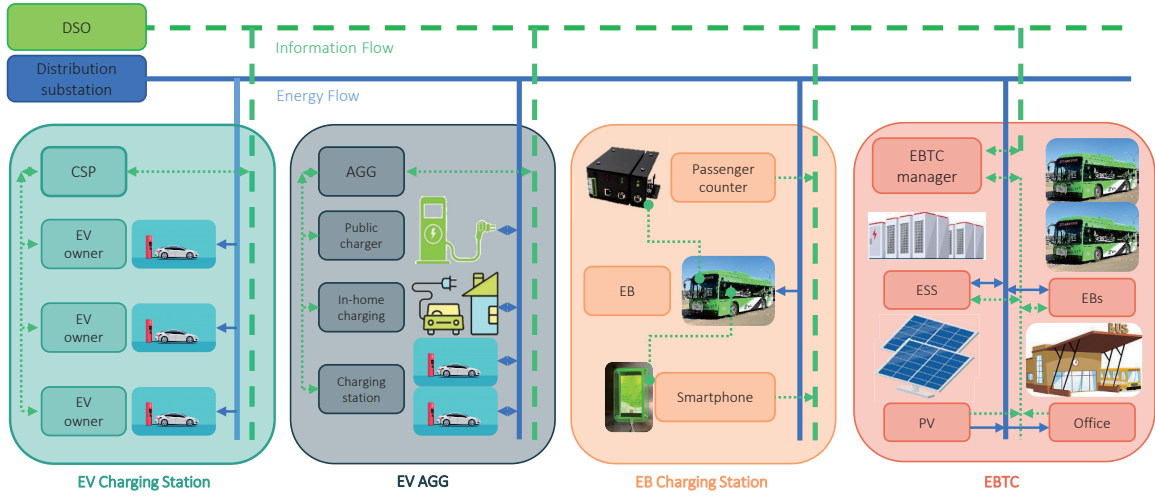


Figure 1.1: An illustration of the smart grid with EV integration.

ing strategies. The pricing scheme of DSO and the charging strategies of EV owners can be optimized to decrease the peak charging load. Secondly, for EV AGGs, the method to integrate EVs as to provide reliable ancillary service is developed. Based on the existing voltage regulation (VR) auction mechanism, AGGs should not only estimate the VR capacity of itself considering the randomness of EBs, but also take into account the impact of other AGGs' auction strategies on the auction result. Then, through optimizing the individual AGG's auction strategy, the revenue of AGGs can be maximized, and the VR capacity requirement of DSO can be satisfied with least cost. Thirdly, compared with general EVs, EBs have larger battery size, higher charging/discharging power, larger daily charging demand, and known operation route and schedule. Accordingly, a real-time energy consumption estimation approach of EBs is developed based on EB motion data collected by smartphone and passenger count. Thereafter, the impact of EB charging load on the distribution system can be estimated accurately. Finally, in the EB transit center (EBTC), the energy management is of great importance. On one hand, the energy demand of the office building and EBs should be satisfied. On the other hand, the impact on the VR process of DSO should be taken into account. In order to minimize the EBTC operation cost and guarantee the voltage quality, we propose a stochastic EBTC energy management approach to control the charging/discharging power of EBs and energy storage system (ESS). Also, the energy consumption of office and the power generation of photovoltaic (PV) are considered in our research.

In the related works, many optimization approaches have been applied to optimize the EV charging schedule to reduce its impact on the distribution systems. Particularly, the robust online algorithms [7, 8], genetic algorithm [9], fuzzy optimization [10, 11], mixed-integer programming [12], dynamic programming [13, 14], game theory [15, 16], and multi-objective optimization [17] are used for optimizing the charging schedule of the EVs con-

sidering multiple issues such as random PV generation, stochastic EV mobility and charging demand, and random electricity pricing scheme. For in-station EV charging, the impact of pricing scheme on the EV charging process is analyzed in [12, 13]. However, few works has taken into account the impact of EV randomness on the pricing strategy of the DSO. The existing works neither consider the revenue of DSO and EVs (via AGGs) together nor involve the randomness of PV, EVs, and distribution system in one system model. In addition, the interaction among DSO's pricing scheme, power grid condition, AGGs' and EV owners' behavior still need to be further analyzed. Among the research works on EV AGG auctions, various game approaches have been applied to optimize the auction strategies of EV AGGs [15, 18, 19]. However, the stochastic game among these AGGs and the impact of distribution system circuit topology on the auction process have not been analyzed in details. In order to evaluate the charging demand of EBs, most of the existing works [20–24] rely on statistic values. A detailed physical energy consumption model based on EVs' motion data needs to be developed. Also, a practical EB motion data collection device is necessary to support this research. Considering the EBTCs, many researchers have made significant efforts to develop an efficient energy flow management scheme in EBTCs with PV and ESSs [25–31]. However, the existing energy flow model is not accurate excluding the randomness of EBTCs. Also, a practical electricity pricing scheme should be considered for EBTC's energy flow management as well as the corresponding impact on the distribution system.

In summary, to achieve efficient energy management of EVs in the future smart grid, additional research effort is still required. In particular, the following four topics are studied in this proposed PhD research.

1. Stochastic in-station charging management and the RTP scheme optimization;
2. Stochastic AGG VR capacity estimation and VR auction strategy optimization;
3. Stochastic EB energy consumption estimation and charging load impact analysis;
4. Stochastic energy management in EBTC with EBs, PV, and ESS.

## 1.2 General Terms and Definitions

In this section, the important terms used in this thesis are defined to clearly identify the scope of work done in this research.

### 1.2.1 G2V and V2G

The charging/discharging modes of EVs/EBs can be divided into two modes: G2V and V2G. Generally, most EVs/EBs work in the G2V mode [32]. In this mode, the EVs/EBs do not need to communicate with the DSO nor to consider the impact on the distribution

system. Their charging processes are determined by their own charging demands and the charging cost. Since the EVs/EBs in this mode are not controlled by the DSO, the DSO have to analyze the charging load impact on the distribution system and reserve enough ancillary service capacity to maintain the security and stability of the distribution system. To mitigate the impact of charging load on the distribution system, the V2G mode is proposed. In this mode, the communication and interaction between EV/EB owners and DSO is emphasized and utilized. Particularly, in the unidirectional V2G mode [33], the EV/EB owners can supply their own profiles such as charging demand, charging power, charging time, charging location, and corresponding adjustable range to the DSO. Accordingly, the DSO will recommend proper charging schedules to the EV/EB owners and reserve corresponding ancillary service capacity. Also, according to the EV/EB owners' response, they can be rewarded by the DSO. In this way, the charging load impact on the distribution system can be mitigated. And both the charging cost of EV/EB owners and the operation cost of DSO can be decreased. Also, the stability and security of the distribution system can be improved. In the bidirectional V2G mode, the EVs/EBs can inject power to the distribution system through discharging according to the control command from the DSO [34]. In this way, the EVs/EBs can provide ancillary services to the distribution system and get more revenue in this process.

### 1.2.2 Markov Decision Process

Markov decision process (MDP) is a discrete-time stochastic decision-making process, which has been widely applied in the EV research for modeling the state of the charging station or EV fleets. As an extension of Markov chain, MDP enables decision makers to take actions and receive revenues. Different from the Markov chain, in MDP, the actions can influence the transition probability of the system state. At each time step, the process is in one deterministic state, and the decision maker may choose any available action in the current system state. In the next time slot, the process will randomly transit into a new system state, and giving the decision maker a corresponding revenue. The goal in a MDP is to find an optimal strategy for the decision maker to take best action in the specific system state. In the scenarios of EV charging, the MDP can be utilized to analyze the charging decision making process of EV owners to minimize the charging cost or maximize the discharging revenue.

### 1.2.3 Stackelberg Game

Generally, a classical Stackelberg game model is expressed as a leader-follower game. To take the optimal action, the leader needs to fully understand not only his/her own feasible actions and the related revenues but also the followers'. In this way, the leader can plan his/her strategy properly to propel the followers to take the actions in favor of the leader. In a normal version, the leader announces his/her action and acts first, while the followers

make their decisions after observing the leader's action. Also, their revenues are partially determined by the leader's action. The leader must know that the follower observes its action. The follower must have no means of committing to a future excluding the leader's expectation and the leader must know this. In particular, if the followers make decision before the leaders announce their actions, the leader-follower relationship will reverse. In this case, the followers have to estimate the leader's action rather than observe directly. Through stochastic optimization approach, the followers can obtain stochastic strategies to optimize the revenues.

#### 1.2.4 Network Topology in VR Market

Network topology refers to the physical topological structure of distribution system. Consider a distribution system with residential loads and PV generators, where under-voltage and over-voltage issues may exist due to the load and generation fluctuations. In the VR market, besides the traditional VR sources, EV AGGs are also potential VR sources for DSO to mitigate the voltage issues [35]. Through injecting or absorbing power in the distribution system, EV AGGs can effectively adjust the voltage magnitudes of neighboring buses. Therefore, in the VR market, since not all the AGGs are suitable for providing the VR services due to random EV mobility and power distribution network topology impact, DSO will periodically select and involve qualified AGGs in the VR process [35].

#### 1.2.5 Stochastic Multi-Player Game

A stochastic multi-player game can be regarded as a repeated game involving stochastic publicly observable states in discrete time slots. In particular, the historical performance scores of all the players (i.e., AGGs) are always broadcast before the auction. Then, they will choose their actions and be paid according to the auction result. In the meantime, their performance scores will be updated according to the actual VR process. Thereafter, the game moves to the next stage, and a new random state is drawn. The distribution of the random state depends on the auction strategies and the results in the previous auction stage. The same process will be repeated in the new stage. In the economic field, such stochastic multi-player game is widely used to analyze the players' actions in the auction process [36,37]. When considering the VR market in the power system, this approach can also be leveraged to analyze the decision process of rational AGGs in the auction process.

#### 1.2.6 Random Decision Forest

Random decision forests is an ensemble learning method for classification, regression and other works that operate by constructing a multitude of decision trees at training time and outputting the class that is the mode of the classification or regression of the individual trees. A random decision forest consists of a group of predefined binary decision trees. In the forest, each decision tree is generated using a bootstrap sample based on the training

dataset. In each tree generation process, a feature subset is randomly chosen from the global feature set. When splitting the node of the tree, one feature in the subset will be selected. In the random decision forest, each tree can make a decision according to the training case. Then, the final decision can be made according to the most popular decision in the forest. Besides, when the importance of features for classification or regression is unknown, the randomness decision forest can help to evaluate the alternative features [38]. Through selecting different feature groups to generate the randomness decision forest and observing the classification or regression performance, the importance of relative features can be quantified. In this way, the important features can be clustered and the unimportant features can be discarded. Particularly, in our research, the randomness decision forest is utilized to estimate the real-time EB acceleration and discard the unimportant features to simplify the computation process.

### 1.2.7 Robust Optimization Over Time

Robust optimization over time (ROOT) can be regarded as a consideration of both robust optimization and dynamic optimization. This approach concerns the cumulative impact of stochastic system states on the decision making efficiency. Therefore, ROOT inherits the properties of robust optimization and has its own new properties. A solution is called robust over time when its expected accumulated revenue remains acceptable and insensitive to the environmental changes in specific term and this solution will be implemented until its future revenue degrades to an unacceptable level. After that, another robust solution must be obtained. The traditional robust optimization mainly concerns the uncertainties in the stationary parameter space, either decision parameters or environmental parameters. By contrast, ROOT not only considers the uncertainties in the parameter space, but also the cumulative effect of these uncertainties in the time space. Generally, in order to obtain the ROOT solution, a time-variant fitness function is required to quantify the acceptability of the strategy. Accordingly, the strategy being implemented can be held or discarded.

### 1.2.8 RTP Scheme

In order to manage EV charging demand, optimizing the operation of charging stations is indispensable for CSP to ensure system reliability, while achieving certain operating objectives such as minimizing the losses in the distribution systems. With advanced smart meters and chargers being deployed in the future smart grid, RTP schemes [39–41] can be leveraged. In particular, by restraining the dense electricity usage via increased electricity price, the EV charging demands can be shifted over time to relieve system peak load.

## 1.3 Research Definition and Literature Review

In this section, the critical terms and problems investigated in this thesis are clarified to identify the scope of this research work. Moreover, the existing research works in literature are discussed.

### 1.3.1 In-Station EV Charging Optimization

In this research, we investigate the operation of multiple EV charging stations in the distribution system. The objective of this study is to maximize both the revenue of DSO and EV owners while considering the randomness of EVs and the impact of RTP scheme on the EV charging decision.

In literature, significant efforts have been devoted to EV charging demand management. The survey in [42] shows the impacts of EVs' demand response to the load shifting in smart grid. An overview of existing dynamic approaches for static EV charging as well as their suitability are presented in [43]. Distributed control method of EV charging is proposed in [44] based on energy demand forecast. Optimization methods are proposed in [45–50] to maximize the unilateral pay-offs of CSPs and EV owners. Here, the authors of [47] develop two revenue optimization frameworks to maximize the revenue from the aspect of EV charging stations. However, as a single-objective optimization method, the charging demand in such model was limited by CSP, which means such methods cannot track the demand response of the actual EV owners in the charging process. Finite horizon optimization (FHO) is applied in [48] for implementing the decentralized optimal demand-side management. As a real-time optimization technique, FHO aims to find an optimal control sequence of a period, which is divided into several time slots, to help handle possible unexpected changes and fluctuations of the system in the later periods. Typically, only the first item of the current time slot in the optimized sequence is applied while others are discarded, which will be optimized again in the next time slot. The results of FHO may vary when the fluctuation of the base load differs. For household load curve with small amplitude and high fluctuation frequency, FHO can work well. However, for the bus load in the distribution system which has a high amplitude and low fluctuation frequency, the finite horizon of FHO can make an overly optimistic estimation of the load condition. Besides, the demand response as well as the interactions between CSPs and EV owners are not considered in FHO. In such optimization frameworks, a single EV owner usually prefers to select a minimum or maximum charging power to maximize the individual revenue. As a result, the station is easier to be saturated so that more EV will be rejected to charge in the station due to the limited charging piles.

To better characterize the interactions between CSPs and EV owners in a competitive power market where they both attempt to maximize their own payoffs, game theoretical models can be used. In particular, non-cooperative game [51], N-person game [52] and

coalition game [53] approaches are developed for EV charging demand scheduling, while the retailer-customer relationship in the charging business (established via charging stations or CSPs) can be modeled by Stackelberg game models [54,55]. Yet, how to integrate the randomness of EV arrivals, departures and charging demands into the game theoretical models and develop optimal RTP schemes accordingly, are still open issues. To model the randomness involved in EV charging, Leou *et al.* [57] prove that the number of EVs starting charging in each time interval can be modeled by a Poisson process according to long-term data of a charging station. Based on similar observations, Markov models [58], and queuing network models [59,60] can be applied to analyze the randomness of EV charging demands. However, how to embed these stochastic models into the game theoretical approaches to characterize the interactions among CSP, charging stations and EV owners is a critical but challenging issue. A recent research work [61] indicates that a stochastic game approach can be potentially used to model a video multi-casting market to characterize the randomness of video subscription by different customers. Another recent paper [62] proposed a distributed charging control method to coordinate large scale EVs without compromising the security of the distribution network based on a non-cooperative game model. However, such approach cannot be directly applied to EV charging station operation since the EV charging decision making processes and distribution system dynamics are significantly different from that of video subscription. Therefore, the development of a novel stochastic game approach is indispensable.

### 1.3.2 EV AGG Energy Management in the Voltage Regulation Market

In this research, the VR auction process among VR service providers including the EV AGGs is investigated. Also, the randomness of EV AGG VR capacity and the impact of distribution system circuit topology on the VR efficiency are taken into account. The objective of this work is to optimize the EV AGGs' auction strategy while minimizing the DSO's VR cost.

In literature, the auction theory has been widely used in the design of V2G ancillary services to characterize the economic properties. In [35,63,64], individual auction is considered and where EV is modeled as an independent ancillary service source. In [65–69], EV AGGs are involved to coordinated a number of EVs so that larger ancillary service capacity can be provided with better performance. In terms of EV actions, the bidirectional V2G auction can be used [66–69]. Besides, the charging/discharging auction mechanisms are also considered independently in [63–65]. According to the existing literature, there are several advantages of analyzing the VR market based on an auction framework: Firstly, based on the auction mechanism, maximizing the individual interests of AGGs can be characterized in details; Secondly, through the auction mechanism, the DSO can select more qualified AGGs as VR sources based on a performance scoring process; Thirdly, due to the performance scoring process, the AGGs can be prevented from providing inaccurate

VR capacity, which could guarantee the reliability of the VR services in power systems.

Based on the auction mechanism, the power quality issue [63,65,68,69] and economic issues such as individual revenue [63,64,68] and social welfare [65,67,69] have been discussed. In particular, stochastic dynamic programming approach is investigated in [64] to optimize the charging process for providing the ancillary service in a smart electric grid environment. The authors of [63] investigate the efficient energy allocation among EVs belonging to one AGG through auction mechanisms. The research work in [65] aims at reducing the system cost while maintaining the system stability. In particular, a demand response approach is proposed, where the EVs are motivated by dynamic pricing for energy requirements. An optimization model is proposed in [67] to determine the day-ahead inflexible auction and real-time flexible auction under market uncertainties, where the concept of conditional-value-at-risk is adopted considering the capacity limitation. In [69], a stochastic optimization model for optimal auction strategies of EV AGGs is developed based on the day-ahead energy and ancillary service markets with variable wind energy. A coordinated auction is considered in [68], where fuzzy optimization and auto-regressive integrated moving average forecasting model are used to deal with the market uncertainties.

Although the auction approaches can ensure that the optimal strategies are followed by AGGs in V2G energy trading, the physical power network topology is neglected by most of the previous works in their V2G auction designs. Considering both economic property and network topology, there are two categories of V2G studies: 1) The non-auction approaches are used while considering power network topology in problem formulation but neglecting economic properties, such as truthfulness and voluntary participation [70,71]; 2) The auction approaches are used to model the economic properties while neglecting the power network topology on auction results [63–69]. In a very recent research work [35], both economic property and network topology are taken into account. However, additional stochastic analysis is still needed to address the uncertainties in the V2G market.

Along with the advancement of game theory, stochastic multiplayer game (SMG) has been developed as a method to solve the stochastic revenue maximization problems involving competitions. In [72], the general form of SMG is analyzed, and a memory mechanism similar to the scoring process is discussed. However, only the cases where the players take actions in turn are considered. Since in the VR auction process, the EV AGGs take actions concurrently and influence the auction results together, a game approach suitable for this application still needs to be developed. The concurrent SMG approach for a single game is proposed in [73], where the players take actions concurrently. This work focuses on the concurrent games with two players. Very recently, the multiplayer stochastic game model is analyzed in [36], where the authors introduce a general condition to guarantee the existence of stationary Markov perfect equilibrium in stochastic games. Yet, we still need to leverage the recent advancement in SMG modeling to address the V2G VR auction

problem.

### 1.3.3 EB Energy Consumption Estimation

In this research, we focus on building an accurate physical EB energy consumption model and estimating the EB energy consumption based on the EB motion data and passenger count. Also, the impact of EB charging load on the distribution system is analyzed based on the proposed estimation approach.

According to the existing works, to mitigate the error of EB energy consumption estimation based on historical data, a correction approach according to the real-time EB motion data is demanded. Therefore, a motion data based EB energy consumption estimation approach is the foundation of various applications, in the following aspects:

1. *Power System Impact Mitigation*: The approach can help estimate EB charging demand so that the impact on the power system can be predicted and mitigated [74,75];
2. *Charging Schedule Optimization*: For EB operators, the estimation can help optimize the charging schedule and reduce the economic cost [76];
3. *Public Transit Upgrade*: Through the approach, the public transit center can collect the motion data of the diesel bus and estimate the corresponding energy consumption and cost, if the diesel buses are replaced by EBs [77];
4. *Battery Lifetime Extension*: The EB manufacturer can estimate and extend the battery lifetime according to the results and provide the customers with better after-sales [78,79].

In literature, many researchers have made significant efforts to develop energy consumption estimation approaches [20–24]. A machine learning-based time series prediction algorithm is applied in [20] to predict the charging demand. In [21], the energy consumption is captured by a bi-level Markov process considering the randomness of wind power supply. With GPS historical data, a genetic algorithm-based optimization model is proposed in [22]. Besides, the population and economic activity indicators are also considered in [23, 24] to improve the accuracy of energy consumption estimation. However, these approaches perform energy consumption estimation based on statistical data only. Considering the specific physical model and regular operation schedule of EBs, more detailed characteristics can be included in the EB energy consumption estimation, to further improve its accuracy.

Notice that most of the above-mentioned works are based on the battery electric vehicles (BEVs) and plug-in hybrid electric vehicles (PHEVs). However, there are many significant differences between the EBs used by public transit services and the BEVs/PHEVs used by regular households. For example, the EB's specifications are usually identical in a certain public transit service, so that accurate physical model of EBs can be leveraged for

energy consumption estimation. Also, the EB route can be known in advance and the operation schedule is usually determined beforehand. In [80], a two-stage EV routing problem is analyzed, and the EV energy consumption estimation is improved by considering detailed route topography and speed profiles. However, compared with EVs, the operation routes of EBs can be determined. Also, the passenger count fluctuation is an important factor because the vehicle mass of an EB can be random due to the highly dynamic passenger count. Considering these unique features, the authors of [81] integrate EB charging demand estimation in a single simulation model. The utilization of a specialized simulator to represent complex technical specifications in the EB operation process is proposed in [82]. Besides, solutions based on dynamic models involving bus design parameters and interaction forces are proposed in [83–85].

Nevertheless, there are still several technical challenges to be addressed. The first challenge is how to build the EB tracking system and collect the motion data since most existing researches are based on the EB motion data. The existing solution can be based on either road-side sensors [86,87], or carry-on devices [88]. However, the corresponding time and economic cost of road-side measurement equipment installation and carry-on device operation can be extremely high. In this case, a simpler and more feasible approach is needed to collect the motion data of EBs so that a large database can be built for the further researches. Besides, the filter for GPS signal noise reduction needs to be developed to increase the accuracy. The traditional filters usually require real-time accelerometer data [90,91] and gyroscope data, which may not be available for most EBs. Thus, there are three critical but challenging issues for modifying the conventional Kalman filter (KF) to estimate real-time EB energy consumption: 1) EB mass estimation considering the impact of stochastic passenger count; 2) Dimension reduction to decrease the computational complexity caused by the high-dimension motion state; 3) Estimation approach for stochastic acceleration, which can be involved as a control input in the KF to improve the accuracy.

### 1.3.4 Stochastic EBTC Energy Management

In this research, the stochastic EBTC energy management is investigated considering the randomness of EBs, PV, and office load. The objective of this research is to minimize the EBTC's operation cost and mitigate the negative impact on the distribution system considering the VR mechanism.

In literature, many researchers have made significant efforts to develop an efficient energy flow management scheme in EBTCs with PV and ESSs [25–31]. In [25], the significance of installing ESS in EBTC is investigated, and a mixed integer nonlinear programming formulation is applied to optimize operation cost. A mixed integer linear programming approach is developed in [26], where the EB battery cost, ESS cost, and charging demand are taken into account. A hierarchical energy storage configuration is considered in [27] involving the coordination among centralized ESS and distributed ESSs. The

work in [28] illustrates the feasibility of PV powered charging station with vehicle-to-grid (V2G) technology and designs a maximum power point tracking controller to manage the energy flow in station. In order to improve the operation efficiency of EBTC, a decentralized energy management system is developed in [29] by utilizing the PV generation. The integration of PV in EB battery swapping station is studied in [30] considering the electricity price fluctuation. In [31], an efficient energy management approach is proposed for a solar powered EV charging station. Particularly, a PCB is designed to implement the management approach in this work. Yet, all the research works above only exploit ESS or PV independently in the EBTC. Thus, more effort is needed for the scenarios involving both of them. Also, a few approaches have been proposed for energy management in EV charging stations with ESS and PV based on stage-variant optimization [92] and multi-agent deep reinforcement learning [93].

Yet, the differences between EBTCs and EV charging stations need to be considered. Firstly, the system models are different. For the economic model, the EV charging station manager and EV owners consider their own benefit and cost independently while the EBTC manager has to consider both factors. For the charging demand model, EVs' charging demand is typically estimated based on the historical data. However, for EBs, an accurate physical energy consumption model can be utilized for charging demand estimation. Also, the decision periods are different. The EV owners only care about one charging period and make their decisions accordingly, while the EBTC owners have to consider several billing periods for benefit maximization. Secondly, the known information in these two cases is not the same. For EVs, the vehicle types, driving routes, battery sizes, charging power, start/finish charging time, and the sensitivity to the price are all undetermined for charging station managers. On the other hand, we have sufficient information about EB operation schedule, technical parameters, driving route, and battery characteristics, which can help to achieve higher accuracy and efficiency in EBTC energy flow management. Thirdly, the flexibility of energy management strategy is different. For EVs, not all the EV owners are willing to discharge for charging other EVs. Also, the charging period is limited by the parking time and the charging demand has to be satisfied before departure. So, the decision making process is restricted and the theoretical optimal strategy is usually infeasible due to the random departure times. In the EBTC, we have unified planning and more available charging periods for EBs. Thus, we can explore and implement the optimal solution in a broader strategy space.

Recently, many researchers have made efforts to optimize the energy flow of the charging stations. The authors of [94] proposed a two-stage stochastic optimization approach to enable the fast charging station to provide ancillary services to the transmission system. In [95], an integrated resource planning framework is proposed for EBTC with the coordination of ESS. However, the randomness of EBs is not considered in these works. To manage the complex EBTC energy flow, EB energy consumption estimation is a fundamen-

tal task. Generally, it can be estimated based on the historical data [96]. Yet, the accuracy is limited. In [97], the EB energy consumption is estimated based on the real-time EB motion state measurement. However, the corresponding equipment cost is extremely high and additional communication infrastructure is needed for the centralized optimization. The driving cycle synthesis approach investigated in [98,99] enables EB energy consumption estimation without real-time motion data. Nevertheless, this approach is still highly dependent on the deterministic EB arrival time and a new approach based on stochastic arrival time is needed due to the randomness of EB operation. The impact of charging load on the distribution system has been analyzed in [100]. Similar to the optimization approaches in [25–30], the impact on the distribution system is modeled based on dynamic electricity price. Yet, the practical peak-load based pricing schemes should also be investigated, which is widely adopted by EBTCs as they are typically considered as industrial loads. In [101], an integrated utility-transit model for EB system optimization is developed to find the optimal charging power and charger numbers in the station. However, the impact of the voltage regulation process on the interactions between the EBTCs and distribution systems has not been taken into consideration. Thus, a novel stochastic EBTC energy flow management approach is still needed.

## 1.4 Thesis Motivation and Contribution

Based on the discussions above, many new technical challenges have been brought to the smart grid along with the ever-increasing EV penetration. At first, how the increasing EV charging load affects the power systems and how to mitigate such impact should be investigated. Secondly, how to utilize the EV charging/discharging capacity to provide ancillary services to benefit both power system and the EV owners should be studied. Thirdly, as a special kind of EVs, the EBs' charging demand needs to be estimated according to the known motion data and deterministic operation schedule. At last, for optimizing EB charging within the EBTC, an approach to manage EB charging schedule is demanded to minimize the EBTC operation cost while minimizing the impact on the distribution system. Moreover, the uncertainties such as EV charging demand, EV charging power, EV start-charging time, EB passenger count, EB motion data noise, power system condition, traffic condition, and renewable generation also increase the difficulty to solve these problems. As discussed in the literature review, a lot of outstanding research works have been done to optimize the EV charging process in different scenarios considering these stochastic features. However, there are still many open issues that need to be further investigated. To address these technical challenges, the main contributions of this thesis are summarized as follows.

### 1.4.1 A Stochastic Game Approach for EV Charging Station Operation in Smart Grid

In this research, we investigate the operation of multiple EV charging stations in the distribution system. On one hand, EV owners aim at reducing the charging costs while satisfying their charging demands. On the other hand, the CSP needs to manage the loads of EV charging stations to ensure efficient and reliable distribution system. Thereafter, we propose a novel stochastic game approach for improving EV charging station operation, and develop an RTP scheme for CSPs to optimize system operation. The main contributions of this research are threefold:

1. Developing an MDP approach to initially optimize the individual EV's charging process considering the stochastic charging demand, charging rate, and the charging time in one charging station;
2. Developing a stochastic game model based on the proposed MDP approach to study the iterations among different EV owner's charging decision and stochastic features, i.e, if one EV owner found that a number of EVs would arrive in the charging station and start charging in some specific period, its owner might decide to charge in advance or later to avoid aggregating the peak charging load;
3. Proposing strategies to optimize the RTP scheme while taking into account the response of EV owners to the charging price as well as the relative impact on the distribution through power flow analysis. In this way, the voltage issue and line loss issue caused by the charging load can be mitigated.

### 1.4.2 A Discounted Stochastic Multiplayer Game Approach for V2G Voltage Regulation

In this research, we consider a topology-aware auction framework to model the impact of network topology on the VR efficiency. To further analyze the AGG strategies and the total VR performance, a discounted stochastic multiplayer game (DSMG) approach is proposed. In particular, we model the VR auction process based on a practical auction mechanism, in which the topology issue, stochastic VR capacities, and VR performance scoring mechanism are considered. In order to obtain the optimal auction strategies, we prove the existence of the stationary Markov perfect equilibrium and provide an algorithm to calculate the corresponding solutions. Based on extensive simulations, we evaluate the performance of the proposed DSMG approach and compare it with other game approaches. The main contributions of this research are threefold:

1. Developing a detailed VR auction model based on practical ancillary service providing mechanism, in which a VR performance evaluation process is used to ensure the

truthfulness, such that each AGG always reports its actual VR capacity in the auction process;

2. Embedding the impact of both power distribution network topology and stochastic EV mobility in the auction process to analyze the rational response of AGGs;
3. Proposing a DSMG approach based on the VR auction model. The existence proof of the stationary Markov perfect equilibrium is presented, and the corresponding algorithm to obtain the equilibrium is developed.

### **1.4.3 A Data-Driven Approach for Electric Bus Energy Consumption Estimation**

In this research, we propose a detailed EB energy consumption estimation approach based on a modified KF. A physical model of EB energy consumption is built considering the impact of stochastic passenger count on the EB mass. Then, the dimension of the EB motion state is reduced based on the known EB operation route so that the computation of KF is simplified. In addition, an EB acceleration estimation approach is developed to simulate the decision process of the driver based on an extended random decision forest algorithm. Accordingly, the EB acceleration can be computed as control input rather than noise, which can significantly improve the accuracy of conventional KF. The main contributions of this research are fourfold:

1. A detailed physical model for KF is built to estimate the EB energy consumption, in which the impact of random passenger count on the EB mass is involved;
2. The dimension of the motion state is reduced through proposed simplification mapping based on the known EB operation route, which can reduce the computational complexity of KF;
3. A random decision forest algorithm is applied to estimate real-time acceleration of the bus, which can improve the accuracy of the KF. Also, a feature importance weight rank approach is extended to optimize the forest generation process;
4. The proposed EB energy consumption estimation approach is tested with the real data collected from St. Alberta Transit, AB, Canada. An Android APP is developed to collect real-time EB motion data, based on which the accuracy of the proposed approach is evaluated.

### **1.4.4 A Three-Layer Stochastic Energy Management Approach for Electric Bus Transit Centers with PV and Energy Storage Systems**

In this research, we propose a three-layer stochastic energy management approach for EBTC. Stochastic models are developed to characterize the randomness associated with

the EBTC. Based on synthetic driving profiles, a stochastic EB energy consumption estimation approach is proposed, where both the randomness of passenger count and EB arrival/departure time are taken into account. Considering the EBTC operation cost including the electricity cost, service charge of capacity, and power generation revenue, an EB/ESS charging/discharging margin is obtained with modified ROOT. Then, the on-load tap changer (OLTC) tap selection process is analyzed so that the impact of the EBTC load on the local voltage magnitude can be evaluated, based on which the optimal strategy for EB charging/discharging can be determined. The main contributions of this research are fourfold:

1. A stochastic model is developed to characterize the EBTC operation considering the randomness of the transit center office load, PV generation, EB energy consumption, and practical electricity pricing scheme;
2. A stochastic EB energy consumption estimation approach is developed based on synthetic driving profile, where random passenger count, stochastic EB motion, and uncertain EB availability are taken into account.
3. A modified ROOT approach is proposed to calculate the feasible EB/ESS charging/discharging margin;
4. A modified greedy algorithm is developed to optimize the EB/ESS charging/discharging strategy, and we mathematically prove that the proposed algorithm can achieve the global optimal solution.

## 1.5 Thesis Outline

As shown in Fig. 1.2, the EV charging station is investigated at first in Chapter 2. The revenues of EV owners and charging service provider (AGG) have been maximized. Thereafter, the EV AGGs participating in the voltage regulation market are studied in Chapter 3 considering the EV fleet contribution to the power system based on auction mechanism. Then, considering the special features of EBs, a data-driven EB energy consumption estimation approach is proposed in Chapter 4, along with the corresponding EB motion data collection application. Finally, the EBTC energy flow management is analyzed in Chapter 5 so that the operation cost of EBTC is minimized while the impact on the power system is mitigated. More specifically, this thesis consists of six chapters which are organized as follows:

- **Chapter 1: Introduction** - The research background is introduced along with the research definitions. Then, the related works in the recent years are reviewed and the technical challenges are highlighted. At last, our research motivation and contributions are presented.

	EV	EB
<u>Grid to Vehicle</u>	<ul style="list-style-type: none"> <li>➤ Individual EV charging demand estimation</li> <li>➤ Charging cost minimization</li> <li>➤ EV charging station peak load shaving</li> <li>➤ Pricing scheme impact on in-station charging</li> </ul>	<ul style="list-style-type: none"> <li>➤ EB motion data collection</li> <li>➤ Physical EB energy consumption model</li> <li>➤ Data-driven energy consumption estimation</li> <li>➤ Impact analysis on distribution system</li> </ul>
<u>Vehicle to Grid</u>	<ul style="list-style-type: none"> <li>➤ EVs coordination</li> <li>➤ Providing VR capacity</li> <li>➤ Decision making in VR auction</li> <li>➤ System topology impact on VR efficiency</li> </ul>	<ul style="list-style-type: none"> <li>➤ Stochastic EB energy consumption model</li> <li>➤ Stochastic EBTC energy flow model</li> <li>➤ EBTC energy management involving VR</li> <li>➤ Voltage quality optimization</li> </ul>

**Chapter 2:** Stochastic Game Approach for EV Charging Station Operation;

**Chapter 3:** Discounted Stochastic Multiplayer Game Approach for VR;

**Chapter 4:** Data-Driven EB Energy Consumption Estimation Approach;

**Chapter 5:** Three-Layer Stochastic Energy Management Approach for EBTC.

Figure 1.2: Structure of this thesis.

- **Chapter 2: A Stochastic Game Approach for EV Charging Station Operation in Smart Grid** - This chapter presents an stochastic EV charging station model considering the highly dynamic EV mobility, which results in random EV arrivals, departures and charging demands. A stochastic game approach is proposed in this chapter to characterize the interactions among CSP, charging stations and EV owners, where the randomness in charging decision making processes of EV owners is modeled by a Markov decision process. Based on the Nash equilibrium solution of the stochastic game, a RTP scheme is proposed for the CSP to minimize power distribution losses while ensuring system reliability. The performance of the proposed approach is evaluated via extensive simulations based on the IEEE 123-bus test feeder with real vehicle mobility data from 2009 NHTS and 2010 NTS.
- **Chapter 3: A Discounted Stochastic Multiplayer Game Approach for V2G Voltage Regulation** - This chapter presents a practical voltage regulation auction model involving EV AGGs. Then, the challenges to optimize the strategy of each EV AGG in the auction process due to the stochastic EV mobility, various distribution network topology, and the competition mechanism are analyzed. To address these challenges, we proposed a DSMG approach to analyze the competition among EV AGGs. Due to the constraint of distribution network topology, the efficiency of the VR sources at different locations can be different. Thus, the impact of distribution network topology on the VR efficiency is investigated by DSO when evaluating the capacity of AGGs. The randomness of EV numbers is considered when predicting the AGGs' available VR capacity so that the tendency for the AGGs to follow the optimal strategies can be modeled accurately. Accordingly, a linear power flow analysis approach and a battery pool model are developed to address the distribution network topol-

ogy and EV mobility, respectively. Then, the DSMG approach is used in the VR auction process to optimize the AGGs' strategies. The existence proof of the stationary Markov perfect equilibrium is presented, and the corresponding algorithms to obtain the equilibrium is proposed. The performance of the proposed DSMG approach is evaluated and compared with other approaches based on the IEEE 33-bus test feeder, IEEE 123-bus test feeder, and the real-world generation and load data from PVWatts Calculator and Market Analysis and Information System, respectively.

- **Chapter 4: A Data-Driven Approach for Electric Bus Energy Consumption Estimation** - This chapter presents a data-driven approach for EB energy consumption estimation. In particular, a detailed physical model of EB is constructed to model its energy consumption considering the randomness in EB operation, including speed, acceleration, and passenger count. In order to improve the estimation accuracy, the conventional KF is modified involving EB mass estimation considering stochastic real-time passenger count, motion data dimension deduction based on EB operation route, and EB acceleration estimation by extending random decision forest algorithm. In the case study, an Android application is developed to collect the motion data of buses so that any general Android smartphone can be used for data collection. The performance of the proposed approach is evaluated based on real-world EB operation data collected from St. Albert Transit, AB, Canada. Compared with the existing approaches, the proposed approach achieves more accurate real-time energy consumption estimation of EBs, which in turn, provides a better characterization of power system loading and voltage variation.
- **Chapter 5: A Three-Layer Stochastic Energy Management Approach for Electric Bus Transit Centers with PV and Energy Storage Systems** - This chapter presents a three-layer stochastic energy management approach in EBTCs to reduce the operation cost while maintaining local voltage quality. In the first layer, a modified ROOT approach is developed to obtain the charging/discharging margin with minimum EBTC operation cost. In the second layer, the voltage regulation impact on the local voltage quality is estimated through power flow analysis considering voltage fluctuation and line loss minimization. In the third layer, the charging/discharging strategy is optimized with dynamic programming based on a modified greedy algorithm. The performance of the proposed approach is evaluated in a case study based on the IEEE 123-bus test feeder and the real operation data obtained from St. Albert Transit in Alberta, Canada. The results indicate that the proposed approach can not only minimize the EBTC operation cost but also well maintain the local voltage quality, in comparison with existing energy management approaches.
- **Chapter 6: Conclusions and Future Works** - The contribution of this research and the future works are summarized in this chapter.

# 2

## A Stochastic Game Approach for EV Charging Station Operation in Smart Grid

In this chapter, we propose a stochastic game approach for EV charging station operation considering the EV randomness, the interaction among different EV charging stations, and the impact of the electricity price to the charging load. A repeated inverse Stackelberg game is developed to model the interactions among in-station charging EVs taking into account the dynamic arrival and departure processes. Thereafter, an MDP optimization approach is embedded in the game to optimize the charging decision of EV owners with specific known information of other EVs. With the EV owners' charging strategy, an optimal RTP scheme is developed based on the power flow analysis so that the power loss can be reduced. The proposed approaches are evaluated based on IEEE 123-bus test feeder with real vehicle mobility data obtained from NHTS.

### 2.1 System Model

An illustration of charging station operation in distribution system is shown in Fig. 2.1. Consider a distribution system with  $K$  buses in the set  $\mathbf{K} = \{1, 2, \dots, K\}$  managed by a DSP. Let  $\mathbf{K}_C \subseteq \mathbf{K}$  be a subset of buses with EV charging stations which are marked by  $a_1, \dots, a_i, \dots, a_I$ , respectively. Here,  $I$  is the total number of charging stations. In order to manage the EV charging demands, the DSP offers an RTP scheme. Dividing the business hours of charging stations into  $T$  time slots with equal duration  $\Delta t$ , the RTP of bus  $k$  ( $k \in \mathbf{K}$ ) can be expressed as  $p_{k,t}$  [\$/kWh] for all  $t = 1, 2, \dots, T$ . Note that the RTP is location dependent as the charging stations on different buses can have different impacts on distribution system operation, to be discussed in Section IV. Let  $\mathcal{B} = \{\mathbf{B}_t | t = 1, 2, \dots, T\}$  be the base load of the distribution system (without EV charging), where  $\mathbf{B}_t =$

$\{B_t^1, B_t^2, \dots, B_t^K\}$  and  $B_t^k$  is the base load of bus  $k$  in time slot  $t$ .

When a EV arrives at a charging station, if there are available charging piles, the owner can set up a charging reservation in terms of charging power and duration on the charging pile. Otherwise, the owner will be rejected to charge. Actually, if the DSP cannot manage the EV owners' charging process well, it will be easier for stations to be saturated so that some of the arrival EVs do not have the chance to charge. As a result, both the peak charging load and the total charging demand are reduced. However, these rejected EVs will not disappear but charge on other buses of the distribution system and the actual total charging load of the system will not be reduced. So the rate of the rejected EVs should be considered seriously to prevent inaccurate estimation of charging load reduction. Besides, during the charging process, we consider a constant charging power which is the same as the charging reservation [56].

After finishing charging, the owner will pick up the EV and pay the charging fee calculated based on the RTP scheme. Charging service providers (CSPs) are responsible for distributing the RTP and occupancy rate information of charging stations to the EV owners. Generally, the RTP is higher in the peak load hours and lower in other periods. As rational EV owners are willing to pay at a lower price in off-peak load hours, the DSP can achieve peak load shifting through the price incentives.

### 2.1.1 Charging Station Model

When a EV owner arrives the charging station, he always prefer to minimize the charging cost which is influenced by his charging power, duration and the RTP directly. Since both the charging power and duration can be determined by the EV owner, the RTP is the only objective factor he should estimate which depends on the charging power and duration of the other EV owners in the station currently and arriving later. Accordingly, as a reference of EV owners to optimize their charging process, the state of a charging station can be defined by the number of EVs charging in different power levels. Assume that there are  $G$  levels of charging power available in the charging station given by  $\mathbf{P} = \{P_1, \dots, P_G\}$ . Each EV will select a determined charging power in the reservation and maintain a constant power during the charging process. We define the state of charging station  $i$  as a vector  $\mathbf{s}^{a_i} = (n_1^{a_i}, \dots, n_g^{a_i}, \dots, n_G^{a_i})$ , where  $n_g$  is the number of EVs charging with power  $P_g$ . In this way, the load of charging station  $i$  can be calculated as

$$L_t^{a_i} = [P_1, P_2, \dots, P_G][\mathbf{s}^{a_i}]^T, \quad (2.1)$$

where  $[\cdot]^T$  represents vector/matrix transpose. Further, define the system state which includes the states of all the charging stations as  $\mathbf{q} = (\mathbf{s}^{a_1}, \dots, \mathbf{s}^{a_i}, \dots, \mathbf{s}^{a_I})$ . Let  $\mathbf{S} = \{\mathbf{s}_1, \mathbf{s}_2, \dots, \mathbf{s}_S\}$  be the set of all possible charging station states, where  $S$  is the total number of charging station states. Then, we can define  $\mathbf{Q} = \{\mathbf{q}_1, \mathbf{q}_2, \dots, \mathbf{q}_Q\}$  as the set of all possible system states, where  $Q = S^I$  is the total number of system states. In charging station  $a_i$ ,

the number of arrival EVs in each time slot can be modeled as a Poisson process according to [57–60]. Also, since the duration of each time slot ( $\Delta t$ ) is short, we can consider that there is at most one arrival or departure EV per time slot in the whole system.

Theoretically, this assumption can be made if the cumulative Poisson probability is close to 1 when the arrival EV number is less than or equal to 1. According to the Poisson cumulative distribution function, the shorter the time slot duration  $\Delta t$  is, the higher the accuracy we can achieve. However, for practical applications, some limitations such as the computation capacity, reference data sampling frequency, and communication bandwidth need to be considered. As a result, it is not feasible to select a very small value of  $\Delta t$ . Generally, for an MDP problem with a finite horizon  $T$ , the time complexity for obtaining the optimal solution grows exponentially with the value of  $T$  [103]. Therefore, we usually prefer to select a relatively large value of  $\Delta t$  in the premise of satisfying the requirement of accuracy. Let  $\lambda^{a_i}$  be the probability for a EV to arrive at charging station  $i$ , which may depend on various factors such as traffic volume and EV penetration rate. Such information can be obtained by the information and communications infrastructures of intelligent transportation systems (ITSs), which are expected to be part of the future smart grid during the process of transportation electrification [60, 102]. The CSPs are expected to distribute the related information to EV owners.

### 2.1.2 EV Charging Model

Each EV owner needs to make a decision on charging reservation once arriving at the charging station. The reservation is denoted by  $R_{P,D}$ , where  $P \in \mathbf{P}$  is the charging power, and  $D$  is the charging duration, given by

$$D = E_C/P, \quad (2.2)$$

where  $E_C$  is the charging demand of an individual EV including energy conversion losses. Generally,  $E_C$  can be modeled as a random variable with a probability density function (PDF) of  $f_{E_C}(\cdot)$ . In literature, log-normal distribution and exponential distribution are widely used to characterize  $E_C$  based on extensive analysis of real traffic data [59]. Also, we can derive the total charging cost of a EV with reservation  $R_{P,D}$  at a charging station  $i$  as

$$c_T = \sum_{t=t_0}^{t_0+D} P\Delta t p_{a_i,t} = P\Delta t \sum_{t=t_0}^{t_0+D} p_{a_i,t}, \quad (2.3)$$

where  $t_0$  is the arrival time, and  $p_{a_i,t}$  is the RTP of bus  $a_i$  at time  $t$ . In our model, each EV owner aims at satisfying his/her charging demand with the minimum cost  $c_T$ . In this work, we just involve a simple RTP model, where the total charging cost of the charging station is a linear function of the total load. In practical pricing scheme, there might be other cost, including the service charge for capacity, which depends on the peak charging

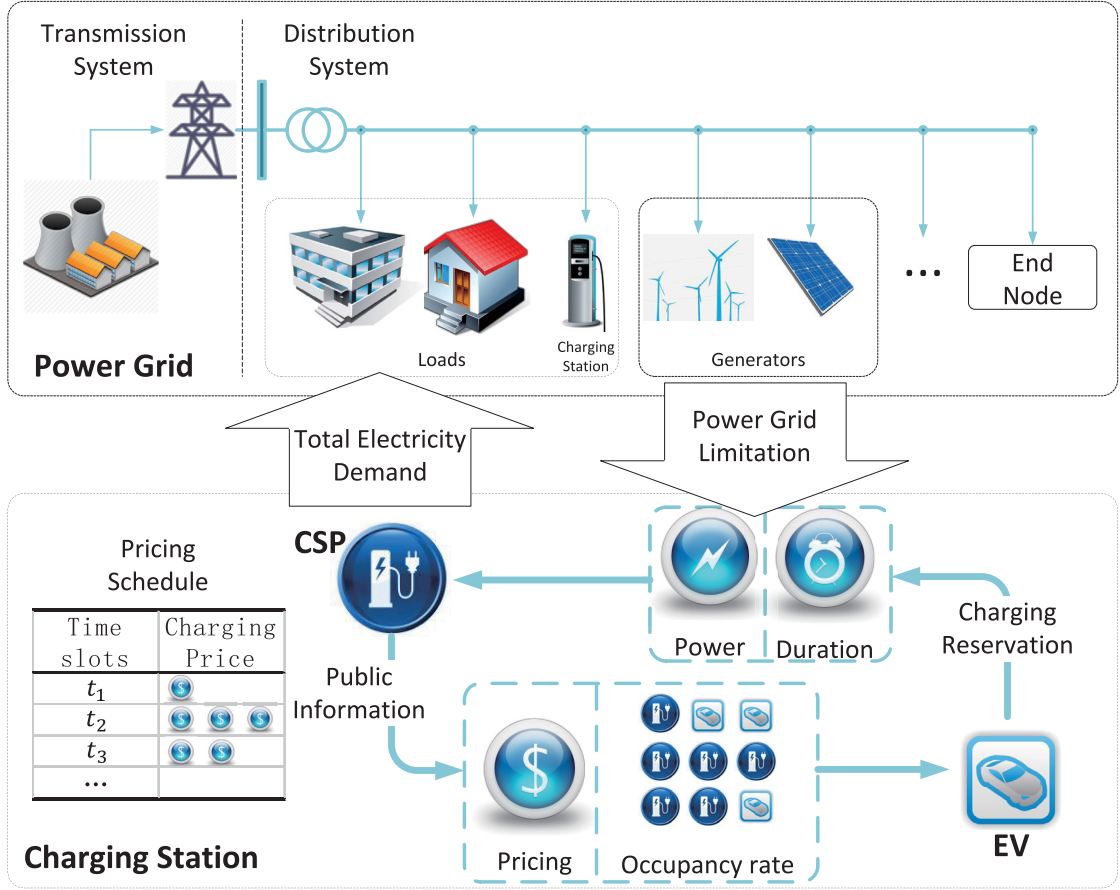


Figure 2.1: An illustration of charging station operation in distribution system.

Table 2.1: STATE TRANSITION PROBABILITIES.

Current state $\mathbf{q}$	Next state $\mathbf{q}'$	Transition probability $Pr(\mathbf{q}' \mathbf{q}, \pi_t, t)$
$(s^{a_1}, \dots, s^{a_i}, \dots, s^{a_I}), a_i$ is not full	$(s^{a_1}, \dots, s^{a_i} + e_g, \dots, s^{a_I})$	$\lambda_{g,t}^{a_i} = \lambda_t^{a_i} \Psi_{g,t}^{a_i}$
$(s^{a_1}, \dots, s^{a_i}, \dots, s^{a_I}), a_i$ is not empty	$(s^{a_1}, \dots, s^{a_i} - e_g, \dots, s^{a_I})$	$\mu_{g,t}^{a_i} = n_g^{a_i} \cdot \Delta t / \int_{E_{g,t}^{a_i}}^x f_{E_C}(x) dx$
$(s^{a_1}, \dots, s^{a_i}, \dots, s^{a_I})$	$(s^{a_1}, \dots, s^{a_i}, \dots, s^{a_I})$	$\delta_t = 1 - \sum_{i=1}^I \sum_{g=1}^G (\lambda_{g,t}^{a_i} + \mu_{g,t}^{a_i})$
$(s^1, \dots, s^{a_i}, \dots, s^{a_I})$	else	0

load in the whole billing period. In this thesis, such a pricing scheme will be discussed in Chapter 4. Since the service charging for capacity is a piecewise linear function of peak load, we can extend the pricing scheme in this chapter through analyzing each pricing segment separately.

## 2.2 Stochastic Game Formulation

The operation of charging stations in smart grid consists of two steps. The first step is to analyze the charging demands of EVs in response to RTP, while the second step is to

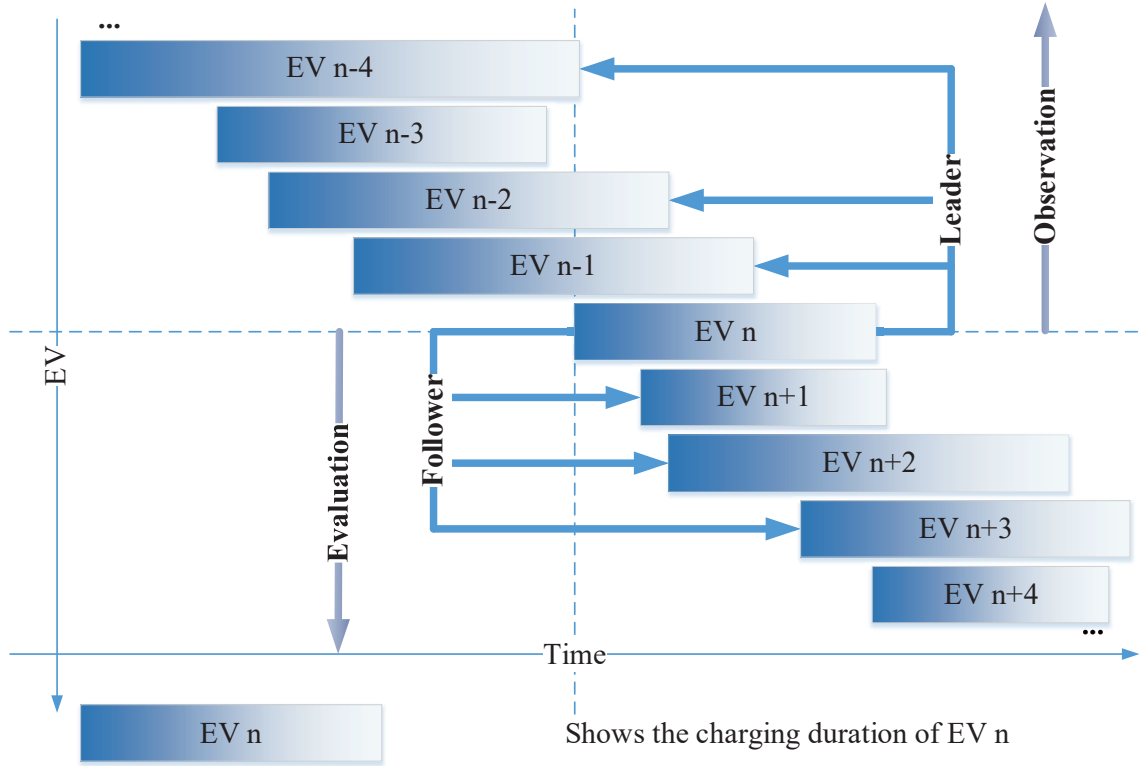


Figure 2.2: A diagram of EV charging leader-follower relationship.

determine the optimal RTP scheme accordingly. In the first step, the total charging cost of each EV can be affected by the decisions of other EV owners, which may lead to different charging station states and in turn, affect the RTP scheme. In this section, we model this phenomenon by using a repeated inverse Stackelberg game to characterize the interactions among EV owners. An MDP is embedded in the game model to describe the decision making processes of EV owners given the randomness of EV arrivals, departures, and charging demands. Based on the solution of this game model, the optimal RTP scheme can be determined, which will be discussed in details in Section IV.

### 2.2.1 Repeated Inverse Stackelberg Game

The repeated inverse Stackelberg game model is a variation of the classical Stackelberg game model. Generally, a classical Stackelberg game model is expressed as a leader-follower game. To take the optimal action, the leader needs to fully understand not only his/her own feasible actions and the related revenues but also the followers'. In this way, the leader can plan his/her strategy properly to propel the followers to take the actions in favor of the leader. In a normal version, the leader announces his/her action and acts first, while the followers make their decisions after observing the leader's action. However, the information structure in our model significantly differs.

In our model, the most recently arrived EV acts as the leader of all previously arrived

(and not yet departed) EVs, as shown in Fig. 2.2. In this way, the dynamics of the arrivals and departures of EVs can be characterized as the role changes of players in the game. Since the leader always arrives later than the followers, the information structure is in an inverse version [104], where the action of the leader can be estimated as a function of the followers' actions, and the leader acts after the followers. For example, if the owner of EV  $n$  wants to minimize the total charging cost, his/her only concern is the reservations of subsequent EVs ( $n + 1, n + 2, n + 3, \dots$ ) since the reservations of previous EVs are already made. The subsequent EVs are the leaders of EV  $n$ . On the other hand, EV  $n$  is also the leader of the previous EVs who concern about EV  $n$ 's action while making decisions. In other words, the role of a EV switches from leader to follower when a subsequent EV arrives. With new EVs arriving continuously, such leader-follower switching process repeats constantly. However, such repeated game process is not infinite. Since most typical charging station will be closed at night, there is always a final time slot, after when there is no more EVs arriving in the station. In other words, the EV owners arrives in the final time slot do not have leaders anymore. So when optimizing these owners' strategies, only the charging reservations of the owners arriving before need to be considered. This characteristic is very useful for our further analysis when calculating the optimal strategies.

We define this game in its strategic form,  $\Gamma = \{\mathcal{N}, \{R_{P,D}\}_{P \in \mathbf{P}}, U(\cdot), \boldsymbol{\lambda}, \mathcal{B}, f_{EC}(\cdot)\}$ , with the following components:

1.  $\mathcal{N}$  is a set of all EV owners in the charging station, who are the players in our model;
2.  $\{R_{P,D}\}_{P \in \mathbf{P}}$  is a set of all the alternative actions for all the players, where  $R_{P,D}$  is the charging reservation of a EV owner. Each reservation consists of charging power  $P$  and duration  $D$ . Such a bivector can describe all the actions for players, where the power and duration should satisfy (2.2);
3.  $U(\cdot)$  is utility function of EV charging in each time slot;
4.  $\boldsymbol{\lambda} = \{\boldsymbol{\lambda}_t | t = 1, 2, \dots, T\}$  is the arrival probability of EVs, where  $\boldsymbol{\lambda}_t = \{\boldsymbol{\lambda}_t^{a_1}, \dots, \boldsymbol{\lambda}_t^{a_i}, \dots, \boldsymbol{\lambda}_t^{a_T}\}$ . For charging station  $i$ ,  $\boldsymbol{\lambda}_t^{a_i} = (\lambda_{1,t}^{a_i}, \lambda_{2,t}^{a_i}, \dots, \lambda_{G,t}^{a_i})$  is the arrival probability of EVs charging at different power levels after the charging decision making;
5.  $\mathcal{B}$  represents the base load of the distribution system;
6.  $f_{EC}(\cdot)$  is the PDF of individual EV charging demand.

## 2.2.2 MDP for Charging Decision Making

For each EV owner, the total charging cost can be calculated by (2.3). However, when making a reservation, the owner does not know the RTPs in the following time slots. Therefore, it is necessary to find a way to evaluate the RTP sequence while considering the randomness of EV arrivals, departures, and charging demands. In this chapter, the decision make

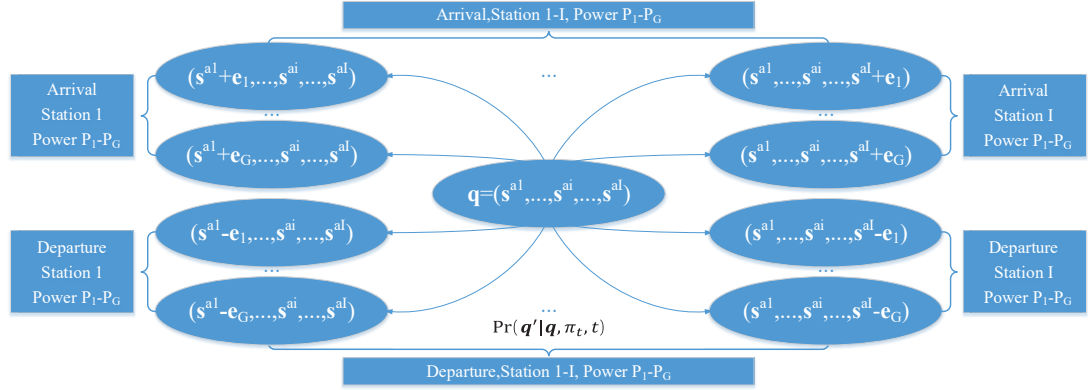


Figure 2.3: An illustration of system state transitions.

process of each EV owners is modeled by an MDP. Given the system state  $\mathbf{q}$  in time slot  $t$ , the utility function of a EV can be calculated as the current revenue adding the estimated future revenue, given by

$$U(\mathbf{q}, t, a_i, R_{P,D}) = -c(\mathbf{q}, t, a_i, P) + \sum_{\mathbf{q}' \in \mathbf{Q}} [Pr(\mathbf{q}'|\mathbf{q}, \pi_t, t) \times U(\mathbf{q}', t + 1, a_i, R_{P,D-1})]. \quad (2.4)$$

Here  $\mathbf{q}$  is the initial system state,  $\mathbf{q}'$  is one of the possible following system states, and  $c(\mathbf{q}, t, a_i, P)$  is the per-slot charging cost, given by

$$c(\mathbf{q}, t, a_i, P) = P\Delta t p_{a_i,t}, \quad (2.5)$$

where  $p_{a_i,t}$  is the RTP for bus  $a_i$ . In (2.4),  $Pr(\mathbf{q}'|\mathbf{q}, \pi_t, t)$  is the transition probability from state  $\mathbf{q}$  to state  $\mathbf{q}'$ , and  $\pi_t$  is the charging strategy in time slot  $t$ , given by

$$R_{P^*,D^*} = \pi_t(\mathbf{q}, t, a_i, E_C) = \arg \max_{P,D} U(\mathbf{q}, t, a_i, R_{P,D}), \quad (2.6)$$

where  $R_{P^*,D^*}$  is the reservation with minimum cost, and  $P^*, D^*$  satisfy (2.2). Specially, when charging duration  $D = 1$ , (2.4) becomes

$$U(\mathbf{q}, t, a_i, R_{P,1}) = -c(\mathbf{q}, t, a_i, P). \quad (2.7)$$

An illustration of system state transitions is shown in Fig. 2.3, while the state transition probabilities are detailed in Table 2.1. In order to obtain the state transition probability  $Pr(\mathbf{q}'|\mathbf{q}, \pi_t, t)$ , it is necessary to analyze the arrival and departure processes of EVs, where the arrival process depends on the charging power selection and the departure process depends on the charging duration. According to (2.6), if a EV owner arrives at charging station  $i$ , the proper charging power and duration depend on the charging demand  $E_C$ . Given the PDF of  $E_C$ , the probability for the EV owner to select charging power  $P_g$  can be calculated as

$$\Psi_{g,t}^{a_i} = \int_{\mathbf{E}_{g,t}^{a_i}} f_{E_C}(x) dx, \quad (2.8)$$

where  $\mathbf{E}_{g,t}^{a_i} = \{x | \pi_t(\mathbf{q}, t, a_i, x) = R_{P_g, x/P_g}\}$  is the integral interval. In this way, we can find the relationship between the charging strategy and the station state changes. Firstly, we can obtain the arrival probability of EV charging with power  $P_g$  as  $\lambda_{g,t}^{a_i}$ . Secondly, given the station state and the PDF of charging demand, we can obtain the departure probability of EV charging with power  $P_g$  as  $\mu_{g,t}^{a_i}$ . Thirdly, getting rid of the arrival and departure probability, we can define the maintaining probability  $\delta_t$  of the system, Table.2.1. At last, we can derive the station state transition matrix, given by

$$\mathbf{Pr}(t) = [\vec{Pr}(\mathbf{q}_1, t), \vec{Pr}(\mathbf{q}_2, t), \dots, \vec{Pr}(\mathbf{q}_Q, t)]^\top, \quad (2.9)$$

where  $\vec{Pr}(\mathbf{q}_i, t)$  with  $i = 1, 2, \dots, Q$  is a row vector of transition probabilities from state  $\mathbf{q}_i$  to any other system states, given by

$$\vec{Pr}(\mathbf{q}_i, t) = [Pr(\mathbf{q}_1 | \mathbf{q}_i, \pi_t, t), Pr(\mathbf{q}_2 | \mathbf{q}_i, \pi_t, t), \dots, Pr(\mathbf{q}_Q | \mathbf{q}_i, \pi_t, t)]_{1 \times Q}. \quad (2.10)$$

With this station state transition matrix, we can track the state changes of the charging station given any charging strategy of EV owners.

### 2.2.3 Nash Equilibrium Solution

In conventional dynamic game models, the Nash equilibrium solution can be obtained by iterating the Bellman function [105]. However, for charging station operation in smart grid, we have to address the randomness of EV arrivals, departures and charging demands. As a result, the conventional iteration approach cannot be applied directly. In the following, we will derive the Nash equilibrium solution of the proposed game model, as well as an algorithm to find the optimal strategy for EV charging decision making.

Each EV owner arriving in time slot  $t$  can optimize his/her own strategy if the system state transition matrices in the following time slots are given. Since the transition probabilities from time slot  $t + 1$  (i.e.,  $\mathbf{Pr}(t + 1), \mathbf{Pr}(t + 2), \dots$ ) are derived based on the optimal strategy,  $\pi_{t+1}, \pi_{t+2}, \dots, \pi_T$  are exactly the Nash equilibrium solution when all the EVs arriving in time slots  $t + 1, t + 2, \dots$  can obtain their maximum revenue. Notice that in (2.4), the first term is the deterministic current revenue and the second term is the estimated future utility which is stochastic. We rewrite the second term as a product of matrices, given by

$$U' = \vec{Pr}(\mathbf{q}, t) \mathcal{U}(t + 1, a_i, R_{P, D-1}), \quad (2.11)$$

where  $\mathcal{U}(t + 1, a_i, R_{P, D-1})$  is a  $Q \times 1$  column vector of the utilities of reservation  $R_{P, D-1}$  for all the station state  $\mathbf{q}^1, \dots, \mathbf{q}^Q$  in the next time slot, given by

$$\begin{aligned} \mathcal{U}(t + 1, a_i, R_{P, D-1}) = [ & U(\mathbf{q}_1, t + 1, a_i, R_{P, D-1}), U(\mathbf{q}_2, t + 1, a_i, R_{P, D-1}), \dots, \\ & U(\mathbf{q}_Q, t + 1, a_i, R_{P, D-1})]^\top. \end{aligned} \quad (2.12)$$

Further, define a  $Q \times 1$  column vector of per-slot costs as

$$\mathbf{C}(t, a_i, P) = [c(\mathbf{q}_1, t, a_i, P), \dots, c(\mathbf{q}_Q, t, a_i, P)]^\top. \quad (2.13)$$

Then, we can transform (2.4) as follows.

$$\begin{aligned} & U(\mathbf{q}, t, a_i, R_{P,D}) \\ &= -c(\mathbf{q}, t, a_i, P) + U' \\ &= -c(\mathbf{q}, t, a_i, P) + \vec{P}r(\mathbf{q}, t)U(t+1, a_i, R_{P,D-1}) \\ &= -c(\mathbf{q}, t, a_i, P) - \vec{P}r(\mathbf{q}, t) \times [\mathbf{C}(t+1, a_i, P) + \sum_{d=1}^{D-2} (\prod_{i=1}^d \mathbf{Pr}(t+i))\mathbf{C}(t+d+1, a_i, P)], \end{aligned} \quad (2.14)$$

where the last equality holds based on induction. Since  $U(\mathbf{q}, t, a_i, R_{P,D})$  is an element in  $\mathcal{U}(t, a_i, R_{P,D})$ , we can derive the vector form of (2.14) as

$$\mathcal{U}(t, a_i, R_{P,D}) = \sum_{d=1}^D (\prod_{i=1}^{d-1} \mathbf{Pr}(t+i))\mathbf{C}(t+d-1, a_i, P). \quad (2.15)$$

Then, the full utility matrix for a EV owner who arrives in time slot  $t$  with charging demand  $E_C$  is given by

$$\mathbf{U}(t, a_i, E_C) = [\mathcal{U}(t, a_i, R_{P_1, E_C/P_1}), \mathcal{U}(t, a_i, R_{P_2, E_C/P_2}), \dots, \mathcal{U}(t, a_i, R_{P_G, E_C/P_G})]_{S \times G}. \quad (2.16)$$

The maximum term in each row is the maximum utility corresponding to each initial state  $\mathbf{q}_1, \dots, \mathbf{q}_Q$ . The corresponding charging reservation  $R_{P, E_C/P}$  is the optimal strategy. In this way, we can obtain  $\pi_t$  as well as the state transition matrices in the following time slots.

Consider that there is almost no EV staying overnight in typical charging station. So the proposed game model will stop at the final time slot  $t_f$ , after when there is no new EV arrival, which means  $\lambda_t^{a_i} = 0, \forall t > t_f (i = 1, 2, \dots, I)$ . In other words, the EV owners arrive in the final time slot do not have “leaders” and the transition matrices after time slot  $t_f$  only depends on the departure probability. Based on (2.15) and (2.16), the utility matrix in time slot  $t_f - 1$  can be obtained. Then we can obtain the optimal strategy  $\pi_{t_f-1}$  as well as  $\mathbf{Pr}(t_f - 1)$ . Repeating this process, we can optimize all the strategies in the previous time slots one by one which is the Nash equilibrium solution we need. The procedure to find the optimal strategy is summarized in **Algorithm 1**.

### 2.3 Optimal Real Time Pricing Scheme

Based on the Nash equilibrium solution, EV charging demands can be estimated based on the optimal strategy. Then, the DSP can manage the charging demands through pricing

---

**Algorithm 1** Optimal strategy calculation.

---

**Require:**  $t_f, \boldsymbol{\lambda}, f_{E_C}(\cdot), D_{\max}, I$ ;  
**Ensure:**  $\pi_1, \dots, \pi_{t_f}$ ;  
**for**  $D = 0, D \leq D_{\max}, D++$  **do**  
  **for each**  $i \in [1, I]$  **do**  
    Calculate  $\mu_{g,t_f+D}^{a_i}$ ;  
  **end for**  
  Calculate  $\Pr(t_f + D)$ ;  
**end for**  
Calculate  $\pi_{t_f}$ ;  
**for**  $d = 1; d < t_f; d++$  **do**  
  **for each**  $i \in [1, I]$  **do**  
    Calculate  $\lambda_{g,t_f-d}^{a_i}, \mu_{g,t_f-d}^{a_i}$ ;  
  **end for**  
  Calculate  $\Pr(t_f - d)$ ;  
  Calculate  $\pi_{t_f-d}$ ;  
**end for**  
**return**  $\pi_1, \dots, \pi_{t_f}$ .

---

adjustment. In the following, we will show how the charging demand of a EV can be affected by different RTP schemes. Further, since the impacts of charging demands on different buses of a distribution system are different, we develop an optimal RTP scheme based on power flow analysis for the DSP to efficiently and reliably operate the distribution system.

### 2.3.1 Impact of RTP on EV Charging Demand

Consider a EV owner arriving at charging station  $i$  in time slot  $t_0$  with charging demand  $E_C$ . Suppose there are two charging power levels  $P_1 > P_2$  (while an extension to multiple power levels is straightforward). We can rewrite (2.5) in the matrix form, given by

$$\mathbf{C}(t, a_i, P) = P\Delta t \mathbf{p}_{a_i,t}, \quad (2.17)$$

where  $\mathbf{p}_{a_i,t} = [p_{a_i,t}^1, \dots, p_{a_i,t}^Q]^T$  is a column vector of RTP schedule of station  $a_i$  corresponding to system state  $\mathbf{q}_1, \dots, \mathbf{q}_Q$ , which is calculated by the DSP. According to (2.14) and (2.17), we can derive

$$\begin{aligned} & U(\mathbf{q}, t_0, a_i, R_{P,D}) \\ &= -P\Delta t p_{a_i,t_0} - P\Delta t \vec{P}r(\mathbf{q}, t_0) \mathbf{p}_{a_i,t_0+1} - P\Delta t \vec{P}r(\mathbf{q}, t_0) \Pr(t_0 + 1) \mathbf{p}_{a_i,t_0+2} - \dots \end{aligned} \quad (2.18)$$

Notice that  $\vec{P}r(\mathbf{q}, t_0) \Pr(t_0 + 1) \dots$  is the probability distribution of the system state given the initial system state  $\mathbf{q}$ . Therefore, each term on the right side of (2.18) is the expectation of per-slot charging cost. Define  $F_{\mathbf{q}}(t_0 + i) = \vec{P}r(\mathbf{q}, t_0) \Pr(t_0 + 1) \dots \Pr(t_0 + i - 1) \mathbf{p}_{a_i,t_0+i}$

with  $F_{\mathbf{q}}(t_0) = p_{a_i, t_0}$  and  $F_{\mathbf{q}}(t_0 + 1) = \vec{P}r(\mathbf{q}, t_0)\mathbf{p}_{a_i, t_0+1}$ . Then, we have

$$U(\mathbf{q}, t_0, a_i, R_{P,D}) = -P\Delta t \sum_{i=0}^{D-1} F_{\mathbf{q}}(t_0 + i). \quad (2.19)$$

Generally, each EV can find the better charging power by comparing the utility. Since  $P_1 > P_2$ , we have the charging duration  $D_1 < D_2$  given certain  $E_C$  according to (2.2). Then, the utility difference can be calculated as

$$\begin{aligned} & U(\mathbf{q}, t_0, a_i, R_{P_1, D_1}) - U(\mathbf{q}, t_0, a_i, R_{P_2, D_2}) \\ &= -\frac{E_C}{D_1} \Delta t \sum_{i=0}^{D_1-1} F_{\mathbf{q}}(t_0 + i) + \frac{E_C}{D_2} \Delta t \sum_{i=0}^{D_2-1} F_{\mathbf{q}}(t_0 + i) \\ &= -E_C \frac{D_2 - D_1}{D_2} \Delta t \left[ \frac{1}{D_1} \sum_{i=0}^{D_1-1} F_{\mathbf{q}}(t_0 + i) - \frac{1}{D_2 - D_1} \sum_{i=D_1}^{D_2-1} F_{\mathbf{q}}(t_0 + i) \right] \\ &= -E_C \frac{D_2 - D_1}{D_2} \Delta t (\overline{F_{\mathbf{q}}}|_{\mathbf{t}_1} - \overline{F_{\mathbf{q}}}|_{\mathbf{t}_2}). \end{aligned} \quad (2.20)$$

where  $\overline{F_{\mathbf{q}}}|_{\mathbf{t}}$  is the average RTP over period  $\mathbf{t}$ , with  $\mathbf{t}_1 = [t_0, t_0 + D_1 - 1]$  and  $\mathbf{t}_2 = [t_0 + D_1, t_0 + D_2 - 1]$ . If  $\overline{F_{\mathbf{q}}}|_{\mathbf{t}_1}$  is larger, the EV owner will select the lower charging power  $P_2$  to avoid the higher cost. Otherwise, the EV owner will select the higher charging power  $P_1$  to finish charging quickly in order to avoid charging in period  $\mathbf{t}_2$ . In this way, the DSP can achieve load control through a special pricing scheme.

### 2.3.2 Optimal RTP Scheme

Two main factors are considered in the pricing scheme, i.e., the energy cost which is related to the usage of electricity and the operation cost which is related to the transmission and distribution (T&D) of electricity<sup>1</sup>. Due to the integration of EV charging stations, additional costs should be considered with respect to extra energy losses and power quality (especially voltage profile) correction [108].

In terms of the energy cost, according to the existing practice in power markets, the DSP can determine the unit price  $p_{k,t}^L$  of energy through dividing the total cost equally. The cost of energy consumption can be calculated with background load, charging load as well as the loss power, which can be calculated through power flow analysis. Besides, the payoff for voltage regulation is also a part of the total cost. Generally, the cost for voltage regulation consists of device cost and operation cost [52, 109]. In this research, we consider the minimum active power losses optimal power flow method (MAPL-OPF) to calculate the voltage regulation cost [110, 111].

By solving the MAPL-OPF problem, the cost for voltage regulation  $C_t^V$  can be obtained. Due to the impedance of the distribution feeders, the EV charging stations at different

<sup>1</sup>Some other factors such regulatory charges, administration charges and debt retirement charges are relatively small in amount and can be added to the pricing scheme as constants [106, 107].

Table 2.2: RESULTS OF THE FOUR APPROACHES WITH DIFFERENT  $\eta$  AND AVERAGE CHARGING DEMAND.

$\eta$	$E_C$	Peak-to-average ratio (PAR)				Rejection rate (RR)				$\bar{p}$				$\bar{p}/(1-RR)$			
		OCL	SG	NNG	FHO	OCL	SG	NNG	FHO	OCL	SG	NNG	FHO	OCL	SG	NNG	FHO
1	30	2.6682	2.1385	2.1633	1.9332	0.0748	0.0381	0.0413	0.0571	0.0941	0.0770	0.0829	0.0762	0.1017	0.0800	0.0865	0.0808
1	35	2.5897	2.1231	2.1714	1.9276	0.0861	0.0530	0.0499	0.0912	0.1104	0.0928	0.0978	0.0892	0.1208	0.0980	0.1029	0.0982
1	40	2.5502	2.1071	2.1890	1.9067	0.0921	0.0729	0.0684	0.1269	0.1236	0.1057	0.1185	0.1037	0.1361	0.1140	0.1272	0.1188
1	45	2.5009	2.0980	2.2081	1.9058	0.0999	0.0832	0.0882	0.1385	0.1401	0.1218	0.1330	0.1182	0.1556	0.1329	0.1459	0.1372
1	50	2.4234	2.0854	2.2603	1.8950	0.1126	0.0976	0.1405	0.1638	0.1560	0.1334	0.1515	0.1256	0.1758	0.1478	0.1763	0.1502
1	55	2.3857	2.0725	2.2936	1.8844	0.1192	0.1125	0.1726	0.1940	0.1716	0.1523	0.1616	0.1394	0.1948	0.1716	0.1953	0.1730
1	60	2.3261	2.0545	2.3321	1.8625	0.1299	0.1337	0.2086	0.2254	0.1961	0.1704	0.1849	0.1528	0.2254	0.1967	0.2336	0.1973
2	40	2.5360	2.0945	2.1754	1.8919	0.0943	0.0845	0.0810	0.1707	0.1496	0.1312	0.1436	0.1296	0.1652	0.1433	0.1563	0.1563
3	40	2.5227	2.0177	2.1431	1.8251	0.1064	0.1109	0.1461	0.2495	0.1685	0.1505	0.1639	0.1458	0.1886	0.1693	0.1919	0.1943
4	40	2.5111	1.9072	2.1306	1.7370	0.1202	0.1454	0.2093	0.3346	0.1911	0.1752	0.1776	0.1626	0.2172	0.2050	0.2246	0.2444

buses/locations may have different impacts on the voltage profile. Thus, it is inappropriate to allocate uniformly to all EV charging stations. Here, we propose an alternative RTP scheme to allocate the cost. At first, the cost is allocated to each bus with different weight. Then, the customers connected to the same bus share the cost according to their load, given by

$$p_{k,t} = \begin{cases} p_{k,t}^L + \frac{\omega_t^k C_t^V}{B_t^k}, & k \notin \mathbf{K}_C \\ p_{k,t}^L + \frac{\omega_t^k C_t^V}{B_t^k + \sum_{i=1}^I L_t^{a_i} I(a_i=k)}, & k \in \mathbf{K}_C \end{cases}, \quad (2.21)$$

where  $I(x)$  is an indicator function which equals 1 if  $x$  is true and 0 otherwise,  $\omega_t^k$  is the weight of bus  $k$  in time slot  $t$ . Since it is the load on each bus that causes the extra voltage regulation cost, we can calculate the total cost  $C_{k,t}^{V-}$  assuming that there is no load on bus  $k$  and then subtract it from the original cost  $C_t^V$  to obtain the extra cost. Normalizing the extra cost of each bus, the weight is given by

$$\omega_t^k = [C_t^V - C_{k,t}^{V-}] / \sum_{\kappa \in \mathbf{K}} (C_t^V - C_{\kappa,t}^{V-}). \quad (2.22)$$

In this way, we can integrate the voltage regulation cost into the RTP while reflecting the location dependency and estimate the power grid condition through RTP.

## 2.4 Simulation Results

To evaluate the performance of the proposed approach, we use the IEEE 123-bus test feeder which was redeveloped in [112] as a symmetric balanced tested for voltage profile study. In particular, the nodes on the branches of the IEEE 123-bus test feeder are merged to the main feeder to facilitate the study. As shown in Fig. 2.4, there are two EV charging stations on bus 20 and bus 40, respectively. In each charging station, there are 10 charging piles with two charging levels of 10 kW and 20 kW, respectively. On bus 11 and bus 43, there are two DGs for voltage regulation. The time-varying base load is obtained from the Energy Information datasets of OpenEI [113]. The statistics of EV arrivals are obtained from 2009 National Household Travel Survey (NHTS) [114], while the PDF of EV charging demands is estimated according to the driving distances from 2010 National Travel Survey

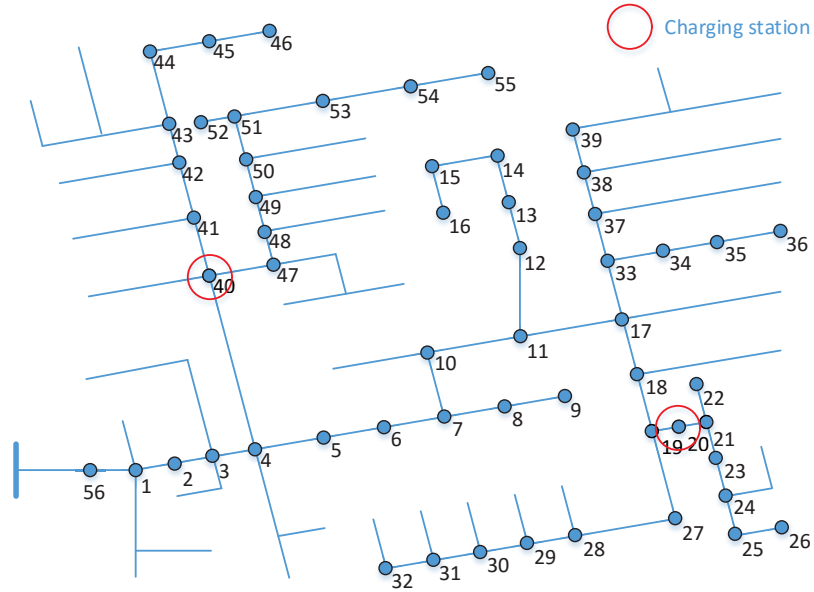


Figure 2.4: Modified IEEE 123-bus test feeder [112].

(NTS) [115]. Considering the size of charging stations as well as the arrival EV number, the slot duration of each time slot  $\Delta t$  is set to 0.5 minute in our simulation. With this value, the arrival EV number per time slot is always less than or equal to one based on the NHTS data. At the same time, the whole simulation process can be finished in finite time.

Four EV charging approaches are tested in our simulations: 1) The original charging load (OCL) is obtained based on uncontrolled EV charging, which can be considered as the benchmark; 2) The stochastic game (SG) approach proposed in this research; 3) The noncooperative N-player game (NNG) approach [51] which is able to address the interactions between DSPs and EV owners in a competitive power market, while the randomness of EV mobility in terms of arrivals, departures and charging demands is not embedded in the game; 4) The finite horizon optimization (FHO) approach [46] estimates the load profile in a finite horizon and optimizes the revenue accordingly. In all cases, we apply Monte Carlo simulations to generate random sequences of EV arrivals and charging demands. The simulation results are obtained from  $10^4$  times of Monte Carlo simulation runs.

In Table 2.2, we show the test results for different average individual charging demand  $\bar{E}_C$  while changing the number of arrival EVs by  $\eta = 1, \dots, 4$  times. Here, we choose 4 indices to show the efficiency of EV charging demand management. According to the peak-to-average ratio (PAR), our approach reduces the peak load obviously and its performance is better than the NNG approach, due to the consideration of the randomness in EV mobility. The EV owners are charging at a relatively low average unit price ( $\bar{p}$  in \$/kWh). Although the PAR and average unit price of the FHO approach seems better, more EVs are rejected from been charged in this case (i.e., higher rejection rate (RR)), because more EVs are charging in such low power that the station is easier to be saturated. Considering that

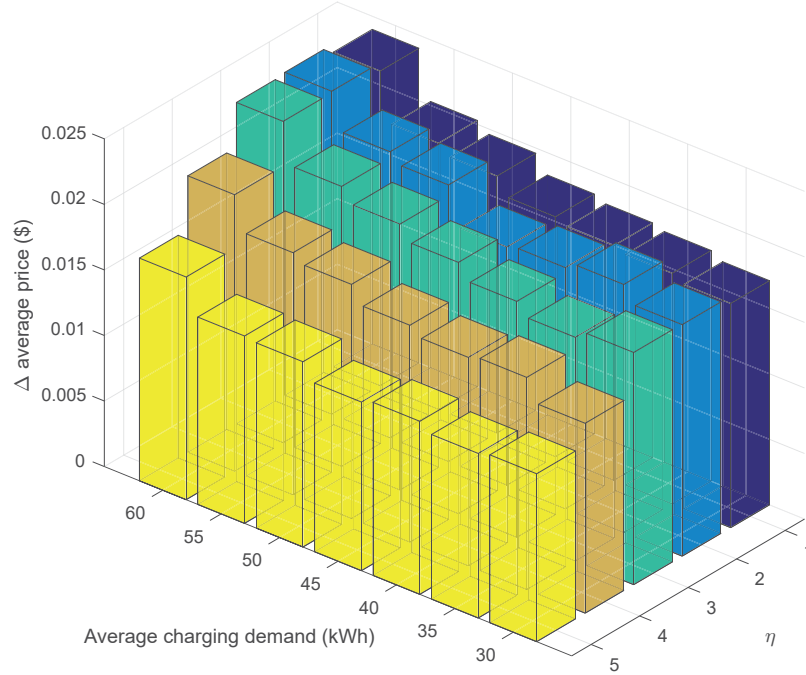


Figure 2.5: The reduction of average unit price versus average charging demand and  $\eta$ .

Table 2.3: AVERAGE UNIT PRICE OF THE FOUR APPROACHES.

Approach	OCL	SG	NNG	FHO
$\bar{p}$	0.1517	0.1365	0.1494	0.1388

these rejected EVs will not disappear but continue to charge somewhere else in the distribution system, the actual charging load is not reduced. In other words, only the charging load of specific buses are reduced due to the decreasing charging EV number but the total charging load of the whole distribution system might not be mitigated.

To avoid the interference of the rejection rate, we consider another estimation index in this research. As we mentioned in Section IV.B, a lower electricity can reflect a better power grid condition. From the DSP's point of view, when satisfying the same amount of charging demands from EVs, the method with a lower electricity price will have a better performance for improving the power grid condition, which can be mathematically reflected by the index  $\bar{p}/(1 - RR)$ . To further clarify this point, we conduct another simulation where there are on average a total of 100 EVs (excluding the rejected ones) charging in the stations in one day, and the average unit price is shown in Table 2.3. As we can see, the average unit price of our approach is lower than the others including the FHO approach. The reason is that the FHO approach only considers the EV group in a finite horizon, while the proposed stochastic game approach considers not only the EV group that can influence the decision maker directly but also the statistics of other EVs which may arrive at the charging stations in the future.

Fig. 2.5 shows the differences between the average unit prices of the proposed stochas-

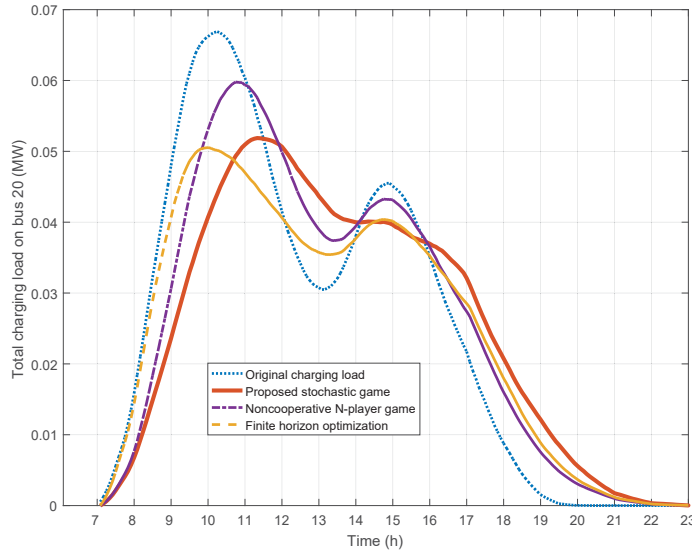


Figure 2.6: Load of charging station on bus 20.

tic game approach and that of the uncontrolled EV charging. As we can see, the average unit price of the proposed approach is lower. More importantly, the price reduction becomes more obvious as the average charging demand increases, since the charging duration of each EV is longer which provides more flexibility for the proposed RTP scheme to manage the charging demands. The price reduction is less obvious with a larger number of arrival EVs since the charging stations are becoming more saturated, such that the RTP scheme becomes less effective.

To take a closer look at the efficiency of charging load management, we use the case  $\eta = 1$  and  $E_C = 40$  as an example. For the station at bus 20, there are two peaks of EV arrivals. The first one starts at around 8:30am, while the second and smaller one starts at around 2:00pm. For the station at bus 40, we have two peaks of EV arrivals at around 11:00am and 3:00pm, respectively. The loads of charging stations on bus 20 and bus 40 are shown in Fig. 2.6 and Fig. 2.7, respectively. Compared with the NNG approach, both the proposed approach and the FHO approach are more effective for PAR reduction. By involving a stochastic game model in the proposed approach, the EV owners can estimate the future charging loads based on the statistics of EV arrivals, departures and charging demands. Then, they can select a higher charging power to finish charging sooner, before the peak load arrives, as shown in Fig. 2.7. In this way, the first peak load on bus 40 is shifted forwards. As a result, compared with the FHO approach where the first peak load of both charging stations arrives at around 10:00am, such peak load overlapping is avoided based on the proposed stochastic game approach.

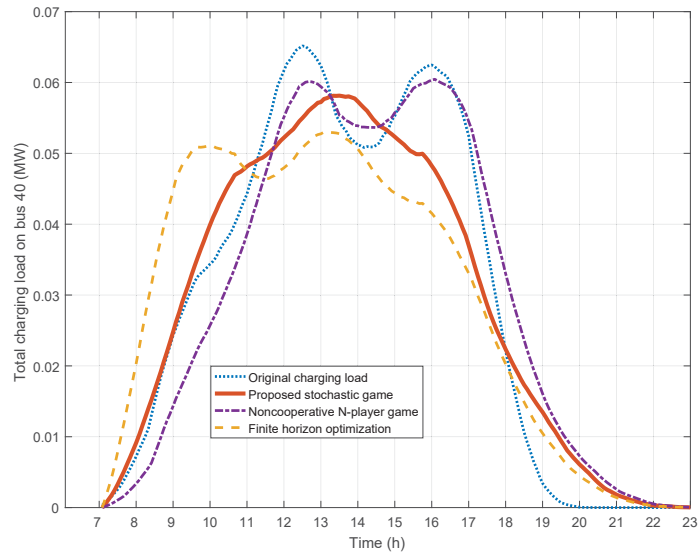


Figure 2.7: Load of charging station on bus 40.

## 2.5 Summary

In this chapter, a stochastic game approach is proposed to characterize the interactions among DSP, charging stations and EV owners in a smart grid. A MDP is embedded in the game to model the decision making processes of EV owners by considering the randomness of EV arrivals, departures, and charging demands. An RTP scheme is developed based on the Nash equilibrium solution of the stochastic game, such that the DSP can minimize power distribution losses while ensuring the reliable operation of distribution system. Simulation results based on IEEE 123- bus test feeder and real vehicle mobility data from 2009 NHTS and 2010 NTS indicate that our proposed scheme can achieve efficient EV charging demand management and reduce the charging costs of EV owners.

# 3

## A Discounted Stochastic Multiplayer Game Approach for V2G Voltage Regulation

In this chapter, we proposed a DSMG approach for V2G VR to analyze the integration of EV AGGs in the VR market with auction mechanism. Based on practical ancillary service providing mechanism, a detailed VR auction model is developed, where the VR performance evaluation process is involved to ensure the truthfulness. In the auction process, the impact of both power distribution network topology and stochastic EV mobility are embedded to analyze the rational response of AGGs. Then, a DSMG is proposed to optimize the auction strategy of AGGS, and the existence proof of the stationary Markov perfect equilibrium is presented. Besides, the corresponding algorithm is also developed. Based on the IEEE 33-bus test feeder and IEEE 123-bus test feeder with real data from the PVWatts Calculator and the Market Analysis and Information System, the performance of the proposed approach is evaluated in the case study.

### 3.1 System Model

Consider a distribution system with residential loads and photovoltaic generators, where under/over-voltage issues may exist due to the load and generation fluctuations. In the VR market, besides the traditional VR sources, EV AGGs are also potential VR sources for DSO to mitigate the voltage issues [35]. Through injecting or absorbing power in the distribution system, EV AGGs can effectively adjust the voltage magnitudes of neighboring buses. Since not all the AGGs are suitable for providing the VR services due to random EV mobility and power distribution network topology impact, DSO will periodically select and involve qualified AGGs in the VR process [35].

During the evaluation and selection process, the primary target of DSO is to select

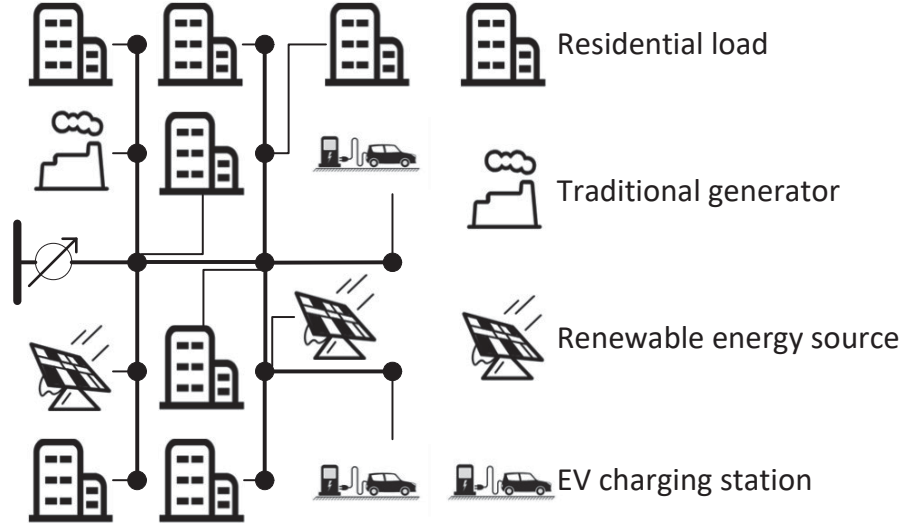


Figure 3.1: An illustration of the distribution system.

the AGGs with the minimum cost while satisfying the total VR capacity requirement. It is worth mentioning that, even if these AGGs' capacities are not realized in the actual operation, the AGGs still get paid as preparation for the emergent case [116].

Fig. 3.1 shows a schematic diagram of a distribution system with EV charging stations serving as the AGGs. In the distribution system under consideration, there are a total of  $I$  buses belonging to the set  $\mathcal{I} = \{1, \dots, i, \dots, I\}$ . On a subset of buses  $\mathcal{T} \subset \mathcal{I}$ , traditional VR sources are installed. The EV AGGs are connected to the buses in the set  $\mathcal{A} = \{1, \dots, A\} \subset \mathcal{I}$ . One day is divided into several periods  $1, \dots, h, \dots, H$  for VR, and we define  $\Delta t$  as the duration of a VR period. In each period, the load on each bus of the distribution system is considered as a constant, given by  $\mathbf{L}_h = \{L_{i,h} | L_{i,h} = (P_{i,h}, Q_{i,h})\}$ , where  $P_{i,h}$  and  $Q_{i,h}$  are the active and reactive power, respectively. At the same time, the voltage of each bus is measured and collected by the DSO, given by  $\mathbf{V}_h = \{V_{i,h} | V_{i,h} = (v_{i,h}, \theta_{i,h})\}$ , where  $v_{i,h}$  and  $\theta_{i,h}$  are the voltage magnitude and phase angle, respectively. Generally, in the voltage regulation market of distribution system, only the voltage magnitude  $v_{i,h}$  is emphasized, and the main target of DSO is to guarantee that all the voltage magnitudes are within the nominal range  $[V_{\min}, V_{\max}]$ . Since the VR process is repeated periodically, we define the VR process in each period as a stage. In the following, we will focus on the VR process in one stage as an example.

In each stage, the VR cost of DSO consists of two parts: the payment for AGGs' VR service and the payment for traditional VR sources, given by

$$C^D = \sum_{i \in \mathcal{A}} C_i^A + \sum_{i \in \mathcal{T}} C_i^T, \quad (3.1)$$

where  $C^D$  is the DSO's total cost for voltage regulation,  $C_i^A$  is the payment to AGG on bus  $i$ , and  $C_i^T$  is the payment to the traditional VR sources.

Accordingly, in each stage, only the AGGs selected by the DSO will be paid for VR service. The stage revenue of one AGG is determined by the price and capacity of its offer. However, due to the randomness of EV number of an AGG, the actual VR capacity may not satisfy the promised value in the offer. In this case, the extra cost will be paid for utilizing other energy resources [35]. Therefore, the actual stage revenue of AGG on bus  $i$  is given by

$$r_i = r_i^D - c_i^T, \quad (3.2)$$

where  $r_i^D$  is the revenue paid by DSO and  $c_i^T$  is the cost paid for the traditional VR sources.

### 3.1.1 Impact of Network Topology on VR

Considering the network topology, the efficiency of AGGs connected to different buses in the distribution system may vary. This distinguishing characteristic should be considered by the DSO in the VR process. Thus, the power flow analysis is involved to indicate the differences of AGGs in the VR process.

The line flow from sending bus  $i$  to its neighboring bus  $k$  is given by

$$S_{ik} = V_i \frac{(V_i - V_k)^*}{z_{ik}} = \frac{v_i^2 - v_i v_k \cos \theta_{ik} - j v_i v_k \sin \theta_{ik}}{r_{ik} - j x_{ik}}, \quad (3.3)$$

where  $z_{ik}$ ,  $r_{ik}$  and  $x_{ik}$  are the impedance, resistance and reactance, respectively, of branches  $i$  and  $k$ . Here,  $\theta_{ik}$  represents the voltage angle difference between buses  $i$  and  $k$ . According to [117], we can approximate  $\theta_{ik} \approx 0$  and  $v_i \approx 1$  p.u. In this way, the power flow equations can be linearized as follows:

$$\begin{bmatrix} \theta' \\ v' \end{bmatrix} = \begin{bmatrix} M'_2 & M'_1 \\ -M'_1 & M'_2 \end{bmatrix}^{-1} * \left( \begin{bmatrix} P' \\ Q' \end{bmatrix} - \begin{bmatrix} M_2^c \\ -M_1^c \end{bmatrix} \theta_1 - \begin{bmatrix} M_1^c \\ M_2^c \end{bmatrix} v_1 \right), \quad (3.4)$$

where  $\theta'$ ,  $v'$ ,  $P'$  and  $Q'$  are the voltage phase angle, voltage magnitude, active power and reactive power vectors, respectively, of all the buses, except the slack bus. Also,  $M_1^c$  and  $M_2^c$  are the first columns of matrices  $M_1$  and  $M_2$  respectively, while  $M'_1$  and  $M'_2$  are the sub-matrices of matrices  $M_1$  and  $M_2$ , respectively, excluding the first column and row. Here, the matrices  $M_1$  and  $M_2$  are constant matrices obtained by the admittance matrix with their elements given by

$$M_1(i, k) = \frac{r_{ik}}{r_{ik}^2 + x_{ik}^2}, \quad i \neq k \quad (3.5)$$

$$M_2(i, k) = \frac{x_{ik}}{r_{ik}^2 + x_{ik}^2}, \quad i \neq k \quad (3.6)$$

$$M_1(i, i) = \sum_{k=1, k \neq i}^I \frac{r_{ik}}{r_{ik}^2 + x_{ik}^2} \quad (3.7)$$

$$M_2(i, i) = \sum_{k=1, k \neq i}^I \frac{x_{ik}}{r_{ik}^2 + x_{ik}^2}. \quad (3.8)$$

According to the aforementioned equations, due to the different impedance, resistance and reactance among different buses, the values in different lines of matrices  $M_1$  and  $M_2$  may vary. Thus, the impact of injecting/absorbing energy to/from different buses to the voltage of a specific bus can be different, which is the reason for evaluating the VR source efficiency based on the network topology.

### 3.1.2 Auction Process and Selection Mechanism

In order to select EV AGGs with better VR performance, auction mechanisms are used. As shown in Fig. 3.2, during the auction process, EV AGGs firstly submit offers with the maximum charging/discharging power available for VR request as well as the corresponding price. According to the VR requirement, AGGs' offers, performance scores, and topology efficiency, DSO selects the qualified VR sources in each VR stage. When an AGG's available EVs are not enough to provide the promised VR capacity in the offer, it needs to pay extra for the traditional VR sources to ensure the quality of service [35]. Such insufficient VR capacity will be detected and recorded by DSO as a performance score, to be referred in the future auction process. Accordingly, to optimize the auction strategy of an AGG, there are mainly three steps: 1) Evaluate VR capacity of the AGG; 2) Estimate the performance score corresponding to a specific VR offer; 3) Analyze the impact of other AGGs' offers. In this section, we present the VR capacity evaluation method. The other two steps will be discussed in Section IV and Section V, respectively.

In this work, we assume an instant communication between the AGGs and the DSO, which means there is not message lost and delay during the communication process. In practical, the voltage regulation interval can vary from one minutes to 15 minutes [118]. So, a few seconds delay is tolerant in this case. Also, each AGG can communicate with a number of EVs and manage their charging/discharging processes. In order to provide the VR service, each AGG needs to estimate the number of its available EVs and the corresponding total VR capacity. Then, an offer with VR capacity and price will be submitted to DSO for selection. Once selected by DSO, AGG has to guarantee the promised VR capacity. Otherwise, the AGG will have to pay extra for the traditional VR sources for making up the insufficient VR capacity. Mathematically, the auction process can be described by the following steps:

1. **Evaluation:** AGG on bus  $i \in \mathcal{A}$  evaluates its number of available EVs and submits an offer  $a_i = \{c_i^U, P_i^U, c_i^D, P_i^D\}$ , where  $c_i^U$  and  $c_i^D$  are the auction price for regulation up and down capacities respectively, with a lower bound  $c_{\min}^A$  corresponding to the basic cost to pay for each EV;
2. **Selection:** Based on the AGGs' auction offers, the DSO selects the AGGs for providing the VR service with minimum cost while satisfying the total VR requirement. The result  $\{\omega_i | i \in \mathcal{A}\}$  is broadcast to all the AGGs, where  $\omega_i = 1$  if AGG on bus  $i$  is

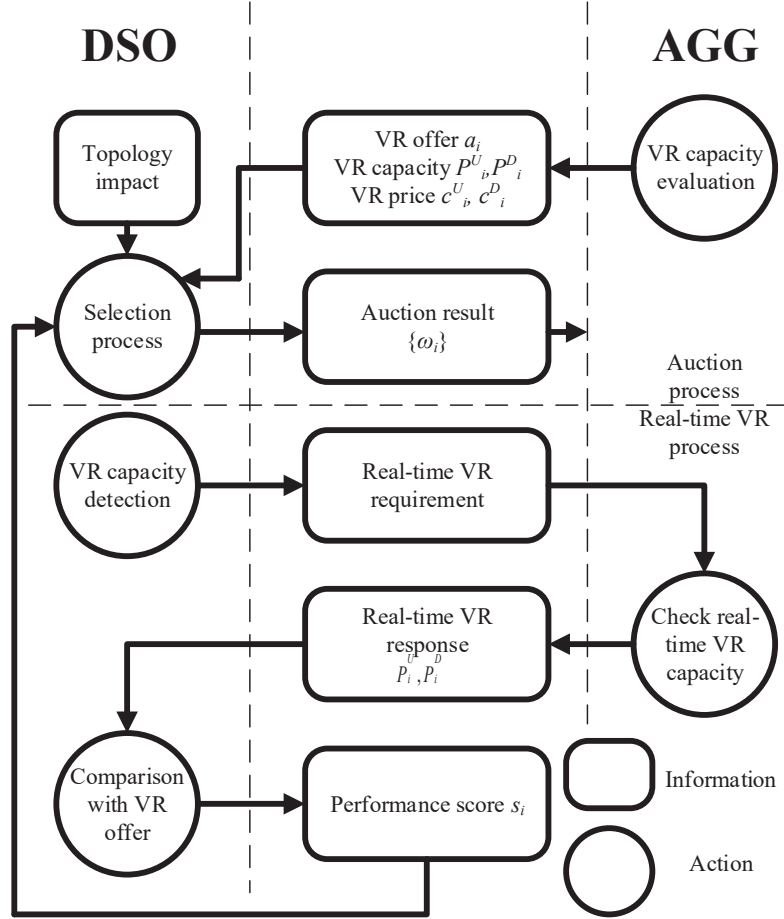


Figure 3.2: An illustration of the VR process of for DSO and AGG.

selected, and vice versa;

3. **Real-time operation:** During the actual VR process, if the real-time VR capacity  $\hat{P}_i^U$  or  $\hat{P}_i^D$  is smaller than the promised value on the auction offer, the EV AGG has to pay for extra VR capacity  $P_i^U - \hat{P}_i^U$  or  $P_i^D - \hat{P}_i^D$  from traditional VR sources on a different bus with price  $c^T$ .

Based on (3.2), we can calculate the revenue of each AGG as follows:

$$r_i = \omega_i (r_i^D - c_i^T) \quad (3.9)$$

$$r_i^D = c_i^D P_i^D \Delta t + c_i^U P_i^U \Delta t \quad (3.10)$$

$$c_i^T = \max(0, c^T (P_i^U - \hat{P}_i^U) \Delta t) + \max(0, c^T (P_i^D - \hat{P}_i^D) \Delta t). \quad (3.11)$$

Based on (3.1), the cost of DSO is given by

$$C^D = \sum_{i \in \mathcal{A}} \omega_i (c_i^D P_i^D + c_i^U P_i^U) \Delta t + \sum_{i \in \mathcal{T}} C_i^T, \quad (3.12)$$

where  $C_i^{T'}$  is the updated cost paid for traditional VR sources. If the total VR capacity provided by AGGs satisfies the total requirement, this term becomes zero.

Notice that the standard in the second auction step of selecting the proper AGGs can be different for different DSOs. The main target is to minimize the cost while guaranteeing the VR capacity requirement. In this chapter, we utilize mechanism of PJM for selecting the AGGs as VR sources [119]. Mathematically, this selection mechanism can be described by the following optimization problem.

$$\min_{\omega_i \in \mathcal{A}, P_i^T \in \mathcal{T}} C^D \quad (3.13)$$

$$\text{s.t. } \Delta v_i^U \leq \sum_{k \in \mathcal{A}} m_{ik} P_k^U, \forall i \in \mathcal{I} \quad (3.14)$$

$$\Delta v_i^D \leq \sum_{k \in \mathcal{A}} m_{ik} P_k^D, \forall i \in \mathcal{I} \quad (3.15)$$

$$\frac{c_i^D P_i^D + c_i^U P_i^U}{P_i^U + P_i^D} \leq \frac{c_k^D P_k^D + c_k^U P_k^U}{P_k^U + P_k^D}, \text{ if } \omega_i = 1 \text{ and } \omega_k = 0, \forall i, k \in \mathcal{A} \quad (3.16)$$

$$\omega_i \in \{0, 1\}, \forall i \in \mathcal{A}, \quad (3.17)$$

where  $C^D$  is the total cost given in (3.12); Constraints (3.14) and (3.15) guarantee the VR capacity requirement, while constraint (3.16) indicates the selected AGG's cost is always lower than the others'. Therefore, if the total AGGs' VR capacity is enough to satisfy the requirement, the payment to the traditional VR sources  $P_i^T$  becomes zero. Otherwise, all the AGGs will be selected in the auction process ( $\omega_i = 1, \forall i \in \mathcal{A}$ ), and  $P_i^T$  will make up for the remaining VR capacity requirement.

### 3.1.3 Controllability-based EV Queue Model

According to the auction process, one vital issue for AGG is to estimate the real-time VR capacity. Since one AGG can dispatch all the available EVs and follow a unitary control signal, it can be modeled as a large dynamic energy storage, which is usually called "battery pool" [120] or "virtual energy storage system" [121]. The capacity of each AGG may vary due to the random number of EVs available for providing VR services.

We can divide the EVs into two categories according to their controllability [122]. The uncontrollable EVs leave the charging station immediately once they finish charging. For the controllable EVs, they are not available for VR services before satisfying their charging demand. After the charging is finished, the controllable EVs will stay idle in the station, whose power is adjustable between the maximum discharging power and the maximum charging power. In such idle period, the EVs will be available for providing VR services. Generally, we can use an M/M/ $\infty$  queue to model this scenario [123]<sup>1</sup>. Define the average

<sup>1</sup>It is worth mentioning that it is straightforward to extend our model based on other types of queues such as G/G/ $\infty$  queues depending on the assumptions of arrival and departure processes [124].

arrival and departure rates as  $\lambda_i$  and  $\mu_i$ , respectively, for all  $i \in \mathcal{A}$ . Then, we can derive the probability distribution of the queue length as follows:

$$P(X_i = n) = (1 - \frac{\lambda_i}{\mu_i})(\frac{\lambda_i}{\mu_i})^n, \quad (3.18)$$

where  $X_i$  is the queue length of AGG on bus  $i$ . Based on [125], the maximum charging power and maximum discharging power of one EV can be regarded as the same value. Since both the actual regulation up/down capacities are linear functions of the number of available EVs, we can define the maximum VR up/down capacity as a single value. Accordingly, the regulation up/down capacities can be merged as total VR capacity in the aforementioned equations. Then the total VR capacity probability distribution of one AGG is given by  $P(P_i^a = n) = P(X_i = \frac{n}{p})$ , where  $P(P_i^a)$  can be abbreviated as a probability mass function  $f_i(\cdot)$ .

## 3.2 Topology-Aware VR Auction Formulation

According to [35], for different buses, the power flow constraints are not the same. Besides, the corresponding line losses of injecting the same amount of power into different buses are different. Additionally, for the same VR capacity, the efficiency in regulating the voltages of different buses are also different. Therefore, it is necessary to consider the network topology while evaluating the VR capacity of the sources connected to different buses [35]. Based on the aforementioned linear power flow model, we can transform the VR capacity connected to different buses to a general one. Then the weight parameter for VR capacity evaluation can be calculated to modified the selection mechanism in the auction model.

### 3.2.1 Topology-aware VR Efficiency

According to Section III-A, we can simplify the relation between the active power injection  $P_k$  and voltage magnitude  $v_i$  with a linear function, given by

$$v_i = m_{ik}P_k + f(P_k^-), \quad (3.19)$$

where  $m_{ik}$  is a constant coefficient which can be obtained with the linearized equations above, which is also known as the participation factor. Here,  $f(P_k^-)$  is a constant value representing the influence of  $P_k^-$  on voltage  $v_i$ , where  $P_k^-$  represents the power injections except  $P_k$ . Thereafter, for regulating the voltage magnitude on bus  $i$ , the VR capacity provided by AGG can be linearly represented with the corresponding voltage ranges, given by

$$\Delta v_i = m_{ik}\Delta P_k, i \in \mathcal{I}, k \in \mathcal{A}. \quad (3.20)$$

Generally, the model of power distribution system can be abstracted based on a one-line diagram with multiple buses [35, 126]. Because of the fluctuations of photovoltaic

generation and residential load, the voltage distribution on the main feeder may vary. However, according to the historical data, DSO can evaluate some foreseeable worst cases, in which the node voltage magnitude reaches the maximum/minimum value due to the peak photovoltaic generation and the peak residential load [121]. Accordingly, the DSO can set the adjustable voltage derivation on each bus as the VR requirement, given by

$$\mathbf{V}^R = \{(v_i^D, v_i^U) | i \in \mathcal{I}\}, \quad (3.21)$$

where  $v_i^D$  and  $v_i^U$  are respectively the maximum regulation down and up ranges, respectively. Then, we can convert the VR capacity requirement to the power injection/absorption capacity constraints for all the AGGs, given by

$$\Delta v_i^U \leq \sum_{k \in \mathcal{A}} m_{ik} P_k^U, \forall i \in \mathcal{I} \quad (3.22)$$

$$\Delta v_i^D \leq \sum_{k \in \mathcal{A}} m_{ik} P_k^D, \forall i \in \mathcal{I}, \quad (3.23)$$

where  $P_k^U$  and  $P_k^D$  are respectively the regulation up/down capacity of AGG  $k$ . In this way, the topology impact on the AGG VR capacity can be quantified.

### 3.2.2 Scoring Mechanism Based on VR Performance

Due to the deviations of the auction VR capacities of AGGs from their actual magnitudes, DSO usually involves performance scoring mechanism to evaluate the performance of AGGs so that their instability can be recorded, which can be referred to as a significant parameter in the future auction process. The criteria of PJM [119] provided us a feasible scoring mechanism to evaluate the actual frequency regulation capacity in transmission system. Based on the VR auction model in [35], we develop a scoring mechanism to evaluate the VR capacity in distribution system. With unit responses measured on a 10-second basis, the performance scores are calculated as an average value in each 5-minute interval. The final hourly average performance score  $S_n$  consists of three parts [127]: The precision sub-score, which measures the average errors between the regulation signal and the unit response; The delay sub-score, which is the maximum value of the statistical correlation between the 5-minute regulation signals and multiple sets of responses, each with a 10-second incremental shifting over the 5 minutes; The correlation sub-score, which can be calculated at the time when the maximum correlation happens. According to [128], in VR cases, the response time of EVs is so short that it can be ignored. As a result, the precision is the most significant factor of performance score in comparison with delay accuracy and correlation accuracy. Therefore, in our study, the performance score can be expressed as

$$s_i \approx s_i^P = 1 - \frac{1}{T} \sum_{t=1}^T |(\max(P_i^U - \hat{P}_i^U, 0) + \max(P_i^D - \hat{P}_i^D, 0))|_t / (P_i^U + P_i^D), \quad (3.24)$$

where  $T = 30$  is the number of time intervals.

Based on the weak law of large numbers, if the period is long enough, the performance score can converge to the expected value, given by

$$s_i \approx s_i^P = 1 - E((\max(P_i^U - \hat{P}_i^U, 0) + \max(P_i^D - \hat{P}_i^D, 0)) | t / (P_i^U + P_i^D)). \quad (3.25)$$

In this way, the performance of AGGs can be quantified with a score in the range  $[0, 1]$ . Thereafter, constraints (3.14) and (3.15) can be modified as follow:

$$\Delta v_i^U \leq \sum_{k \in \mathcal{A}} s_k m_{ik} P_k^U, \forall i \in \mathcal{I} \quad (3.26)$$

$$\Delta v_i^D \leq \sum_{k \in \mathcal{A}} s_k m_{ik} P_k^D, \forall i \in \mathcal{I}. \quad (3.27)$$

Besides, when DSO compares the offer prices of AGGs, the performance scores are also considered [119]. Generally, the price in constraint (3.17) is modified as the performance-score-weighted price, given by

$$\bar{c}_i^U = c_i^U / s_i \quad (3.28)$$

$$\bar{c}_i^D = c_i^D / s_i. \quad (3.29)$$

### 3.2.3 Stochastic VR Capacity Evaluation and Score Estimation

Based on the controllability-based EV queue model above, we can calculate the expected revenue of an AGG given its auction capacity  $P_i^A$  as follows:

$$\bar{r}_i(P_i^A) = r_i^D - \bar{c}_i^T = c_i^A P_i^A \Delta t - \Delta t c^T \int_0^{P_i^A} f_i(P)(P_i^A - P) dP. \quad (3.30)$$

Besides, we can estimate the expected value of the performance score. At first, we need to calculate the expected value and variance of  $\max(P_i^A - P_i^a, 0)$  in (3.24), given by

$$E(P_i^A) = \int_0^{P_i^A} (P_i^A - P) f(P) dP = \int_0^{P_i^A} F(P) dP. \quad (3.31)$$

Here,  $E(\cdot)$  can be considered as a function of  $P_i^A$ , which is defined based on the cumulative distribution function  $F(\cdot)$ . Then we can calculate the variance as follows:

$$\begin{aligned} Var(P_i^A) &= \int_{P_i^A}^{\infty} E^2 f(P) dP + \int_0^{P_i^A} (P_i^A - P - E)^2 f(P) dP \\ &= 1 - 2E^2 + 2 \int_0^{P_i^A} E dP, \end{aligned} \quad (3.32)$$

where  $E$  is given in (3.31). According to the classical central limit theorem, we can regard the second term in (3.24) as a sequence of independent and identically distributed random variables. Since the expected value  $E$  and finite variance  $Var$  exist, the average value converges in probability to a normal distribution, whose expected value is  $1 - E$ , and the variance is  $Var/T$ .

### 3.3 Discounted Stochastic Multiplayer Game

During the repeated auction processes, the total VR requirement of DSO is constant. Each rational AGG competes for a higher market share in order to maximize the revenues. Considering the stochastic issues and competition characteristics in this case, the DSMG model is applied to analyze the optimal auction strategies of AGGs. Generally, this model can be regarded as a repeated game involving stochastic publicly observable states in discrete time slots. In particular, the historical performance scores of all the players (i.e., AGGs) are always broadcast before the auction. Then, they will choose their actions and be paid according to the auction result. In the meantime, their performance scores will be updated according to the actual VR process. Then, the game moves to the next stage, and a new random state is drawn. The distribution of the random state depends on the auction strategies and the results in the previous auction stage. The same process will be repeated in the new stage. In the economic field, such DSMG is widely used to analyze the players' actions in the auction process [36, 37]. When considering the VR market in the power system, DSMG can also be leveraged to analyze the decision process of rational AGGs in the auction process.

#### 3.3.1 Game Formulation

Mathematically, we describe the DSMG in its strategic form, given by

$$\Gamma = \{\mathcal{A}, \{\mathbf{A}_{i \in \mathcal{A}}\}, (\mathbf{S}, \mathcal{S}), r_i(\cdot), U(\cdot), \beta\}, \quad (3.33)$$

where the components are given by

- $\mathcal{A}$  is the set of players;
- For each  $i \in \mathcal{A}$ ,  $\mathbf{A}_i = \{a_i = (c_i^A, P_i^A)\}$  is player  $i$ 's action space, and  $a_i$  is the specific action;
- $(\mathbf{S}, \mathcal{S})$  is a measurable space representing the states  $\mathbf{s} = \{s_i | i \in \mathcal{A}\} \in \mathbf{S}$ ;
- $r_i(\cdot)$  is the stage payoff function;
- $U(\cdot)$  is the utility function;
- $\beta \in [0, 1)$  is the discount factor.

Here,  $\mathcal{S}$  is countable [129], [130], and  $\mathbf{A}_i$  is a nonempty compact metric space endowed with its Borel- $\sigma$ -algebra  $\mathcal{B}(\mathbf{A}_i)$ . Define  $\mathbf{A} = \prod_{i \in \mathcal{A}} \mathbf{A}_i$  as the space of all possible action profiles. Accordingly, we have  $\mathcal{B}(\mathbf{A}) = \otimes_{i \in \mathcal{A}} \mathcal{B}(\mathbf{A}_i)$ , which is the extended Borel  $\sigma$ -algebra of the whole action space, where  $\otimes$  represents the tensor product. For each state  $\mathbf{s}$ , the AGG on bus  $i$  has feasible action space  $A_i(\mathbf{s})$ , which is an  $\mathcal{S}$ -measurable, nonempty, and

compact valued correspondence from  $\mathbf{S}$  to  $\mathbf{A}_i$ . Then, we define the feasible action space as  $A(s) = \prod_{i \in \mathcal{A}} A_i(\mathbf{s})$ .

Based on the aforementioned equations, we can define the stage payoff of AGG on bus  $i$  as  $r_i : \mathbf{S} \times \mathbf{A} \rightarrow \mathbb{R}^*$ . Since the revenue cannot be infinite, the stage payoff  $r_i(\mathbf{s}, \mathbf{a})$  is an  $\mathcal{S}$ -measurement for each  $\mathbf{s} \in \mathbf{S}$ , where  $(\mathbf{s}, \mathbf{a}) \in \mathbf{S} \times \mathbf{A}$ ,  $\mathbf{a} = \{a_1, \dots, a_A\}$ . Mathematically, the stage payoff is given by

$$r_i(\mathbf{s}, \mathbf{a}) = \omega_i \bar{r}_i. \quad (3.34)$$

Besides, we can also define the transition probability  $Q: \mathbf{S} \times \mathbf{A} \times \mathcal{S} \rightarrow [0, 1]$ , which means, given the stage state  $\mathbf{s}$  and a group of AGG actions  $\mathbf{a}$ , the probability of the next stage state  $\mathbf{s}' \in \mathbf{E}$  can be described as  $Q(\mathbf{E}|\mathbf{s}, \mathbf{a})$ , given by

$$Q(\mathbf{E}|\mathbf{s}, \mathbf{a}) = \sum_{\mathbf{s}' \in \mathbf{E}} Pr(\mathbf{s}'|\mathbf{s}, \mathbf{a}) \quad (3.35)$$

$$Pr(\mathbf{s}'|\mathbf{s}, \mathbf{a}) = \prod_{i \in \mathcal{A}} Pr(s'_i|s_i, a_i). \quad (3.36)$$

According to (3.31) and (3.32),  $Pr(s'_i|s_i, a_i)$  can be calculated as follows:

$$Pr(s'_i|s_i, a_i) = \frac{T}{Var\sqrt{2\pi}} e^{-\frac{T^2(s'_i - (1-E))^2}{2Var^2}}. \quad (3.37)$$

Define the strategy profile  $\pi_i$  as the mapping between all the states and corresponding actions. Then, the utility of AGG can be derived as follows:

$$U_i(\mathbf{s}, \pi_i, \pi_{i-}) = \left( \sum_{h=1}^{\infty} \beta^{h-1} r_i(\mathbf{s}, \mathbf{a})_h \right), a_i = \pi_i(\mathbf{s}), \quad (3.38)$$

where  $\pi_{i-}$  is the other AGGs' strategy profile except  $i$ . Such strategy profile  $\pi = (\pi_1, \dots, \pi_A)$  is called a stationary Markov perfect equilibrium if it satisfies the following condition:

$$\forall \pi_{i-}, \mathbf{s} \in \mathbf{S}, U_i(\mathbf{s}, \pi_i, \pi_{i-}) \geq U_i(\mathbf{s}, \pi_{i-}, \pi_{i-}), \quad (3.39)$$

where  $\pi_{i-}$  is any other strategy profile except  $\pi_i$ . Considering the stationary Markov perfect equilibrium in a recursive structure, we have

$$\pi_i = \arg \max_{a_i \in A_i(\mathbf{s})} \int_{\mathbf{A}_{i-}} [(1 - \beta)r_i(\mathbf{s}, \pi_i, \pi_{i-}) + \beta \int_{\mathbf{S}} U(\mathbf{s}', \pi_i, \pi_{i-}) Q(ds'|\mathbf{s}, \pi_i, \pi_{i-})] \pi_{i-}(da_{i-}|\mathbf{s}). \quad (3.40)$$

### 3.3.2 State-based Feasible Action Space

Based on (3.30), we can derive the first order condition for maximizing the expected revenue, given by

$$\frac{\partial \bar{r}_i}{\partial P_i^A} = c_i^A - c^T F(P_i^A) = 0 \quad (3.41)$$

$$\frac{\partial \bar{r}_i}{\partial c_i^A} = P_i^A > 0. \quad (3.42)$$

---

**Algorithm 2** Winning Set and Strategy Generation
 

---

**Require:**  $\mathcal{A}, P(\cdot), c^T, \{m_{ei}\}, \mathbf{s}, V^R, c_{\min}^A$ .

**Ensure:**  $\mathcal{A}_s^+, \mathcal{A}_s^-, \{(c_i^{A*}, p_i^{A*})\}$ .

- 1: Initialize  $\mathcal{A}_s^+ = \emptyset$  and  $\mathcal{A}_s^- = \mathcal{A}$ .
  - 2: Initialize each AGG's auction price  $c_i^A = c_{\min}^A$ .
  - 3: Calculate the equivalent auction price  $\bar{c}_i^A$ .
  - 4: Rank  $\mathcal{A}$  in ascending order  $(i_1, \dots, i_A)$  according to  $\bar{c}_i^A$ .
  - 5: Initialize counter  $k = 1$ .
  - 6: **repeat**
  - 7:  $\mathcal{A}_s^+$  append  $i_k, \mathcal{A}_s^-$  pop  $i_k$ .
  - 8: Calculate  $c_i^{A*} = \frac{m_{ei}s_i\bar{c}_i^A}{m_{ek}s_k}, i \in \{i_j | j = 1, \dots, k\}$ .
  - 9: Calculate  $P_i^{A*}, i \in \{i_j | j = 1, \dots, k\}$ .
  - 10: Calculate total VR capacity  $V^T = \sum_{i \in \mathcal{A}_s^+} P_i^{A*}, k++$ .
  - 11: **until**  $V^T \geq V^R$
  - 12: **return**  $\mathcal{A}_s^+, \mathcal{A}_s^-, \{(c_i^{A*}, p_i^{A*})\}$ .
- 

So, for each AGG winning the auction, the revenue monotonically increases along with the increase of price. Given any specific price, the optimal auction VR capacity always exists, given by  $P_i^{A*} = F^{-1}(c_i^A/c^T)$ . Therefore, the auction space can be reduced to  $\{(c_i^A, P_i^{A*})\}$ .

Since the AGG's revenue is zero if it fails in the auction process, which is much less than the revenue that the AGG can obtain if it wins, we consider that for each state  $\mathbf{s}$ , each AGG is rational enough that the winning strategy is always chosen if it exists. The algorithm for generating the AGG set with winning strategies is shown in **Algorithm 2**.

Based on the winning strategy we generated above, we can find out that the AGGs in set  $\mathcal{A}_s^-$  cannot win the auction unless they submit a price lower than their basic cost and receive a negative revenue. So their optimal auction price is  $c_i^A = c_{\min}^A$ . Besides, in order to obtain a high performance score in the next auction, they need to submit a minimal VR capacity. For the AGGs in set  $\mathcal{A}_s^+$ , they can always win the auction as long as they select a price in the range  $[c_{\min}^A, c_i^{A*}]$ . So the feasible action space can be reduced as follows.

$$A_i(\mathbf{s}) = \begin{cases} \{(c_i^{A*}, P_i^{A*}) | c_i^{A*} = c_{\min}^A, P_i^{A*} = 0\}, i \in \mathcal{A}_s^- \\ \{(c_i^{A*}, P_i^{A*}) | c_i^{A*} \in [c_{\min}^A, c_i^{A*}], \\ P_i^{A*} = F^{-1}(C_i^{A*}/c^T)\}, i \in \mathcal{A}_s^+. \end{cases} \quad (3.43)$$

In this reduced feasible action space, the auction result can be transformed into a state independent variable, which no longer depends on the AGGs' auction strategies. Accordingly, we can prove the existence of the stationary Markov perfect equilibrium in our game model.

### 3.3.3 Existence of Stationary Markov Perfect Equilibrium

In this section, we will investigate the existence of the stationary Markov perfect equilibrium. At first, we need to involve the following two lemmas, which have been proved

in [36].

**Lemma 1** *A discounted stochastic game has a coarser transition kernel if for some sub- $\sigma$ -algebra  $\mathcal{G}$  of  $\mathcal{S}$ ,  $q(\cdot|\mathbf{s}, \mathbf{a})$  is  $\mathcal{G}$ -measurable for all  $\mathbf{s} \in \mathbf{S}$  and  $\mathbf{a} \in \mathbf{A}$ , and  $\mathcal{S}$  has no  $\mathcal{G}$ -atom.*

**Lemma 2** *Every discounted stochastic game with a coarser transition kernel has a stationary Markov perfect equilibrium.*

In the following, we prove that the conditions of these two lemmas are satisfied by our game model. According to (3.35)-(3.37),  $\mathcal{Q}(\cdot|\mathbf{s}, \mathbf{a})$  is absolutely continuous with respect to the probability measure. Based on (3.37), we can define  $q$  as an  $\mathcal{S} \otimes \mathcal{S} \otimes \mathcal{B}(\mathbf{A})$ -measurable function from  $\mathbf{S} \otimes \mathbf{S} \otimes \mathbf{A}$  to  $\mathbb{R}^*$ . Thus, for all the  $\mathbf{s}$  and  $\mathbf{a}$ ,  $q(\cdot|\mathbf{s}, \mathbf{a})$  is the corresponding Radon-Nikodym derivative of  $\mathcal{Q}(\cdot|\mathbf{s}, \mathbf{a})$ .

Then we generate a sub- $\sigma$ -algebra  $\mathcal{G}$  of  $\mathcal{S}$ . Since the performance score is always in the range  $[0, 1]$ ,  $\mathcal{S}$  is a Borel- $\sigma$ -algebra on  $\prod_{i=0}^{i < A} [0, 1]$ . Accordingly, we define  $\mathcal{G} = \otimes_{i=1}^{i < A} \mathcal{B}([0, 1]) \otimes \{\emptyset, [0, 1]\}$ . Based on (3.37), for all  $\mathbf{s}$  and  $i$ ,  $q_i(\cdot|\mathbf{s}, \mathbf{a})$  is a function of  $a_i$  and does not depend on  $a_{i-}$ . So, the  $\sigma$ -algebra generated by  $\{q_i(\cdot|\mathbf{s}, \mathbf{a})\}$  is  $\mathcal{G}$ . It is clear that  $\mathcal{S}$  has no  $\mathcal{G}$ -atom. According to Lemma 1, we can prove that the density function  $q$  satisfies the condition of a decomposed coarser transition kernel.

In the previous subsection, we have reduced the feasible action spaces. Accordingly, we can update the stage payoff function as follows.

$$r_i(\mathbf{s}, \mathbf{a}) = \begin{cases} \bar{r}_i, & i \in \mathcal{A}_s^+ \\ 0, & i \in \mathcal{A}_s^- \end{cases}. \quad (3.44)$$

In this way, the result weight  $\omega_i$  is removed and for each  $\mathbf{s}$ , and the stage payoff function  $r_i(\mathbf{s}, \mathbf{a})$  is continuous in  $\mathbf{a} \in \mathbf{A}$ .

By now, all the continuity conditions in [36] have been satisfied. Therefore, based on Lemma 2, we can prove the existence of the stationary Markov perfect equilibrium. The corresponding algorithm to obtain the equilibrium solution is given in **Algorithm 3**.

### 3.4 Case Study

Our case study consists of two parts. Firstly, we check the impact of power distribution network topology on V2G voltage regulation based on IEEE 33-bus test feeder [131]. Then, we conduct simulation based on the IEEE 123-bus test feeder [112] to assess the performance of the proposed DSMG approach in a complex environment, in comparison with other existing approaches. In our simulation, the following constant values are selected according to [125]. In particular, there are on average five EVs available for providing VR services arriving in each AGGs' region per minute following a Poisson distribution. The charging/discharging power of each EV is  $p = 6$  kW. The minimum cost of AGG for each EV is  $c_{\min}^A = 0.02\text{¢}$ , and the make-up cost is  $c^T = 0.06\text{¢}$ . The initial performance score is

**Algorithm 3** Stationary Markov Perfect Equilibrium Solution**Require:**  $\mathcal{A}, P(\cdot), c^T, \{m_{ei}\}, \mathbf{s}, V^R, c_{\min}^A, T, S, \epsilon$ .**Ensure:**  $\pi$ .

- 1: Calculate  $m_{ie}$  for all  $i \in \mathcal{A}$ .
- 2: Calculate  $\mathcal{A}_s^+, \mathcal{A}_s^-$  for all  $\mathbf{s} \in \mathbf{S}$  based on **Algorithm 2**.
- 3: Calculate the decreased feasible action space  $A_i(\mathbf{s})$  for all  $\mathbf{s} \in \mathbf{S}, i \in \mathcal{A}$ .
- 4: Initialize  $\pi = \pi^0$  according to  $\{A_i(\mathbf{s})\}$ .
- 5: Calculate the stationary utility  $\{U_i(\mathbf{s}, \pi_i, \pi_i^-)\}$ .
- 6: **repeat**
- 7:   Update  $\pi_i$  based on (3.40) for all  $i \in \mathcal{A}$ .
- 8:   Calculate the stationary utility  $\{U_i'(\mathbf{s}, \pi_i, \pi_i^-)\}$ .
- 9:   Calculate  $\Delta U = \max(\{|U_i' - U_i|\})$ .
- 10:   Update  $\{U_i(\mathbf{s}, \pi_i, \pi_i^-)\} = \{U_i'(\mathbf{s}, \pi_i, \pi_i^-)\}$ .
- 11: **until**  $\Delta U \leq \epsilon$
- 12: **return**  $\pi$ .

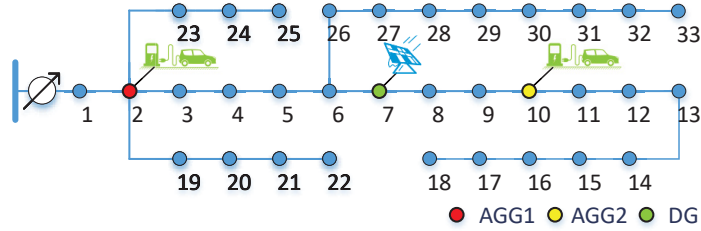


Figure 3.3: An illustration of the IEEE 33-bus test feeder [131].

set to 1. The VR requirement on each bus is  $\{-0.1, 0.1\}$ . In the VR process, the VR performance is measured every 15 seconds, and the auction repeats every 5 minutes. Besides, the continuous performance score is uniformly divided into five levels.

In the first case study, as shown in Fig. 3.3, AGG1 is connected to bus 2 and AGG 2 is connected to bus 2 to 18 in turn. A distributed generator (DG) in terms of photovoltaic (PV) farm rated at 3.4 MW is installed on bus 7. To fairly compare the impact of network topology on different AGGs, the departure rates of the two AGGs are set to the same value  $1/80 \text{ min}^{-1}$ . With the optimal strategy calculated based on our approach, we test its performance by varying the base load of the IEEE 33-bus test feeder according to a one-week residential load profiles and PV generation, which are generated based on the database of PVWatts Calculator [132] and Market Analysis and Information System [133], respectively.

According to Fig. 3.4, we can find out that along with AGG 2 moving away from the substation, the total VR capacity for satisfying the DSO's requirement decreases. It means that the AGGs connected to the buses farther from the substation would have better VR performance and higher efficiency. Besides, as shown in Table 3.1, when both AGGs are

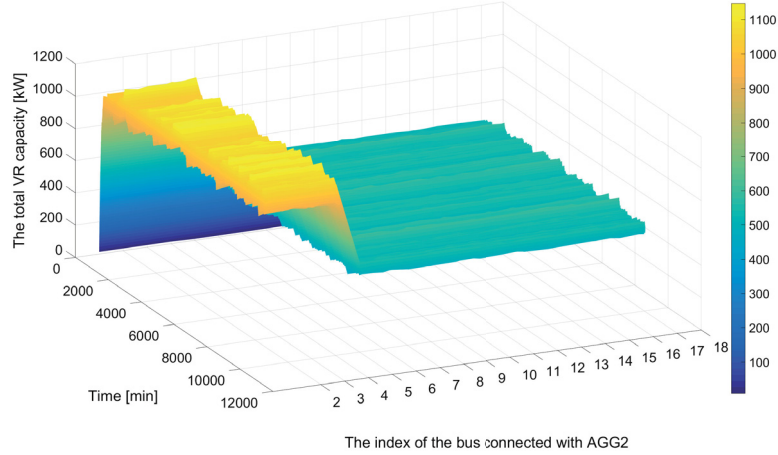


Figure 3.4: The real-time total VR capacity for satisfying the DSO's requirement.

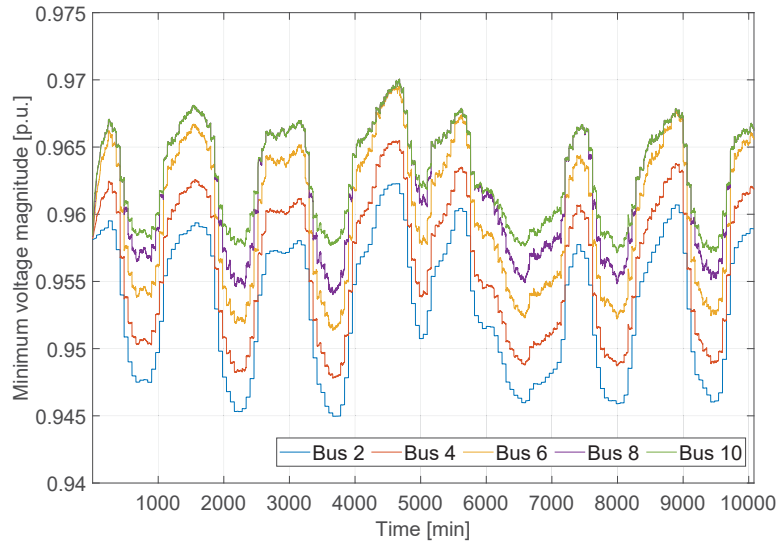


Figure 3.5: The real-time minimum voltage magnitude.

Table 3.1: REVENUE AND SELECTION RATE OF AGG 2

AGG 2 Location	Bus 2	Bus 4	Bus 6	Bus 8	Bus 10
AGG 2 Revenue [ $10^6 \text{€}$ ]	0.383	0.405	0.498	1.260	1.314
AGG 2 Selection Rate	52.6%	59.3%	62.2%	81.5%	84.8%

close to the substation, the selection rates of them are approximately the same, which means neither of them has absolute advantage in the VR auction process. However, when AGG 2 moves to the buses farther from the substation, according to the power flow analysis and the topology awareness of the VR scheme, the equivalent capacity will increase. So AGG 2 has at an advantage with higher selection rate and more revenue. Besides, the

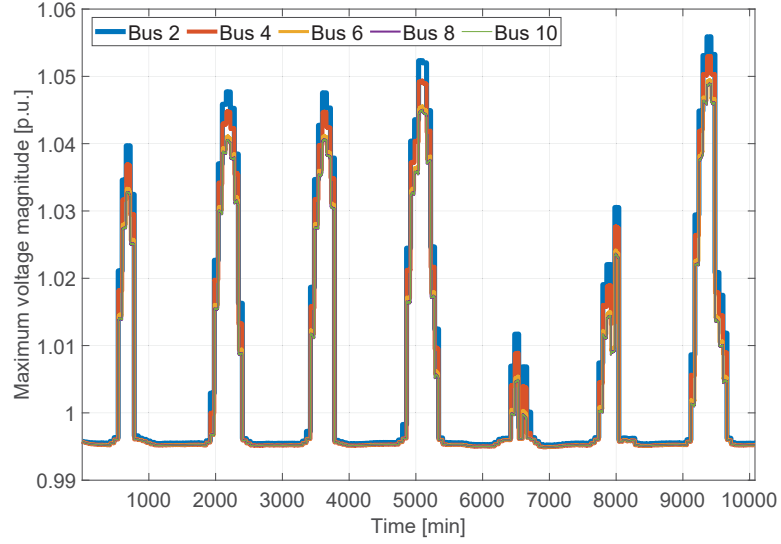


Figure 3.6: The real-time maximum voltage magnitude.

required VR capacity becomes smaller in this process. This phenomenon also shows the importance of considering the network topology in the VR auction process.

In Fig. 3.5, we show the under-voltage case, where no DG is installed. We can find out that, when the AGG is connected to bus 6, 8, or 10, the minimum voltage is always greater than 0.95 p.u., which means that the proposed approach can generally accomplish the VR task. However, when the AGG is connected to bus 2 or 4, the minimum voltage will be lower than 0.95 p.u., which does not satisfy the VR requirement. In other words, an AGG placed closer to the end node has a better performance than the others. Thereafter, we add the DG in the feeder, and the result is shown in Fig. 3.6. When both AGGs are connected to the buses between the substation and the DG, they can hardly overcome the overvoltage issue. On the contrary, when AGG 2 moves to the other side, the maximum voltage can be limited below 1.05 p.u. Through this simulation, we may verify the significance and advantage of our topology-aware analysis in the VR market. In our second case study, there are 2 DGs and 10 AGGs located in the simplified IEEE 123-bus test feeder, as shown in Fig. 3.7. The departure rate of AGG 1-10 are, respectively, given by  $\mu_1 = 1/80 \text{ min}^{-1}$ ,  $\mu_{2,3} = 1/50 \text{ min}^{-1}$ ,  $\mu_{4,5,6} = 1/30 \text{ min}^{-1}$ , and  $\mu_{7,8,9,10} = 1/10 \text{ min}^{-1}$  according to [125]. Three optimization approaches are tested in our simulations: 1) The game approach developed in [69], in which the topology issue is not considered; 2) The topology-aware approach applied in [35], where the uncertainties are not taken into account; 3) The proposed DSMG approach in this chapter. In all the cases, we apply Monte Carlo simulations to generate random available EV numbers for each AGG. To compare the performance of the 3 approaches, we generate a one-week load profiles for the buses, and the data is obtained from [132] and [133]. The actual real-time available VR capacities

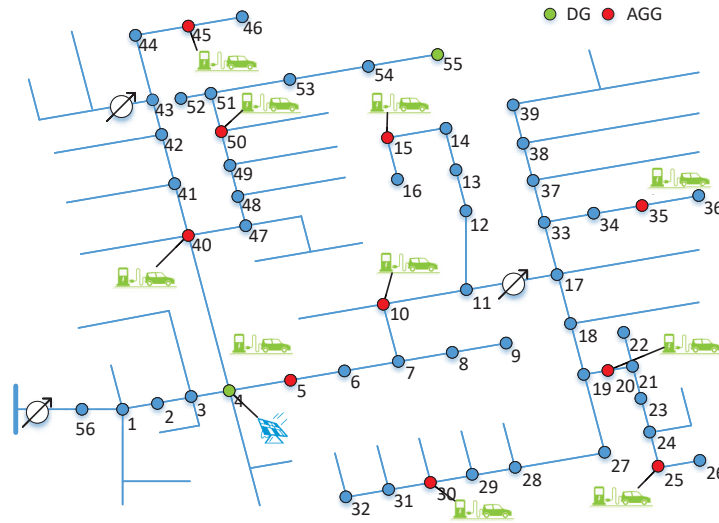


Figure 3.7: An illustration of the modified IEEE 123-bus test feeder [112].

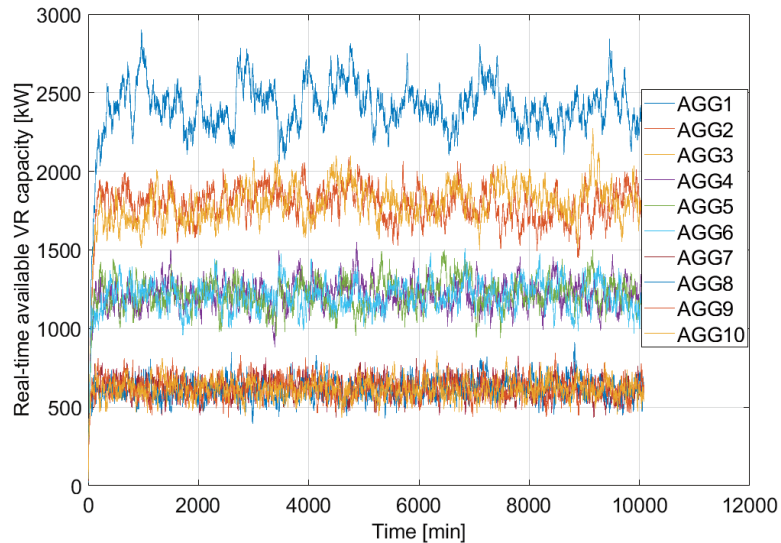


Figure 3.8: The real-time available VR capacities.

for the ten AGGs are shown in Fig. 3.8.

In Fig. 3.9, the convergence process for solving the stationary Markov perfect equilibrium is given. Even the size of the state space ( $5^{10}$ ) is extremely large, our proposed algorithm can still obtain the stationary Markov perfect equilibrium within 40 iterations. The VR performance of the three approaches is shown in Fig. 3.10 and Fig. 3.11. We can find out that in most cases, the voltage magnitudes are above 0.95 p.u. In other words, all the approaches can accomplish the VR target. Compared with the traditional VR ap-

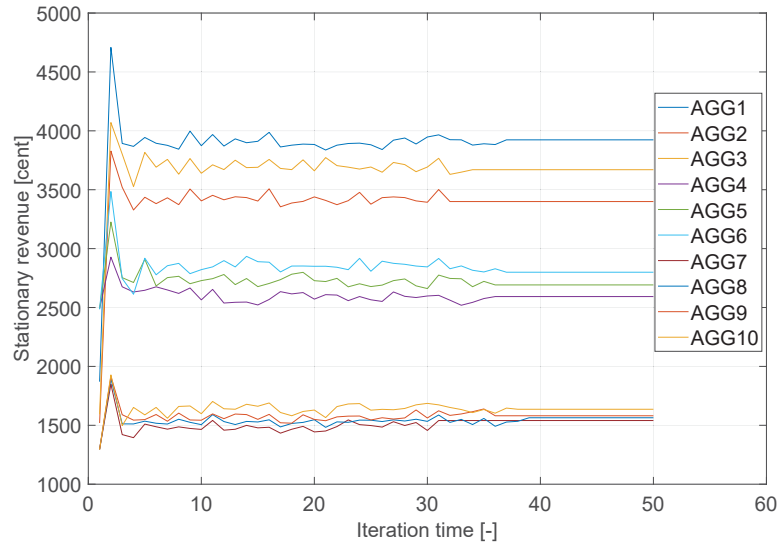


Figure 3.9: The convergence process for solving the stationary Markov perfect equilibrium.

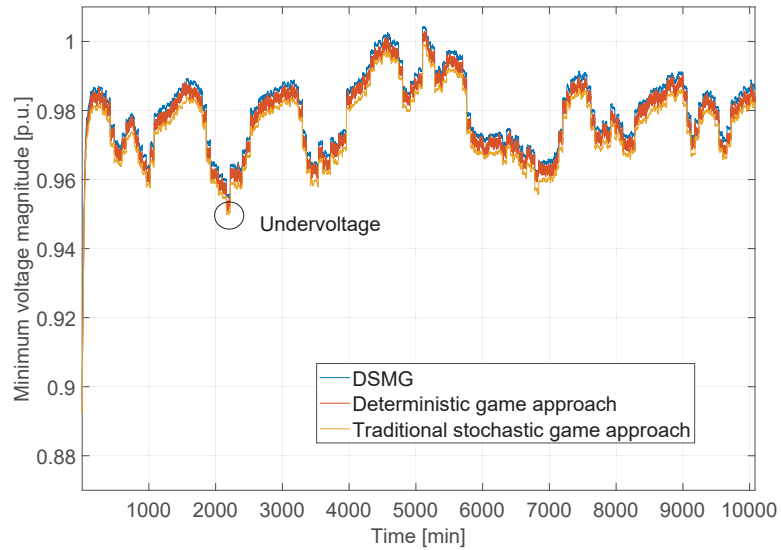


Figure 3.10: The real-time minimum voltage magnitude.

proaches, we can find out that the VR capacity based on the proposed DSMG approach is the lowest, which means the proposed DSMG approach is able to adjust the minimum voltage to the highest level while consuming less VR capacity. This result indicates that the DSMG approach can make full use of the network topology information. By distinguishing the VR efficiency caused by the topology differences, the DSO can evaluate the VR capacity provided by the AGG more accurately. In this way, the unnecessary VR capacity consumption is avoided while the VR requirement is satisfied. As for the deterministic game approach, we can find out that its performance is very close to DSMG. However,

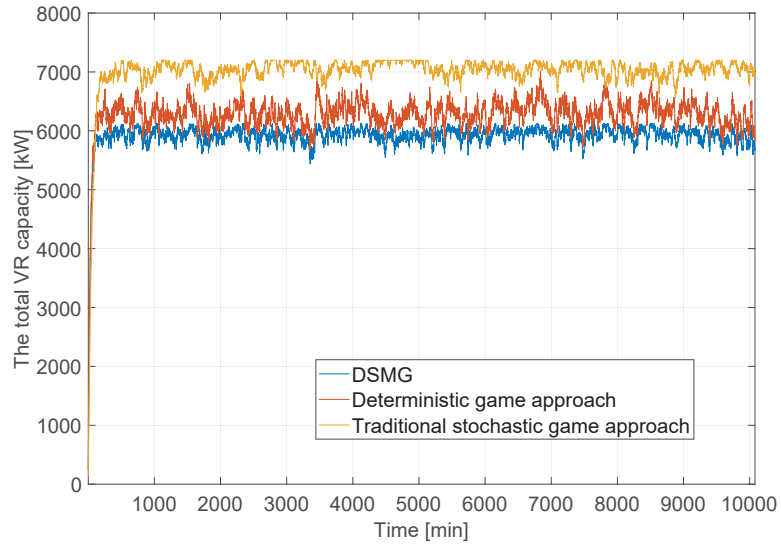


Figure 3.11: The real-time total VR capacity.

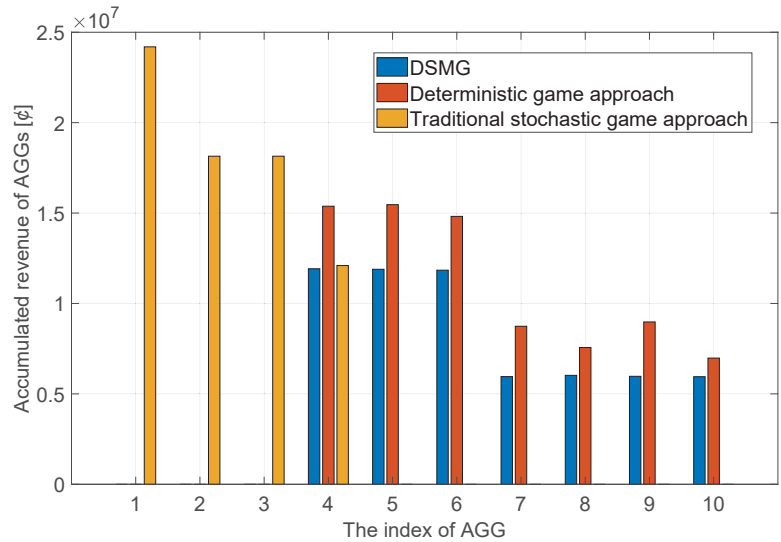


Figure 3.12: The accumulated revenue of AGGs.

since we have carefully considered the stochastic factors such as available EV numbers, the available VR capacity of the DSMG approach is more stable and reliable. In a few cases (between 2210-2250 minutes), the unstable feature of deterministic game approach can lead to under-voltage issues.

From Fig. 3.12, we can find out that the consideration of topology issues increases the selection rate and revenue of the AGGs farther from the substation, which means in these cases, the highly effective VR capacity is encouraged to be adopted in the VR market. Besides, the cost of the DSO for VR is lower than the traditional stochastic game approach.

In other words, the DSMG approach can increase the authenticity of the auction prices of AGGs. Besides, the total VR cost of DSO can be reduced.

### **3.5 Summary**

In this chapter, a new approach based on stochastic game model has been proposed for VR auction considering the network topology impact. It aims to mathematically analyze the VR auction process and generate the optimal strategies for AGGs with stochastic available EV numbers while guaranteeing the VR requirement of the distribution system. The problem is formulated as a DSMG, and the existence proof of stationary Markov perfect equilibrium is provided. Based on the IEEE 33-bus test feeder and IEEE 123-bus test feeder, we demonstrate the advantages of the proposed DSMG from the perspectives of network topology impact, VR capacity, regulated voltage magnitude, and accumulated revenue. In particular, we find out that the proposed approach not only helps DSO to select the most efficient AGGs to be the VR sources but also decreases the total required VR capacity.

# 4

## A Data-Driven Approach for Electric Bus Energy Consumption Estimation

In this work, a data-driven approach for EB energy consumption estimation is proposed. In particular, a detailed physical model of EB is constructed to model its energy consumption considering the randomness in EB operation, including speed, acceleration, and passenger count. In order to improve the estimation accuracy, the conventional KF is modified involving EB mass estimation considering stochastic real-time passenger count, motion data dimension deduction based on EB operation route, and EB acceleration estimation by extending random decision forest algorithm. In the case study, an Android application is developed to collect the motion data of buses so that any general Android smartphone can be used for data collection. The performance of the proposed approach is evaluated based on real-world EB operation data collected from St. Albert Transit, AB, Canada. Compared with the existing approaches, the proposed approach achieves more accurate real-time energy consumption estimation of EBs, which in turn, provides a better characterization of power system loading and voltage variation.

### 4.1 System Model

In this section, a physical model is built for estimating EB energy consumption, in which the road condition, EB operation route and schedule, stochastic EB mass, speed, and acceleration are taken into account.

### 4.1.1 Bus Operation Parameters

Consider a bus running on a ring path consisting of  $I$  road intersections and  $S$  EB stops. Accordingly, the route is divided into  $N = I + S$  road segments  $\mathbf{N} = \{1, \dots, N\}$ . Specifically, the last stop  $x_{N+1}$  is considered to be not only the terminal station but also the departure station. Besides, the altitude values along the route are considered to be available (e.g., through Google Earth Pro), given by  $\{alt_1, \dots, alt_N\}$ . For one cycle trip of the EB, we can collect  $T + 1$  GPS locations  $\{(Lat(t), Lon(t)) | t = 1, \dots, T\}$  in time slots  $\{0, 1, \dots, T\}$ , with sampling interval  $\Delta t$ . Thus, the motion state of EB can be presented with a sequence of GPS locations. At the EB stop  $s \in \mathbf{S}$ , there are  $h_s$  passengers getting on the bus, which can be generally modeled with Poisson distribution  $h_s \sim \pi(\lambda_s)$  [89], among which the frequency of the passengers who will take off at stop  $s'$  is  $\mu_{s,s'}$ . The total passenger count taking off at stop  $s'$  is  $d_{s'}$ . The passenger count between any two adjacent bus stations in road segment  $n$  is given by  $f(g_1, \dots, g_S, d_1, \dots, d_S)$ , where  $f(\cdot)$  will be derived in the next section.

### 4.1.2 Physical Model of EB Energy Consumption

According to [81, 135], we can calculate the accumulated energy consumption as follows:

$$C(t) = \sum_{\tau=0}^t E(\tau) = \sum_{\tau=0}^t Pow(\tau)\Delta t, \quad (4.1)$$

where  $C(t)$  is the real-time accumulated energy consumption;  $E(t)$  is the real-time energy consumption in each period;  $Pow(\cdot)$  is the real-time power, given by

$$Pow(t) = (2\pi Tq(t)v^E(t))/(\beta_1\eta^E\eta^D) + Pow^{aux}, \quad (4.2)$$

where  $Pow^{aux}$  is the auxiliary device power;  $\beta_1$  is the angular speed unit transfer from rps to rpm;  $\eta^E$  is the engine efficiency;  $\eta^D$  is the driver efficiency;  $v^E(t)$  is the real-time engine angular speed, given by

$$v^E(t) = (\beta_2 G^r v(t))/(2\pi r), \quad (4.3)$$

where  $\beta_2$  is the time and power unit transfer;  $G^r$  is the gear ratio;  $r$  is the tire radius;  $v(t)$  is the real-time speed. With these parameters, the real-time torque of the engine can be calculated as  $Tq(t) = r \cdot F(t)/G^r$ , where  $F(t)$  is the real-time total force of EB. According to the force analysis diagram shown in Fig. 4.1, the total force can be decomposed into four parts, given by

$$F(t) = F_f(t) + F_a(t) + F_s(t) + F_r(t), \quad (4.4)$$

where  $F_f(t)$  is the friction force, which is determined by the bus mass  $m^B$  and driving speed  $v(t)$ , given by

$$F_f(t) = C^F(t) \cdot m^B(t) \cdot \eta^G \cdot \cos(\theta), \quad (4.5)$$

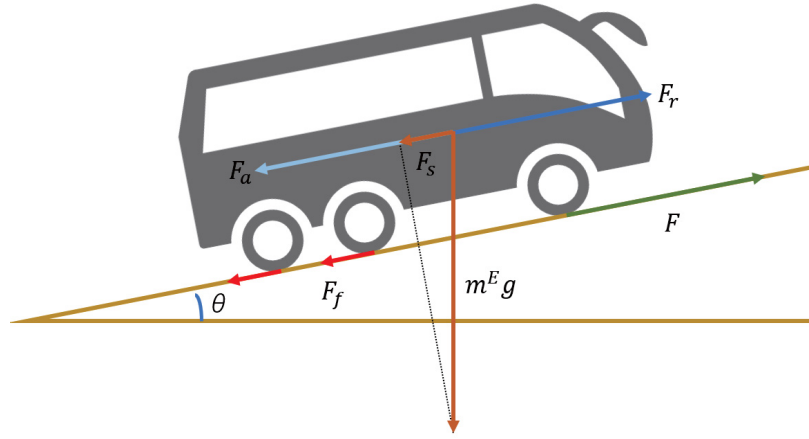


Figure 4.1: Force analysis illustration of EB.

where  $C^F(t) = C^R \cdot (\beta_3 + \beta_4 v(t))$  is the friction coefficient;  $\eta^G = 9.8m/s^2$  is the gravity acceleration;  $C^R$  is the road friction coefficient;  $\beta_3$  and  $\beta_4$  are constant parameters. In (4.4),  $F_a(t)$  is the aerodynamic drag force, which is caused by the air resistance against the movement of the bus. This force depends on the bus shape design properties. Approximately, it can be calculated with the bus frontal area, given by

$$F_a = 0.5 \cdot \varsigma \cdot C^A \cdot A \cdot v(t), \quad (4.6)$$

where  $\varsigma$  is the density of the air;  $C^A$  is the aerodynamic dragging coefficient;  $A$  is the frontal area of the bus. Considering the ups and downs of the road, a part of the decomposed gravity can be applied in the moving direction of the bus, given by

$$F_s(t) = m^B(t) \cdot \eta^G \cdot \sin(\theta), \quad (4.7)$$

where  $\theta$  represents the slope of the road. Consider that the road slope is a constant value for specific position in the route of EB. The slope angle  $\theta$  can be defined as a known function, given by

$$\theta = \theta(\text{Lat}(t), \text{Lon}(t), \text{Lat}(t-1), \text{Lon}(t-1)), \quad (4.8)$$

where  $\theta(\cdot)$  is a mapping from GPS location to road slope, given by

$$\theta(\text{Lat}(t), \text{Lon}(t)) = \arctan((\text{Alt}(\text{Lat}(t), \text{Lon}(t)) - \text{Alt}(\text{Lat}(t), \text{Lon}(t-1)))) \quad (4.9)$$

$$/D(\text{Lat}(t), \text{Lon}(t), \text{Lat}(t-1), \text{Lon}(t-1))), \quad (4.10)$$

where  $Alt(\cdot)$  is the mapping from GPS location to the altitude;  $D(\cdot)$  is the transfer function from two GPS locations to their distance, given by

$$\Delta Lat = Lat(t) - Lat(t - 1) \quad (4.11)$$

$$\Delta Lon = Lon(t) - Lon(t - 1) \quad (4.12)$$

$$k_1 = \sin^2(\Delta Lat/2) + \cos(Lat(t - 1)) \cos(Lat(t)) \sin^2(\Delta Lon/2) \quad (4.13)$$

$$k_2 = 2 \arctan^2(\sqrt{(k_1)(1 - k_1)}) \quad (4.14)$$

$$D(\cdot) = Rk_2, \quad (4.15)$$

where  $R = 6371000$  is the earth's radius;  $k_1$  and  $k_2$  are the intermediate variables.

The last force in (4.4) is the resultant force, which is necessary for driving the bus, given by

$$F_r(t) = m^B(t) \cdot a(t) = m^B(t) \frac{dv(t)}{dt}, \quad (4.16)$$

where  $a(t)$  is the real-time acceleration of EB, which can be computed through the differentiated speed. By now, the mathematical model of EB's energy consumption has been built. Through this model, given the real-time speed, real-time bus mass, and the other corresponding parameters, the real-time energy consumption  $E(t)$  can be calculated.

## 4.2 Data-Driven EB Energy Consumption Estimation Based on Modified Kalman Filter

In this subsection, we propose a data-driven EB energy consumption estimation approach, as shown in Fig. 4.2. Generally, the EB energy consumption can be estimated with the EB mass and motion data. Since the EB mass can be influenced by the stochastic passenger count, a dynamic passenger count estimation approach is proposed improve the estimation accuracy. In order to reduce the noise of EB motion data, KF is widely used. In this work, we develop an EB motion state dimension deduction approach based on know EB operation route to reduce the computational complexity of conventional KF. Besides, an EB acceleration estimation approach is proposed based on random decision forest algorithm so that the EB acceleration can be regarded as control input in KF rather than noise, which can further improve the accuracy of conventional KF. In the following subsections, these three approaches will be introduced, respectively.

### 4.2.1 Real-time Dynamic Passenger Count Estimation

For a typical EB, the maximum loading capacity can be up to 30 passengers, which means the total mass fluctuation of the bus can be up to 2 tons considering that the weight of an adult is around 65kg. In other words, the passenger count has an significant impact on the EB energy consumption. Generally, in order to estimate the passenger count, a constant

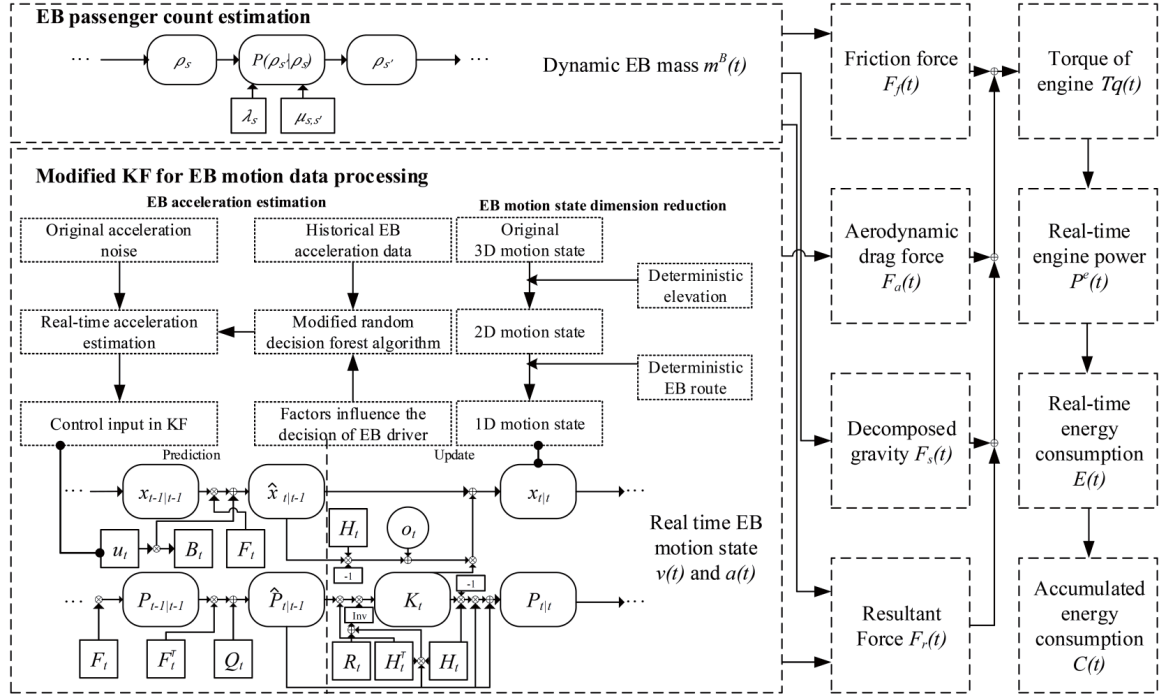


Figure 4.2: An illustration of the data-driven approach for EB energy consumption estimation.

expectation value can be utilized based on the historical data. To improve the accuracy, a real-time dynamic passenger count estimation approach is developed. In the way, given the current passenger count on the EB, we can estimate the passenger count in the near future. From the dataset provided by the public transit service, we can obtain  $\lambda_s$ , and based on the travel survey report like [136,137], the parameter  $\mu_{s,s'}$  can be estimated based on the neighbor area types of the EB stops  $f$  and  $t$ . With the statistic frequency  $\mu_{s,s'}$ , we can have  $\mu_{s,s'} = P(s'|s)$ , where  $P(s'|s)$  represents the probability that one passenger gets off the EB at stop  $s'$  given that he/she got on the bus at stop  $s$ . Define the  $g_{s,s'}$  as the number of passengers travel from stop  $s$  to  $s'$  as follows:

$$P(g_{s,s'} = W) = \sum_{Z \leq W} P(g_{s,s'} = W | h_s = Z) P(h_s = Z), \quad (4.17)$$

where  $P(h_s = Z)$  can be calculated based on the Poisson distribution  $\pi(\lambda_s)$ . The conditional probability can be computed through binomial distribution, given by

$$P(g_{s,s'} = W | h_s = Z) = \left[ \begin{matrix} W \\ Z \end{matrix} \right] (1 - P(s'|s))^{Z-W} P(s'|s)^W. \quad (4.18)$$

Then, we can derive the number of passengers taking off at stop  $s'$ , given by

$$P(d_{s'} = W) = \sum_{\sum_{s=1}^S Z_s = W} \pi_{s=1}^N P(g_{s,s'} = Z_s). \quad (4.19)$$

Based on  $d_{s'}$ , we have

$$P(\rho_{s+1} = W' | \rho_s = W) = \sum_{h_s - d_s = W' - W} P(h_s)P(d_s). \quad (4.20)$$

Given any passenger count in trip from stop  $s$  to  $s + 1$ , we can estimate the passenger count in the next trip, given by

$$\rho_{s+1} = \sum_{W=0,1,\dots} WP(\rho_{s+1} = W | \rho_s). \quad (4.21)$$

Accordingly, we can calculate the total bus mass as following

$$m_t^B = m^b + (\rho_s + 1)m^a, \quad (4.22)$$

where  $m^b$  is the pure bus weight, and  $m^a$  is the average adult weight.

#### 4.2.2 EB Motion State Dimension Deduction

In order to reduce the noise of EB motion data, KF is widely used. Involving the orientation data and acceleration data measured by the corresponding sensors, the KF can use a 10-dimension state variable to track the motion state. It should be noted that most of the existing GPS KFs require an exact model for the inertial sensor bias characteristics. However, for EB applications, this type of sensor is generally unavailable. On the other hand, unlike the traditional GPS location applications, the EB route and the operation schedule can be known in advance. Those features can be used in the data preprocessing process. The original data we can obtain from the EB is the GPS location which is a 3-D variable containing the real time latitude, longitude, and altitude. In this subsection, an EB motion state dimension deduction approach is proposed for the data preprocessing of KF. In this way, the motion state dimension of KF can be reduced to one dimension.

At first, we can track the EB's altitude with the real-time altitude and longitude according to the EB operation route. Thus, the dimension of EB motion state can be reduced from 3 to 2. Also, the real-time road slope can be obtained with the 2-D EB motion state. Based on the 2-D state, the EB speed in each sampling interval can be calculated as

$$v(t) = l(t) / \cos(\theta(t)), \quad (4.23)$$

where  $l(t) = D(Lat(t), Lon(t), Lat(t-1), Lon(t-1))$  is the horizontal distance.

In order to locate the EB with the 2-D motion state, a Cartesian coordinate system needs to be built so that the location of the bus can be represented by a bi-vertical variable. Since the EB route is known, we can assume that an EB always drives on the correct road and never reverses, which means the accumulated horizontal driving distance  $G$  is always increasing, given by the following binary-relation mapping.

$$\mathcal{L} : (X, Y) \rightarrow G = \sum_{i=0}^t l(i). \quad (4.24)$$

In other words, given the EB route and the accumulated driving distance, we can determine the exact EB location. In this way, the EB motion can be simplified as an 1-D linear variable based on the operation route. However, due to the bias and noise of GPS signal, we find out that sometimes the sampled position of the EB is not on the correct route, and the abnormal reverse can also be observed. Thus, before we apply the mapping  $\mathcal{L}$  to reduce the system state dimension, the collected GPS data need to be preprocessed. According to [90, 91], the noise of GPS signal can be modeled by a normal distribution. So, given the accuracy of the GPS module  $\sigma$ , the probability density function can be given by

$$f(X, Y) = \frac{1}{2\pi\sigma^2} \exp\left(-\frac{(X - X^m)^2 + (Y - Y^m)^2}{2\sigma^2}\right), \quad (4.25)$$

where  $(X^m, Y^m)$  is the measured EB location. Based on EB operation route  $L$ , the conditional probability density function can be derived, given by

$$f((X, Y)|(X, Y) \in L) = f(X, Y)/P((X, Y) \in L), \quad (4.26)$$

where  $P((X, Y) \in L)$  is a constant value, given by

$$P((X, Y) \in L) = \int_L f(X, Y) dX dY. \quad (4.27)$$

Then, we can calculate the expected location on the path, which can be regarded as the actual real-time 2-D EB motion state. Also, the mean and variance of  $G$  with the mapping  $\mathcal{L}$  are given by

$$E(G) = \int_L G f(G)/P((X, Y) \in L) dG \quad (4.28)$$

$$Var(G) = \int_L (G - E(G))^2 f(G)/P((X, Y) \in L) dG. \quad (4.29)$$

Based on (4.23) and (4.24), we can locate the EB with 1-D variable  $G(t)$  in real-time and obtain the corresponding real-time speed  $v(t)$ .

### 4.2.3 The Modified One-Dimension KF for EB Motion Tracing

In the above subsection, we have simplified the 3-D EB motion into 1-D linear motion. Thereafter, we proposed a modified 1-D KF for tracking the EB motion. The KF is a recursive estimator for which only the estimated state from the previous time step and the current measurement are needed to compute the estimate for the current state. In contrast to batch estimation techniques, neither history of observations nor estimate is required by KF. Given the road slope data, the three-dimension EB motion can be projected into a two-dimension motion in a plane. With the dimension reduction approach above, the linear EB motion can be represented by a bi-vertical variable  $x_t = [G(t), v(t)]^T$ . According to the traditional KF, we can assume that true state at time  $t$  is evolved from state  $t - 1$ , given by  $x_t = F_t x_{t-1} + B_t$ , where  $F_t = \begin{bmatrix} 1 & \Delta t \\ 0 & 1 \end{bmatrix}$  is the state transition matrix,  $B_t = [\frac{1}{2}\Delta t, \Delta t]^T$

is the control-input matrix, and  $u_t$  is the acceleration controlled by the driver. Besides, the observation is given by  $o_t = H_t x_t$ , where  $H_t = [1, 0]$  is the observation matrix.

Fig. 4.2 shows the KF diagram we applied in our work. Specifically, our modification are marked with dotted lines. A typical KF consists of two steps: prediction and update. The prediction step uses the location estimate from the previous time step to produce an estimate of the state at the current time step, given by

$$\hat{x}_{t|t-1} = F_t \hat{x}_{t-1|t-1} + B_t u_t, \quad (4.30)$$

where  $\hat{\cdot}$  represents estimated value. This predicted location estimate is a *priori* estimate because it does not include observation information (latest GPS signal) from the current time step. In the meanwhile, the *priori* error covariance can be computed as follow:

$$P_{t|t-1} = F_t P_{t-1|t-1} F_t^T + Q_t, \quad (4.31)$$

where  $Q$  is the process noise covariance.

In the update step, the estimated location is combined with current GPS signal to refine actual EB location. This improved estimate is termed the a *posteriori* state estimate. Mathematically, the optimal Kalman gain, *posteriori* state estimate and *posteriori* covariance can be calculated as follows:

$$K_t = P_{t|t-1} H_t^T (R_t + H_t P_{t|t-1} H_t^T)^{-1} \quad (4.32)$$

$$\hat{x}_{t|t} = \hat{x}_{t|t-1} + K_t (o_t - H_t \hat{x}_{t|t-1}) \quad (4.33)$$

$$P_{t|t} = (I^M - K_t H_t) P_{t|t-1} (I^M - K_t H_t)^T + K_t R_t K_t^T, \quad (4.34)$$

where  $K_t$  is the Kalman gain;  $I^M$  is the identity matrix;  $[\cdot]^T$  represents transportation. By now, given the real-time EB acceleration, the KF above can be used to estimate the real-time motion state of the EB.

#### 4.2.4 Real-time EB Acceleration Estimation Based on Modified Decision Forest Algorithm

Given an extremely accurate gyro with high sampling frequency, the EB acceleration can be measured directly. However, this solution is associated with high economic cost and energy consumption. Although there are gyros installed in most smartphones, the sampling accuracy is not good enough for acceleration estimation. Besides, due to the frequent bumps and direction changes during the bus driving, the instantaneous acceleration measured by the smartphone gyro cannot be used directly. For traditional KF, if the acceleration is not measurable, it can be regarded as process noise following the normal distribution. However, according to the statistics in [138], the distribution of acceleration is not a general normal distribution so that the traditional KF cannot be applied directly. In this case, a new approach to estimate the acceleration of the bus is needed.

Considering the behavior of an EB driver, the acceleration value can be regarded as a dynamic decision made according to various conditions, such as the location of the bus, current speed, current acceleration, the distance to the next road cross or EB stop, and the road slope [139–141]. Thus, a decision tree can be utilized to simulate the decision process of the driver. To avoid the over fitting issue of a single decision tree, a modified random decision forest algorithm is applied in our work.

As a popular machine learning algorithm, the random forest algorithm has been widely applied in the field of image processing, pattern recognition, etc. Notice that the estimation accuracy of random decision forest algorithm is not the highest. But it can help select the important features efficiently. With these selected important features, we can utilize other learning approaches to improve the estimation accuracy. Many works have been done to modify the tradition random forest algorithm for discarding the unimportant features [38], improving the efficiency of random feature selection [142], and interpreting the decisions made by individual trees [143]. Since most of the existing works are based on the classification trees, in this work, we will focus on extending the feature evaluation and discarding approach of classification trees to regression ones to simulate the EB driver's decision process and estimate the real-time EB acceleration.

A traditional random decision forest consists of a group of predefined binary decision trees. In the forest, each decision tree is generated using a bootstrap sample based on the training dataset. In each tree generation process, a feature subset is randomly chosen from the global feature set. When splitting the node of the tree, one feature in the subset will be selected. In the random decision forest, each tree can make a decision according to the training case. Then, the final decision can be made according to the most popular decision in the forest.

The first step is the individual decision tree generation. Here, we consider  $Z$  possible conditions, which can affect the acceleration decision made by the driver. According to the traditional classification and regression tree (CART) algorithm, we use the minimum mean-square error (MMSE) as the reference for node splitting when generating decision trees. Then, the best node splitting feature as well as the splitting value can be obtained through the following optimization:

$$(z, \kappa) = \arg \min_{(z, \kappa)} MMSE \quad (4.35)$$

$$MMSE = \min_{e_1} \sum_{D_1|(z, \kappa)} (y_1 - e_1) + \min_{e_2} \sum_{D_2|(z, \kappa)} (y_2 - e_2), \quad (4.36)$$

where  $z$  is the node splitting feature,  $\kappa$  is the threshold value for node splitting,  $D_1$  and  $D_2$  are data-subset after node splitting  $(z, \kappa)$ , while  $e_1$  and  $e_2$  are, respectively the synthesized decisions of the two data-subsets. Repeating the node splitting process until the all the data-subsets are small enough or their MMSE is small enough, the individual tree can be obtained. Repeating this process, a traditional random decision forest can be obtained.

In the data collection process, many features can be obtained influencing the EB driver's decision while the importance of these features is unknown. Thus, the dimension for generating the random decision forest can be extremely large. To avoid spending too much time on unimportant features and the corresponding errors, a modified random decision forest algorithm is needed to determine the importance of the features. In other words, we should distinguish the major factors that the EB driver cares about while driving. As we mentioned in Section I, there have been some improved random forest algorithms proposed in the previous works. However, most of them focus on the classification tree rather than decision tree. So, we extend the approach in [38] to distinguish the important and unimportant features in the random forest with decision trees. Consider  $U$  nodes in a decision tree  $\xi$ . For node  $u$ , the quality  $Q(u, z)$  of splitting by feature  $z$  can be represented by the reciprocal of MMSE as (4.36). Then, we can firstly assign a local weight to the feature  $z$  in tree  $\xi$ , given by

$$w^\xi(z) = \frac{\sum_{u=1}^U Q(u, z)}{U}. \quad (4.37)$$

A higher value of  $w^\xi(z)$  means the quality of split by feature  $z$  is better. Secondly, we need to calculate the weight of each individual tree. Checking the trees through the test set, the sum of square error (SSE) can be calculated, which can reflect the performance of each decision tree. Accordingly, the normalized weight of tree  $z$  is given by

$$\gamma^\xi = \frac{1/SSE^\xi}{\max_{\xi}(1/SSE^\xi)}. \quad (4.38)$$

In this way, higher value of  $\gamma^\xi$  indicates better decisions that one tree can make. Based on the local weight of feature and the weights of the trees, we can compute the global weight of feature  $z$ , given by

$$w(z) = \frac{\sum_{\forall \xi} w^\xi(z) \gamma^\xi}{\max \sum_{\forall \xi} w^\xi(z) \gamma^\xi}. \quad (4.39)$$

This value has a positive correlation with the feature's importance. Accordingly, we can rank the features and select best  $z^b$  features to organize the important feature set  $\mathcal{I}$ . The rest features are organized as unimportant feature set  $\mathcal{U}$ . In set  $\mathcal{U}$ , the mean value  $\mu^u$  and the standard deviation  $\sigma^u$  are calculated. Thereafter, the features in set  $\mathcal{U}$  with weight less than  $\mu^u - 2\sigma^u$  will be permanently discarded [38]. If all the features satisfy this condition, the worst one will be discarded instead. With the rest features, another random decision forest can be generated. In the new forest, if the weight of any feature in set  $\mathcal{U}$  is greater than the minimum weight in set  $\mathcal{I}$ , it will be reevaluated as an important feature and moved from  $\mathcal{U}$  to  $\mathcal{I}$ . Such process will be repeated until the set  $\mathcal{U}$  is empty. According to [38], this approach has two advantages: Firstly, one feature will never be discarded once it is evaluated as important feature. Secondly, none of the features are discarded during

**Algorithm 4** Modified Random Decision Forest Algorithm

**Require:** Dataset, feature number in data-subset, MMSE threshold, minimum data-subset size, nodes limitation, initial import feature number.

**Ensure:** Random decision forest for acceleration estimation.

- 1: **repeat**
- 2:   Generate the training datasets with replacement through bootstrap sampling as well as the test dataset.
- 3:   **for** All training dataset **do**
- 4:     **repeat**
- 5:       According to (4.35), pick the best  $z$ .
- 6:       According to (4.35), pick the best  $\kappa$ .
- 7:       According to  $(z, \kappa)$ , generate two data-subset and repeat the recursive process.
- 8:     **until** The MMSE value, data-subset size, or the total nodes number in a tree satisfies the termination condition.
- 9:   **end for**
- 10: **return** All the decision trees as the random decision forest.
- 11: Calculate the  $w^\xi(z)$  of each feature according to (4.37)
- 12: Calculate the  $\gamma^\xi$  of each decision tree according to (4.38)
- 13: Calculate the  $w(z)$  of each feature according to (4.39)
- 14: For the first time, rank the features and organize  $\mathcal{I}$  and  $\mathcal{U}$
- 15: Calculate  $\mu^u, \sigma^u$
- 16: If any feature in  $\mathcal{U}$  has higher weight than the minimum one in  $\mathcal{I}$ , move the feature to  $\mathcal{I}$ .
- 17: If any feature in  $\mathcal{U}$  has lower weight than  $\mu^u - 2\sigma^u$ , discard the feature. Otherwise discard the worst feature.
- 18: **until**  $\mathcal{U}$  is empty.

the decision tree generation process. Thus, we can significantly reduce the probability of discarding an important feature. The details of the modified random decision forest algorithm are shown in **Algorithm 4**.

In this way, we can generate the random decision forest for estimating the real-time acceleration and determine the importance feature for such estimation process.

## 4.3 Case Study

### 4.3.1 Data Collection

In order to collect the EB motion data, we have developed an Android APP based on Android Oreo 8.0 system. This APP can utilize the internal sensors in the smart phone to collect the attitude and motion data of the EB such as GPS location, time, 3-dimension acceleration data, and 3-dimension direction. In the background mode, all the data is recorded in the internal storage of the smart phone. Also, we have designed a graphic interface for the user to start and pause the recording process and set the sampling frequency. According to our test, the APP can work stably in long-term while utilizing less

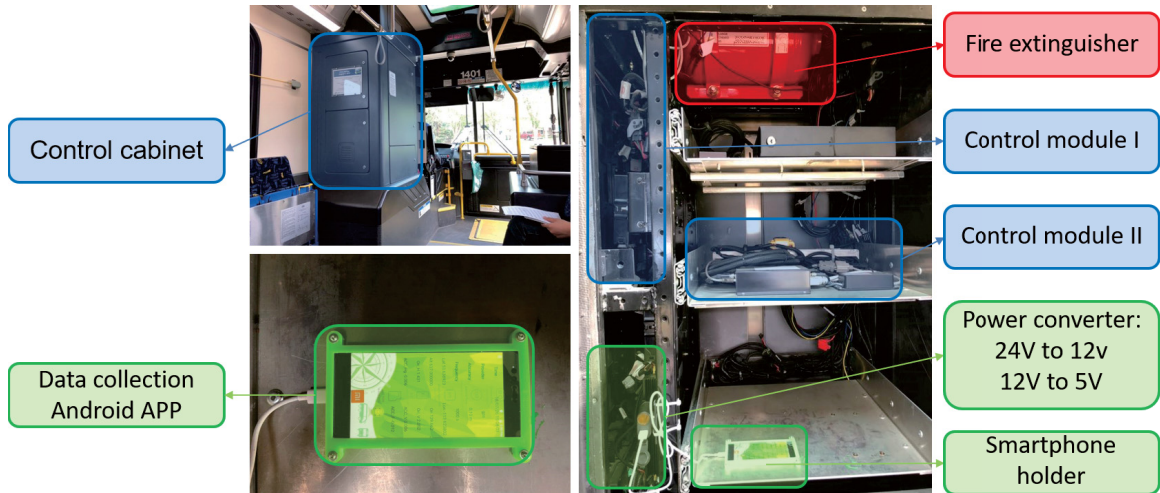


Figure 4.3: An illustration of the smartphone installation on EB.

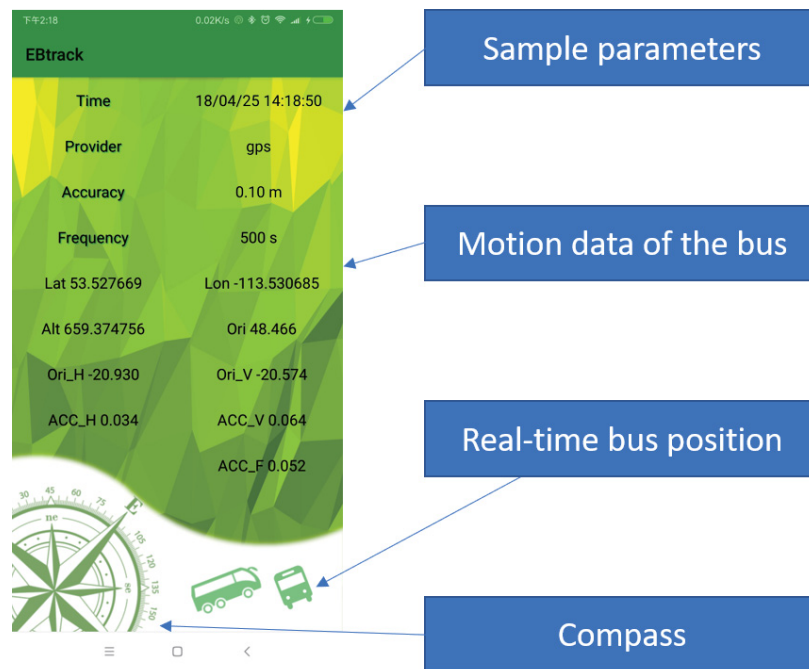


Figure 4.4: Android APP for collecting motion data.

than 5 MB of RAM.

In our work, an Android smartphone with our APP is installed in the control box of the EB. Fig. 4.3 shows the installation of the smartphone. Each day, when an EB finishes the daily operation task and returns to the transit center, the collected data will be sent to the Google drive through St. Albert Transit wireless network. Besides, on each EB, a system named HAMS has been installed, which can roughly record the GPS location of the EB as well as its SOC value every 5-10 minutes. These data can be used to evaluate



Figure 4.5: St. Albert Transit: A1 EB route.

the performance of our approaches. For collecting and recording the GPS data of the EB, a trace data collection Android APP is developed based on Android 8.0 system (Oreo). The user interface is shown in Fig. 4.4. The sampling frequency is set as 1 Hz, and the maximum localization accuracy is 1 meter. The daily data are saved in an independent CSV file and sent to the cloud through wireless network, which consist of the time stamps, GPS locations, 3-dimension orientation and 3-dimension acceleration data. Since most of the Android smartphones have been equipped with the sensors above, the proposed approach and APP can be applied to most of them.

The A1 EB route of St. Albert Transit is selected in our case study [145]. There are 70 EB stops and 116 road crosses in this route. Through the developed APP, the real GPS data and bus operation route is applied. Fig. 4.5 shows the EB route, EB stops, as well as the locations of road crosses. Based on the GPS locations of the route, the corresponding elevation data is obtained from the Google elevation API, as shown in Fig. 4.6. On average, the EB runs 56 minutes per cycle and 7 cycles per day. The corresponding constant parameters are given in Table 4.1, which are obtained from the BYD K9 technique information [78] and our preliminary research [144].

At first, the original data are preprocessed based on (4.23)-(4.29). Fig. 4.7 shows the performance of the proposed data preprocessing approach. It can be observed that, our approach can get rid of a part of the noise of the GPS signal and the preprocessed data always locate on the known EB route, which is more accurate than the original locations. Thus, the system state reduction is feasible and the real-time location of the EB can be represented by the accumulated driving distance from the departure station.

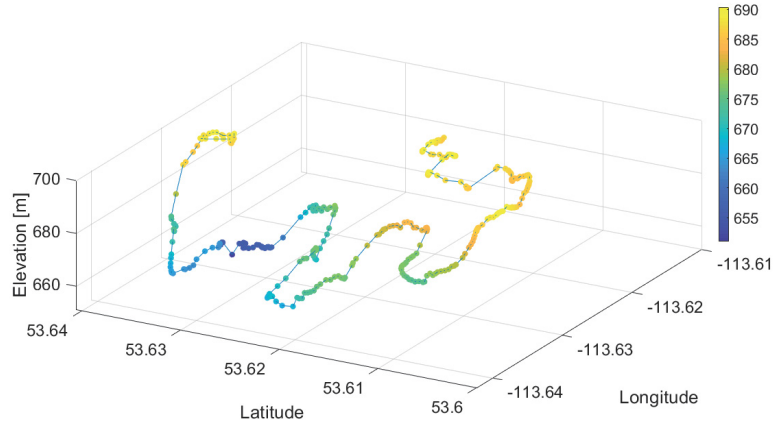


Figure 4.6: Google Elevation API: A1 EB route elevation.

Table 4.1: CONSTANT PARAMETERS IN THE SIMULATION.

Constant	Value	Constant	Value
$\beta_1$	60000	$C^A$	1.17
$\beta_2$	60	$C^R$	1.2
$\beta_3$	0.0041	$r$	0.5 m
$\beta_4$	0.00098	$A$	10 m <sup>2</sup>
$\eta^E$	0.638	$Q_t$	0.00015
$\eta^D$	0.92	$R_t$	10
$g$	9.8 m/s <sup>2</sup>	$m^B$	19000 kg
$\xi$	1.2	$m^a$	70kg

Both the traditional random decision forest algorithm and the modified random decision forest algorithm are applied to estimate the real-time acceleration of the EB. When generating the initial dataset, the following 11 features are considered according to [139–141].

1. The location of the EB.
2. The altitude of the EB.
3. The current speed of the EB.
4. The acceleration of the EB in the previous time slot.
5. The accumulated parking time (0 if EB is moving).
6. The distance from the previous EB stop.
7. The distance to the next EB stop.
8. The distance from the last passed road cross.

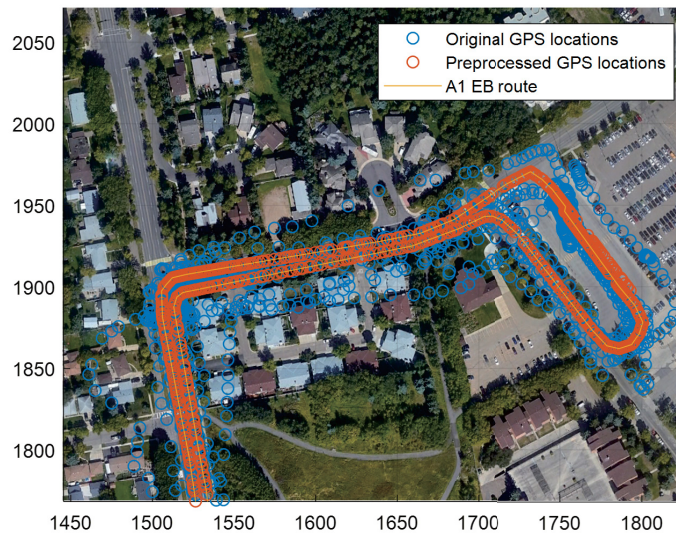


Figure 4.7: An illustration of the data preprocessing process.

9. The distance to the next road cross.
10. The road slope.
11. The rest time to reach the next EB stop (infinite if not required in the schedule).

### 4.3.2 Performance Comparison and Impacts Analysis

In our case study, the performance of the proposed approach is compared with conventional KF in four cases. In the first case, the traditional KF is applied with constant passenger count; The second case involves the route based KF (RKf) with EB motion state dimension deduction and stochastic passenger count estimation; Based on RKf, the acceleration estimated (AKF) through the traditional random decision forest algorithm is tested in the third case; In the last case, we test the proposed modified KF based on the modified random decision forest algorithm.

In the random decision tree generation process, the chosen feature number is 4. The maximum node number in each tree is 100. The minimum data subset size is 10. The threshold of MMSE is 0.001. One random decision forest consists of 1000 decision trees. The initial size of the important feature set  $\mathcal{I}$  is 3. With **Algorithm 4**, the important and unimportant features can be distinguished. Totally, we generated 6 random decision forests, 5 features are discarded, and 6 features are selected as important features. Fig. 4.8 shows the corresponding feature selection/discarding process. Accordingly, we can find out that through calculating and ranking the features' weights in the first random decision forest, the bus location, speed, and the distance to the next EB stop are assessed as important features while the accumulated parking time and the road slope are discarded due to

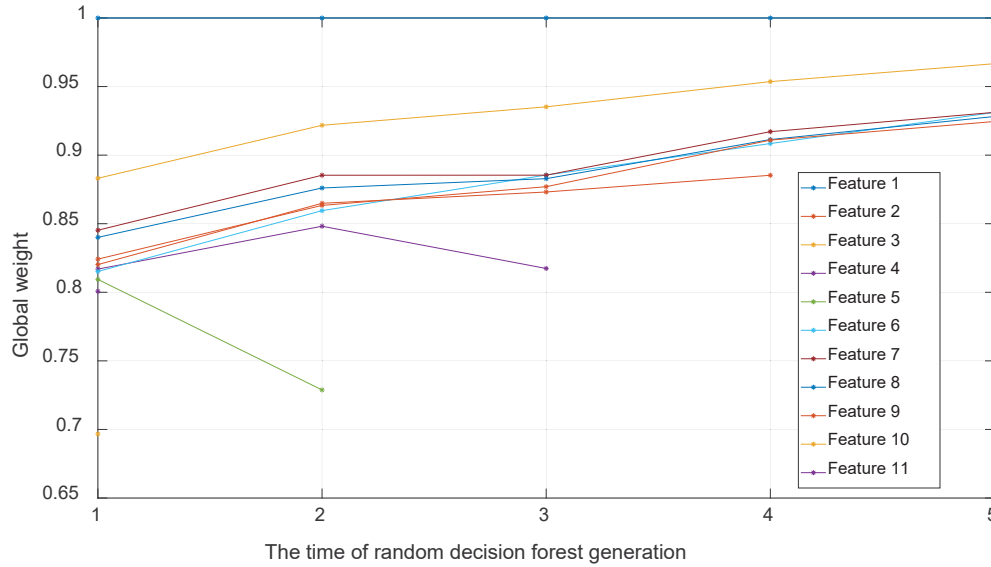


Figure 4.8: Feature selection/discarding process.

Table 4.2: PERFORMANCE OF DECISION FORESTS WITH DIFFERENT FEATURE NUMBERS.

Tree index	1	2	3	4	5
Selected features	11	9	8	8	6
SSE[ $10^3$ ]	2.4535	1.9429	1.6994	1.4526	1.3096
Time[s]	49.791	44.153	43.368	45.896	41.337

their low global weights. In the following steps, the unimportant features including altitude, the accumulated parking time, and the schedule requirement are discarded. Finally, the remaining 6 features are evaluated as important features.

Besides, the SSE of the 5 generated random decision forest trees are given in Table 4.2. We can observe that, while we have discarded some unimportant features, the SSE of the random decision forests decreases. At the same time, the total generation time consumption is not significantly increased. Therefore, the proposed feature discarding process can efficiently increase the accuracy of the predicted values and the time consumption is quite acceptable for solving the problems.

With the generated random decision forests, we can compare the performance of the KFs in the four cases. In Fig. 4.9, the estimated real-time driving mileages are compared with the actual values. We can find out that the traditional KF without acceleration measurement support cannot follow the driving mileage accurately. Since the EB route information is ignored, the traditional KF can only regard the acceleration as Gaussian noise. As a result, the error will be accumulated so that the driving mileage is far greater than the actual value. In the meanwhile, with the proposed data preprocessing approach, such error can be mitigated based on the known EB route. According to the result, the daily accumulated errors in cases 2, 3, and 4 are always within  $\pm 2\%$ .

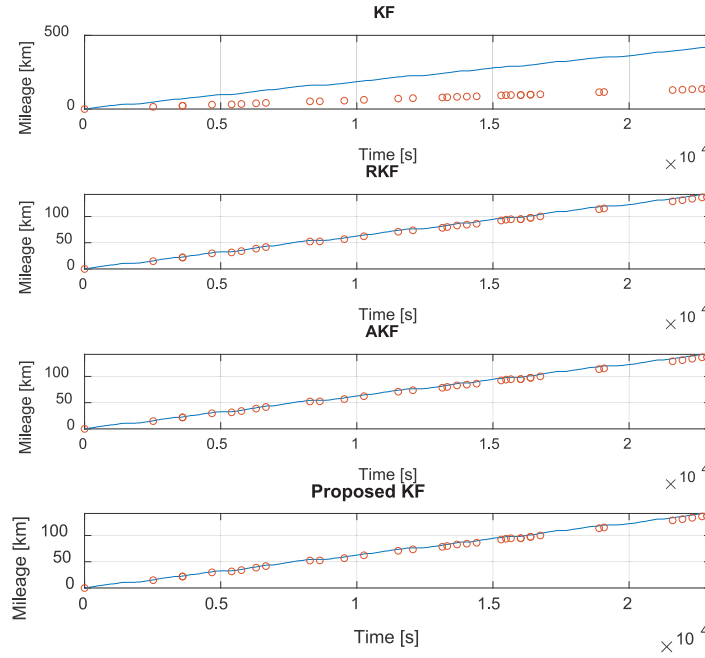


Figure 4.9: A comparison of the driving mileages.

The estimated speed of the EB is shown in Fig. 4.10. For presentation clarity, only the speed in one driving cycle is shown. Based on traditional KF, the estimated speed has dramatic fluctuations. Besides, there are some obvious extreme values, which do not satisfy the normal operation speed of the EB. In the contrary, with the data preprocessing approach, the speeds estimated by the other three KFs are more accurate. Besides, compared with AKF and proposed approach, we can find out that the speed in RKF has obvious high frequency noise, which is caused by Gaussian distribution model of the acceleration noise. Compared with RKF and AKF, the proposed approach can mitigate such noise through the proposed acceleration estimation approach. In addition, the speeds in AKF and proposed approach are similar, and the maximum difference between them is 3.2%. It means that after discarding the unimportant features, the speed estimation accuracy can still be guaranteed.

In Fig. 4.11, we present a comparison of the estimated energy consumption of the four KFs and the actual EB energy consumption data recorded by the EB internal system. We can find out that the proposed approach can estimate the real-time EB energy consumption accurately with shorter sampling time interval compared with the EB recorded data. Besides, the error of traditional KF is extremely large. Through the proposed data preprocessing approach, the accuracy can be significantly improved. Specifically, for RKF without the acceleration estimation, the accumulated error cannot be ignored when estimating a long term energy consumption. The high frequency speed noise also reduces the

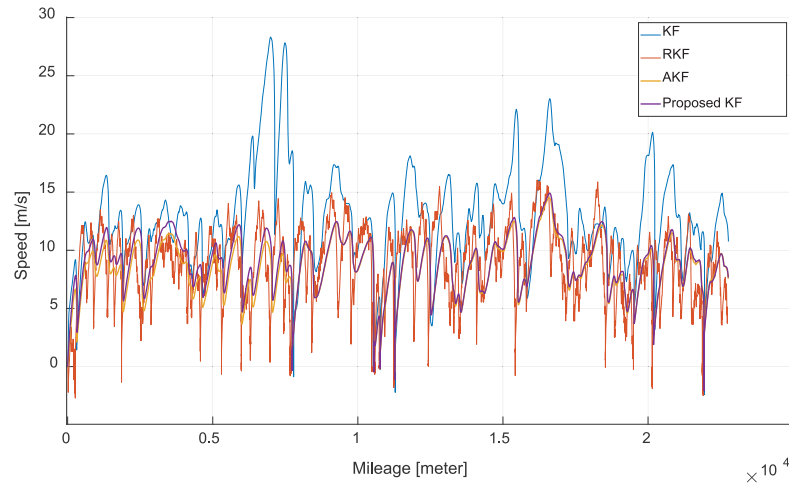


Figure 4.10: A comparison of the driving speed estimation.

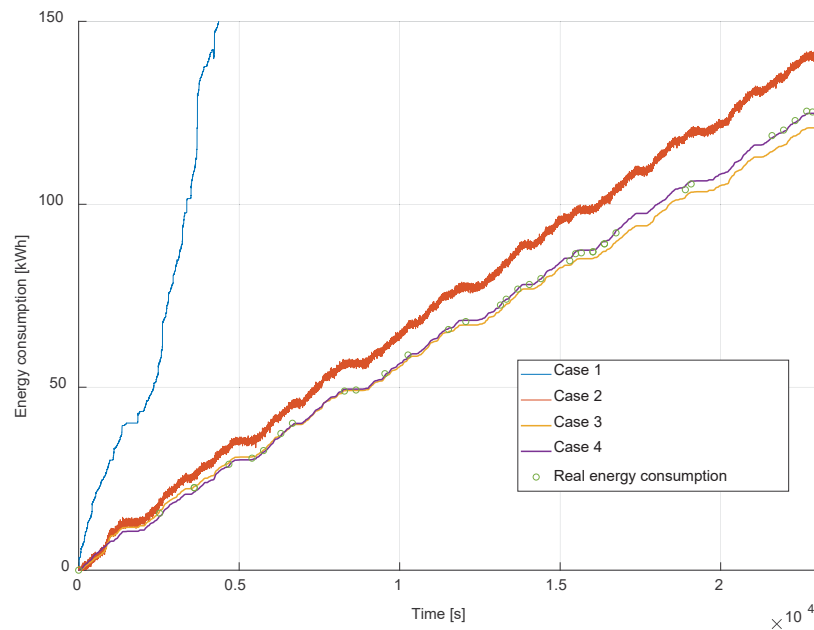


Figure 4.11: A comparison of the estimated energy consumption.

accuracy of RKF. In addition, the curves of AKF and the proposed approach can generally match the actual energy consumption. However, according to the numerical results, the accumulated error in AKF is 4.1%, while the error the proposed approach is 0.8%. It means that, through discarding the unimportant features, the corresponding impact to the estimated acceleration can be mitigated. In this way, the energy consumption can be estimated more accurately.

We also compared the proposed approach with the EB energy consumption estimation approach presented in [146], where neither the passenger count estimation (PCE) nor the motion state estimation (MSE) is taken into account. The comparison study results are

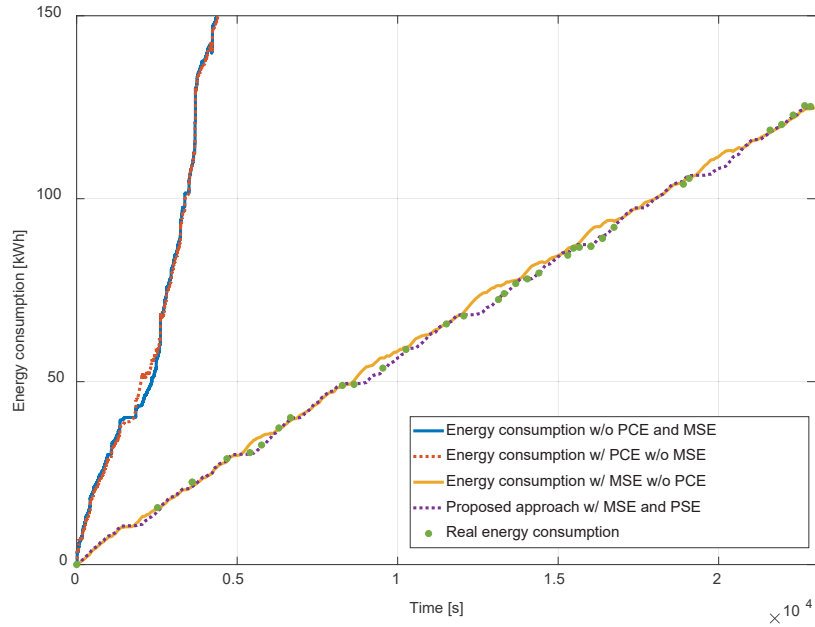


Figure 4.12: A comparison of proposed approach and other EB energy consumption estimation approaches.

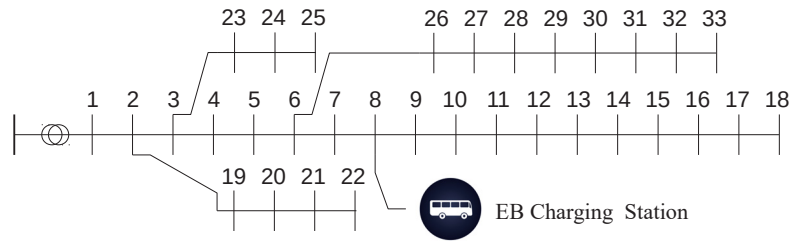


Figure 4.13: An illustration of the IEEE 33-bus test feeder.

Table 4.3: POWER FLOW ANALYSIS RESULTS.

Approach	Charging Demand [MWh]	Charging Duration [Minute]	Peak Charging Load [kW]	Minimum Voltage [p.u.]
Real data	0.7841	198.0	400	0.9969
KF	3.0688	483.6	480	0.9965
RKF	0.9084	213.5	480	0.9965
AKF	0.7806	191.9	400	0.9969
Proposed KF	0.7830	197.9	400	0.9969

shown in Fig. 4.12. According to the blue and red lines, we can find out that without MSE, the noise in the raw motion data is so large that the estimated energy consumption is not accurate at all. In comparison, the orange and purple lines are closer to the real energy consumption data based on the proposed MSE approach. Besides, according to the orange

line, we can find out that without PCE, the local accumulate error is obvious since the real-time passenger count on the EB can be more or less than the average value. Considering the impact of such randomness on the EB energy consumption, we can decrease the estimation error. Numerically, compared with average passenger count value, the proposed PCE can decrease the mean absolute error (MAE) from 11.84 to 1.39. However, in this simulation, the data is obtained from a small town and there would be at most dozen passengers on the EB, which cannot influence the EB total mass to much. If we involve EB operation routes with more passengers, the improvement of energy consumption estimation through considering the stochastic passenger counts would be more obvious.

Finally, we use the IEEE 33-bus test feeder to evaluate the performance of the proposed approach [131]. We assume that the EB charging station and the transit center are connected to the 8<sup>th</sup> bus of the feeder. There are a total of 6 EBs running on A1 EB route and they will start charging as soon as they reach the charging station. The time interval between the EBs' arrival is 20 minutes and the rated charging power of each EB is 80kW. The results are shown in Table 4.3. We can find out that the charging demand and charging duration of all the EBs derived by the proposed approach are closer to the actual data, and the estimated peak charging load are almost the same as the actual value as well as the minimum voltage of the distribution system. Particularly, comparing the results of AKF and the proposed approach, it is obvious that the proposed feature reduction method can make minor improvement to the estimation accuracy.

According to the results, we can find out that the proposed approach can help estimate the real-time EB energy consumption. The total charging time, charging power, and charging demand are all close to the actual value.

## 4.4 Summary

In this work, we develop a new EB energy consumption estimation approach. We take advantage of the known EB route and propose a data preprocessing approach to mitigate the impact of the GPS signal noise on the energy consumption estimation. Then, we model the acceleration of the EB as an control variable in the KF and apply the random decision forest algorithm to estimate it. A feature discarding approach is developed to reduce the error caused by the unimportant features. An Android APP is developed to collect the GPS data through smartphones. The real EB operation data from St. Albert Transit and the geometry data from Google elevation API are used in the case study, and the performance of the proposed approach are tested and compared with the existing approaches.

# 5

## A Three-Layer Stochastic Energy Management Approach for Electric Bus Transit Centers with PV and Energy Storage Systems

In this work, a three-layer stochastic energy management approach is proposed for EBTCs to reduce the operation cost while maintaining local voltage quality. In the first layer, a modified ROOT approach is developed to obtain the charging/discharging margin with minimum EBTC operation cost. In the second layer, the voltage regulation impact on the local voltage quality is estimated through power flow analysis considering voltage fluctuation and line loss minimization. In the third layer, the charging/discharging strategy is optimized with dynamic programming based on a modified greedy algorithm. The performance of the proposed approach is evaluated in a case study based on the IEEE 123-bus test feeder and the real operation data obtained from St. Albert Transit in Alberta, Canada. The results indicate that the proposed approach can not only minimize the EBTC operation cost but also well maintain the local voltage quality, in comparison with existing energy management approaches.

### 5.1 System Model

As shown in Fig. 5.1, the system model involves three major components: power flow model in distribution system; energy flow model in EBTC; EB energy consumption model for daily operation. In this work, we consider one day as an operation cycle including  $T$  time slots  $1, 2, \dots, t, \dots, T$ . The duration of each time slot is  $\Delta t$ .

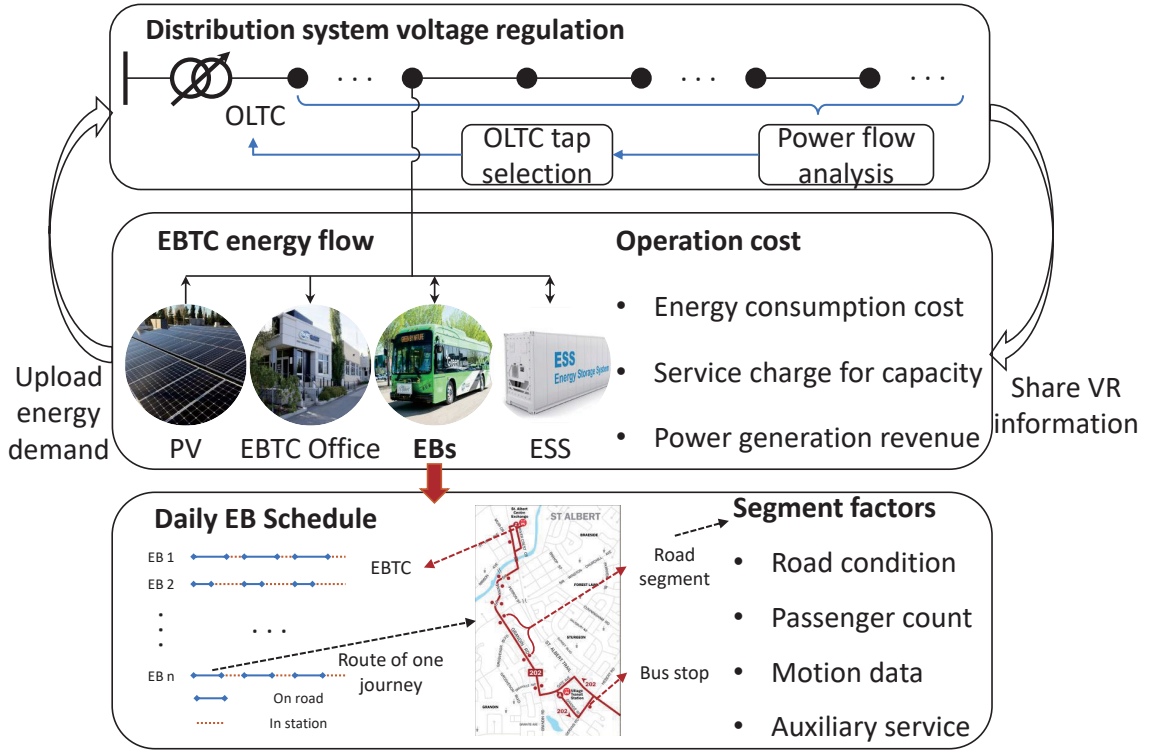


Figure 5.1: An illustration of EBTC energy management.

### 5.1.1 EBTC Operation Cost

The EBTC operation cost mainly consists of the energy consumption cost, service charge for capacity, and power generation revenue. The energy consumption cost corresponds to the total energy consumption of the EBTC, given by  $c^e = p^e \sum_{1 \leq t \leq T, P^{TC}(t) > 0} P^{TC}(t) \Delta t$ , where the price  $p^e$  is usually constant and  $P^{TC}(t)$  is the real-time load of EBTC.

The EBTC service charge for capacity depends on the peak load. Without loss of generality, we adopt a commonly used piecewise charging rate, given by

$$c^s = \begin{cases} p_0^c \hat{P} + p_1^c \hat{P}, & \hat{P} \leq \delta_1 \\ p_0^c \hat{P} + p_1^c \delta_1 + p_2^c (\hat{P} - \delta_1), & \delta_1 < \hat{P} \leq \delta_2 \\ \dots, & \dots, \end{cases} \quad (5.1)$$

where  $\hat{P}$  is the peak load, while the price  $p_0^c, p_1^c, p_2^c, \dots$  represent the stage price corresponding thresholds  $\delta_0, \delta_1, \delta_2, \dots$ . For example, in FortisAlberta's EBTC electricity pricing [147], the stage prices are given by 0.39, 0.24, 0.21 \$/KW. Since the peak load can affect the service charge for capacity in the entire billing period, peak load shaving has very significant impact on cost reduction.

Besides, EBTC can inject the extra power into the distribution system and receive revenue, given by  $c^r = p^r \sum_{1 \leq t \leq T, P^{TC}(t) < 0} P^{TC}(t) \Delta t$ , where  $p^r$  is the power generation price.

### 5.1.2 Energy Flow in the EBTC

The EBTC energy flow consists of five components: distribution system, EBs, office, PV, and ESS. The energy is supplied by distribution system and PV and consumed by the office and EBs. To reduce the EBTC peak load, the ESS can store the energy in the valley load period and supply power during the peak load period. Also, if the capacity of ESS is not sufficient, the idle EBs parking in the EBTC can also discharge for power supply. Mathematically, the real-time total power of EBTC can be decomposed into four parts, given by

$$P^{TC}(t) = P^O(t) + P^E(t) + P^S(t) + P^V(t), \quad (5.2)$$

where  $P^O(t)$  is the office load;  $P^E(t)$  is the total EB charging/discharging power;  $P^S(t)$  is the ESS charging/discharging power;  $P^V(t)$  is the real-time PV generation. To minimize the peak load, we should balance the power consumption, generation, and storage in the right hand side of the equation. Here, the office load and the PV generation are unknown and uncontrollable. Thus, we need to estimated these values for coordinating the energy flow in the EBTC. Considering the their randomness and the EBTC stability requirement, the worst case estimation is utilized in this work. The two remaining items, ESS and EB charging/discharging loads are controllable for EBTC energy flow management. However, since only the EBs parking in the EBTC are available for charging/discharging, we need to extend the EB operation model. Consider  $N$  EBs in the EBTC with indices  $1, \dots, n, \dots, N$ . In one day, the first EB departs from EBTC in time slot 1. Define set  $\mathcal{T}_n^+$  containing the time slots when EB  $n$  is running on the way. The other idle time slots can be defined as a set  $\mathcal{T}_n^-$ . Only the charging/discharging power  $P_n^E(t), t \in \mathcal{T}_n^-$  is controllable. To ensure sustainable EBTC operation, the initial and final state of charge (SOC) of ESS and EBs should be 100%. The real-time SOC can be calculated based on the initial value and real-time charging/discharging power.

### 5.1.3 EB Energy Consumption Model

According to (5.2),  $P^{TC}(t)$  is mainly characterized by the stochastic office load, PV generation, and EB energy consumption. Based on the historical data, we can obtain the real-time probability density functions (PDFs) of office load and PV generation, given by  $f_t^O(P)$  and  $f_t^V(P)$ , respectively. On the other hand, since the randomness of EB energy consumption depends on many factors, a detailed physical model is needed to estimate the EB energy consumption.

The EB energy consumption mainly depends on the real-time tractive force, given by

$$F^{tr} = F^a + F^f + F^s + F^r, \quad (5.3)$$

where  $F^a = 0.5\rho C^a Av^2$  is the aerodynamic drag force,  $\rho$  is the air density,  $C^a$  is the drag coefficient,  $A$  is the front area of EB, and  $v$  is the EB speed. The second term  $F^f = mg\zeta\cos(\alpha)$

represents the friction force, where  $m$  is the total mass of the EB,  $g$  is the gravitational acceleration,  $\zeta$  is the rolling friction coefficient, and  $\alpha$  is the road gradient. Given the altitude difference  $\Delta h$  and GPS distance  $d$  of a straight road, the road gradient can be estimated as  $\alpha = \arctan(\Delta h/d)$ . In addition,  $F^s = mg \sin(\alpha)$  is a part of the decomposed gravity caused by the ups and downs of the road, while  $F^r = \phi ma$  is the resultant force, where  $\phi$  represents the inertia impact of all rotating components in the drivetrain, and  $a$  is the acceleration of EB.

According to [148], passenger mass and auxiliary energy consumption should be involved in the system model. Consider EB  $n$  is scheduled to run journey  $1, \dots, j, \dots, J_n$  in one day, and the passenger count during one journey may vary. The passenger count distributions between different bus stops are regional. Since the EB total mass can influence the energy consumption, a location-dependent passenger count distribution can improve the energy estimation accuracy compared with a rough expectation value. Thus, we divide the  $j^{th}$  journey of EB  $n$  into  $I_{n,j}$  segments  $1, \dots, i, \dots, I_{n,j}$ . Thereafter, we can calculate the energy consumption in each segment separately, while the EB mass in each road segment is a constant value  $m_{n,j,i}$ . Specially, the passenger count in one road segment can be modeled as log-normal distribution<sup>1</sup> [149]. ...Thus, given the historical data, the probability mass function (PMF) of on-bus passenger count can be modeled as  $f_{n,j,i}^p(x)$ , where  $x$  is the passenger count. With the average passenger mass  $m^p$  and EB curb mass  $m^c$ , we can derive that  $x = \frac{m-m^c}{m^p}$ . Thus, the total EB mass is a surjective function of passenger count. Then, the PMF of EB mass can be estimated as follows:

$$f_{n,j,i}^m(m) = f_{n,j,i}^m(m^c + m^p x) = f_{n,j,i}^p\left(\frac{m - m^c}{m^p}\right), \quad (5.4)$$

where  $m = m^p x + m^c$ ,  $x = 1, 2, \dots, X$ . Here,  $X$  is the maximum passenger count of the EB.

Thereafter, involving the auxiliary service power  $P^{aux}$ , the EB energy consumption is given by

$$E_{n,j,i} = \int \eta F^{tr}(t)v(t) + P^{aux}(t)dt, \quad (5.5)$$

where  $\eta$  is a constant efficiency coefficient. Consider the energy recovery mechanism. The EB battery can utilize a part of kinetic energy to charge the battery when braking or driving down a road segment [98], which can affect  $\eta$ , given by

$$\eta(t) = \begin{cases} (\eta^g \eta^{inv} \eta^e)^{-1}, & F^{tr}(t) \geq 0 \\ \eta^r \eta^g \eta^{inv} \eta^e, & F^{tr}(t) < 0 \end{cases}, \quad (5.6)$$

<sup>1</sup>It is worth mentioning that other distributions can also be applied to model the on-bus passenger count [150]. Selecting proper distribution according to specific historical data may help improve the accuracy of our approach, but it is left for our future research.

where  $\eta^r$  is the energy recover efficiency,  $\eta^g$  is the gearbox and drivetrain efficiency,  $\eta^{inv}$  is the inverter efficiency, and  $\eta^e$  represents the efficiency of engine. Then, the energy consumption of one journey can be calculated, given by

$$E_{n,j} = \sum_{i=1}^{I_{n,j}} E_{n,i,j}. \quad (5.7)$$

### 5.1.4 Battery Degradation Cost Model

Besides the energy cost of EBTC, the battery degradation cost of EBs and ESS should also be taken into account. When managing the energy flow in the EBTC, according to [151], the battery degradation cost can be modeled as a function of depth of discharge (DOD), given by

$$\begin{aligned} c^b &= \frac{p^{bc} B^S}{cyc^S} * DOD^S + \sum_{n=1}^N \frac{p^{bc} B_n^E}{cyc_n^E} * DOD_n^E \\ &= p^{bc} \Delta t \sum_{t=1}^T \left( \frac{P^S(t)}{cyc^S} + \sum_{n=1}^N \frac{P^E(t)}{cyc_n^E} \right), \end{aligned} \quad (5.8)$$

where  $p^{bc}$  is the battery cost per kilowatt [152];  $B^S$  and  $B_n^E$  are the battery capacity of ESS and EB;  $cyc^S$  and  $cyc_n^E$  are the battery total life cycle of ESS and EB;  $DOD^S$  and  $DOD_n^E$  are the daily DOD of ESS and EB. Since the daily EB energy consumption is uncontrollable and all the EBs should be fully charged by the end of the day, the corresponding battery degradation cost cannot be mitigated. Thus, only the battery degradation cost caused by the EB/ESS discharging process for peak load shaving needs to be investigated.

## 5.2 Problem Formulation

To manage the EBTC energy flow, the main objective is to minimize the operation cost [25–30]. According to the operation cost models, the total cost can be calculated by adding up  $c^e$ ,  $c^s$ ,  $c^r$ , and  $c^b$ . Then, the optimal EBTC energy management problem can be formulated as:

$$\min_{\substack{P_n^E(t), t \in \mathcal{T}_n^-, n \in [1, N] \\ P^S(t), t \in [1, T]}} c^e + c^s + c^r + c^b, \quad (5.9)$$

$$\text{s.t. Eqs. (1) – (8)} \quad (5.10)$$

$$P_{dis \max}^E \leq P_n^E(t) \leq P_{ch \max}^E, n = 1, \dots, N \quad (5.11)$$

$$P_{dis \max}^S \leq P^S(t) \leq P_{ch \max}^S \quad (5.12)$$

where  $P_{dis \max}^E$ ,  $P_{ch \max}^E$ ,  $P_{dis \max}^S$  and  $P_{ch \max}^S$  are, respectively, the maximum charging/discharging power of EBs and ESS. To minimize the operation cost, we need to estimate the energy

consumption based on certain EBTC energy flow management strategy, given by  $\pi(t) = (P_1^E(t), \dots, P_N^E(t), P^S(t))$ .

During the actual EBTC operation, we can find out that the charging strategy of EBTC in the off-peak load period is vary flexible. Charging in the off-peak period increases neither the total charging cost nor the service charge for capacity. Thus, all of these strategies can achieve the same operation cost for EBTC. However, such strategies can have distinguished impacts on the power system. Thus, if the real-time state of the power system can be known by the EBTC, the strategies which are more friendly to the power system can be selected without increasing the EBTC operation cost. By utilizing the information exchanged in the smart grid, the DSO can share the real-time VR information with EBTC. In this way, the EBTC is able to provide VR capacity to improve the local voltage quality, which benefits both distribution system and EBTC [153, 154]. To quantify voltage quality, the percentage steady-state voltage fluctuation (PSVF) of the EBTC bus is usually applied [155, 156], given by

$$PSVF = \frac{1}{T-1} \sum_{t=2}^T |V^{TC}(t) - V^{TC}(t-1)| \times 100\%. \quad (5.13)$$

After optimizing the operation cost, the EBTC can further optimize the charging/discharging power of EBs and ESS, given by

$$\min_{\substack{P_n^E(t), t \in \mathcal{T}_n^-, n \in [1, N] \\ P^S(t), t \in [1, T]}} PSVF, \quad (5.14)$$

$$\text{s.t. } (P_1^E(t), \dots, P_N^E(t), P^S(t)) \in \{\pi(t)\} \quad (5.15)$$

$$\pi(t) = \{\pi(t) | \arg \min_{\pi(t)} c^e + c^s + c^r + c^b\} \quad (5.16)$$

$$\sum_{t=0}^T P_n^E(t) \Delta t = 0, n \in [1, N] \quad (5.17)$$

$$\sum_{t=0}^T P^S(t) \Delta t = 0 \quad (5.18)$$

where the constraints for ESS, EB charging power and SOC should be satisfied. Also, the ESS and EB should be fully charged after daily operation. Since the cost minimization is a vital objective, we achieve (5.9) firstly and minimize the PSVF value while not increasing the total operation cost in this work.

In order to decrease PSVF efficiently, we consider impact of VR on the EBTC voltage in this work. To build a practical model, the voltage regulation procedure is considered because such operation can influence the EBTC voltage quality, which used to be ignored by most related works [157–159]. In this work, we consider a distribution system with  $K$  buses  $1, \dots, k, \dots, K$  and one OLTC to implement the voltage regulation with tap position  $\lambda$ . To formulate the optimization process for tap selection, both voltage deviation minimization index and line loss minimization index are considered. Given the load

$\{\mathcal{S}_k | \mathcal{S}_k = \mathcal{S}_k^{re} + j\mathcal{S}_k^{img}\}$ , the voltage magnitudes of all the buses can be calculated through power flow analysis.

For any time slot  $t$ , given the power of EBTC  $\mathcal{S}^{TC} = (P^{TC}(t), Q^{TC}(t))$  and the other buses  $\mathcal{S}_k$ , we can calculate the real-time voltage magnitude of EBTC bus  $V^{TC}(t)$  and quantify the impact of the charging/discharging strategy on the local voltage quality mathematically. Here, the active power  $P^{TC}(t)$  can be calculated with (5.2) and the reactive power  $Q^{TC}(T)$  can be estimated with the historical reactive load of the EBTC. In this work, the OLTC VR mechanism in [155] is involved, and the VR objective function can be formulated as the average square voltage deviation to the reference value, given by

$$\min_{\lambda} \frac{1}{K} \sum_{k=1}^K (V^{ref} - V_k)^2, \quad (5.19)$$

where  $V^{ref}$  is the reference voltage,  $V_k$  is the voltage magnitude, which can be controlled by the OLTC tap position  $\lambda$ . Also, the voltage regulation problem can be modeled as network loss minimization program [160], given by

$$\min_{\lambda} \sum_{k,k' \in \{1, \dots, K\}} L(V_k, V_{k'}), \quad (5.20)$$

where  $k'$  is the adjacent bus of bus  $k$ , and  $L(\cdot)$  is the line loss between bus  $k$  and  $k'$ . Besides, the voltage magnitude and tap position should be within the ranges  $[V^{\min}, V^{\max}]$  and  $[\lambda^{\min}, \lambda^{\max}]$ , respectively.

### 5.3 A Three-Layer Stochastic Energy Management Approach

As shown in Fig. 5.2, we can optimize the EBTC energy flow management in three layers: In the first layer, we optimize the EBTC operation cost and calculate the proper charging/discharging margin. In the second layer, the optimal OLTC tap position can be optimized with the real-time load of each bus. In the third layer, the local voltage quality can be optimized within charging/discharging margin obtained in the first layer. Specifically, to optimize the EBTC operation cost, estimation of the EB energy consumption is necessary [98]. Thus, we develop a stochastic EB energy consumption estimation based on synthetic driving profile. Accordingly, the proposed approach will be introduced in details in the following four subsections.

#### 5.3.1 Stochastic EB Energy Consumption Estimation Based on Synthetic Driving Profile

In order to manage the energy flow in the EBTC and minimize the operation cost, the stochastic energy consumption of office and EBs and power generation of PV should be estimated. Generally, the PDFs of office load  $f_t^O(P)$  and PV generation  $f_t^V(P)$  can be estimated based on the historical data [161, 162]. Without the real-time EB motion data, a

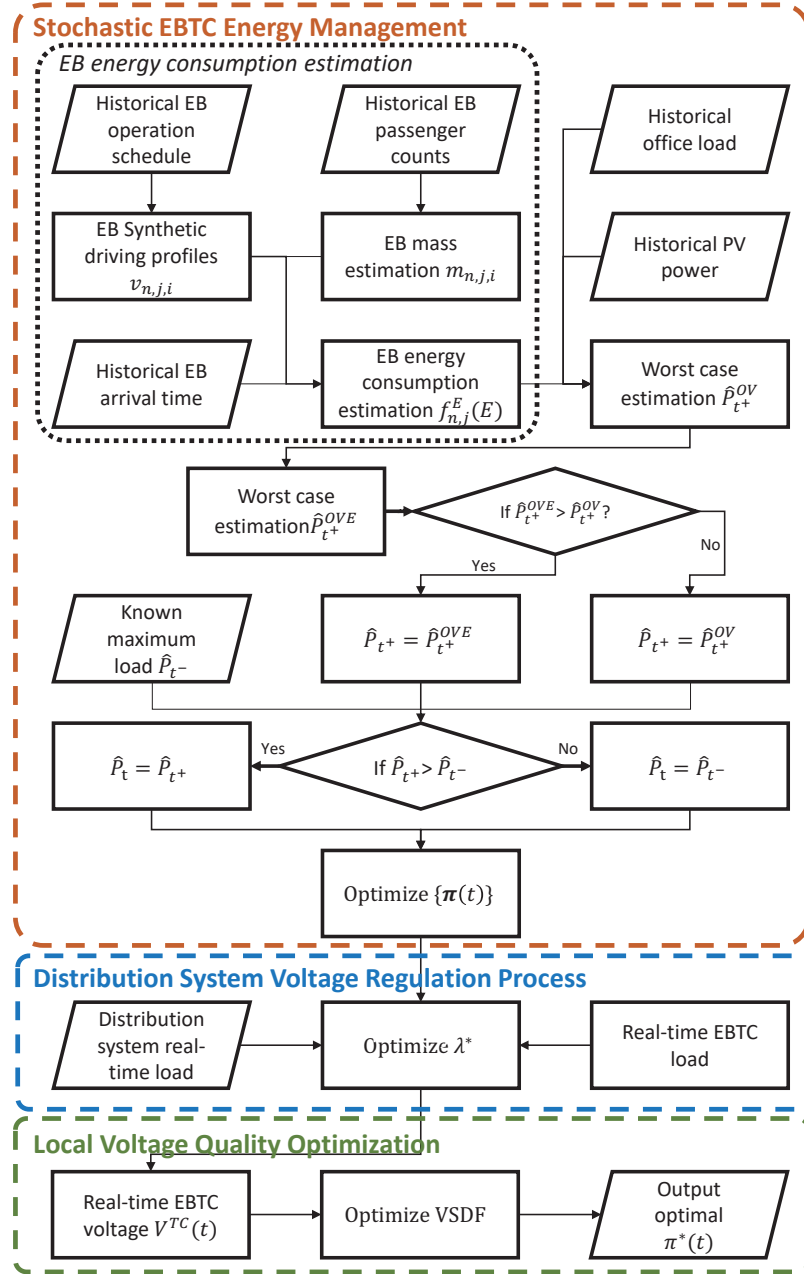


Figure 5.2: Flowchart of the three-layer EBTC energy management approach.

driving profile synthetic approach is proposed in [98, 99] to simulate EB motion based on deterministic EB departure/arrival time. To characterize the randomness in EB energy consumption, in this research, we propose a modified EB energy consumption estimation approach based on synthetic driving profile considering the stochastic EB arrival time, passenger count, and road condition.

Firstly, a synthetic driving profile needs to be generated for bus  $n$  with respect to the trip between two adjacent bus stops  $i$  and  $i + 1$  in the  $j^{th}$  journey. Define the inter-stop

distance as  $D_{n,j,i}$ . Consider there are  $n_{n,j,i}^h$  intermediate halts happening during the trip. The trip can be divided into  $n_{n,j,i}^h + 1$  phases. In each phase, the EB starts with constant acceleration  $a^+$ . Then, it will coast with a constant speed  $v_{n,j,i}^*$  and halt with a constant deceleration  $a^-$ . The driving distances for each process are  $d_{n,j,i}^+$ ,  $d_{n,j,i}^*$ , and  $d_{n,j,i}^-$ , respectively. According to [98], the coasting speed and intermediate halt number can be obtained based on the empirical formula, given by

$$v_{n,j,i}^* = 1.5v_{n,j,i}^{avg} \quad (5.21)$$

$$n_{n,j,i}^h = \begin{cases} 1, & v_{n,j,i}^{avg} \geq 25\text{km/h} \\ 6 - \lfloor v_{n,j,i}^{avg}/5 \rfloor, & \text{else} \end{cases}, \quad (5.22)$$

where  $v_{n,j,i}^{avg}$  is the average speed in the trip,  $\lfloor \cdot \rfloor$  is the floor function. According to [163, 164], the delay arrival time of EB satisfies log-normal distribution  $f_{n,j,i}^d(t)$ . In the actual case, we can install location recording devices on the EBs and collect the real-time EB locations. Based on the collected EB location samples, we can determine  $f_{n,j,i}^d(t)$  for each road segment. Given the scheduled trip time  $Tr_{n,j,i}^*$ , the distribution of the trip time  $Tr_{n,j,i}$  can also be obtained as  $f_{n,j,i}^d(Tr_{n,j,i} - Tr_{n,j,i}^*)$ . Then, we can calculate the distribution of the average speed, given by  $f_{n,j,i}^d(\frac{D_{n,j,i}}{v_{n,j,i}^{avg}} - Tr_{n,j,i}^*)$ . Thereafter, we can compute  $[d_{n,j,i}^+, d_{n,j,i}^*, d_{n,j,i}^-]$  with coasting speed and intermediate number, given by

$$\left[ \frac{v_{n,j,i}^{*2}}{a^+}, \frac{D_{n,j,i}}{n_{n,j,i}^h + 1} - \frac{v_{n,j,i}^{*2}(a^- - a^+)}{2a^+a^-}, -\frac{v_{n,j,i}^{*2}}{a^-} \right]. \quad (5.23)$$

Accordingly, the minimum distance of the synthetic profile is  $(n_{n,j,i}^h + 1)(d_{n,j,i}^+ + d_{n,j,i}^-)$ . If the minimum distance is shorter than the inter-stop trip distance  $D$ , the EB will decelerate before accelerating to  $v_{n,j,i}^*$  and there is no coasting processes. Mathematically, when  $(n_{n,j,i}^h + 1)(d_{n,j,i}^+ + d_{n,j,i}^-) > D_{n,j,i}$  the distance vector in (5.23) should be calibrated as follows:

$$\left[ \frac{D_{n,j,i}a^-}{(n_{n,j,i}^h + 1)(a^- - a^+)}, 0, \frac{D_{n,j,i}a^+}{(n_{n,j,i}^h + 1)(a^+ - a^-)} \right]. \quad (5.24)$$

Given the trip time, we can generate the synthetic driving profile and obtain the real-time speed, acceleration, and the real-time location according to the EB journey route. Besides, the road segment slope  $\alpha_{n,j,i}$  is deterministic for specific location. Thus, the energy consumption of the inter-stop trip can be calculated based on (5.3)-(5.6), given by

$$E_{n,i,j} = SDP(m_{n,j,i}, Tr_{n,j,i}, D_{n,j,i}, \alpha_{n,j,i}), \quad (5.25)$$

where  $\alpha$  is the road segment slope,  $SDP(\cdot)$  represents the computation function based on the synthetic driving profile approach. Since the journey route is available, the corresponding distance and road slope data can be obtained from digital map such as Google Map. The distribution for the passenger count and travel time can be obtained from the

historical data. Thus, the distribution of the EB energy consumption per inter-stop trip can be calculated, given by

$$\begin{aligned}
 f_{n,j,i}^E(E) &= \int_{T_{n,j,i}^*}^{T_{n,j,i}^{\max}} f_{n,j,i}^{dm}(t, \underbrace{SDP^{-1}(E, t, D_{n,j,i}, \boldsymbol{\alpha}_{n,j,i})}_{\text{Mass } m}) dt \\
 &= \int_{T_{n,j,i}^*}^{T_{n,j,i}^{\max}} \int_0^{m_{n,j,i}^{\max}} \omega(t, m) f_{n,j,i}^d(t) f_{n,j,i}^m(m) dm dt, \tag{5.26}
 \end{aligned}$$

$$\omega(t, m) = \begin{cases} 1, & E = SDP(m, t, D_{n,j,i}, \boldsymbol{\alpha}_{n,j,i}), \\ 0, & \text{else} \end{cases}, \tag{5.27}$$

where  $T_{n,j,i}^{\max}$  and  $x_{n,j,i}^{\max}$  are, respectively, the historical longest trip time and maximum passenger count;  $f_{n,j,i}^{dm}(\cdot)$  is the joint probability function of  $t$  and  $m$ ;  $SDP^{-1}(\cdot)$  is the inverse function of mass  $m$  given time  $t$ ;  $\omega$  is a binary weight, which equals to one if (5.25) holds and zero otherwise. According to (5.25), when the trip distance  $D_{n,j,i}$  and road slop  $\boldsymbol{\alpha}_{n,j,i}$  is determined, the probability of specific inter-stop energy consumption is determined by the double integrals on EB mass and EB delay time. Thus, for calculating the probability of specific EB energy consumption, we need to integral the probability of all the possible combinations of EB mass and EB delay time. The binary weight  $\omega$  is a selection function for getting rid of invalid integration interval. Thereafter, the energy consumption distribution per journey can be obtained, as shown in (5.28)-(5.29).

$$\begin{aligned}
 f_{n,j}^E(E) &= \int_0^{E_{n,j,1}^{\max}} \int_0^{E_{n,j,2}^{\max}} \dots \int_0^{E_{n,j,I_{n,j}-1}^{\max}} \\
 &\quad \underbrace{f_{n,j,i}^E(E_{n,j,1}, \dots, E_{n,j,I_{n,j}})}_{\text{Combination } (E_{n,j,1}, \dots, E_{n,j,I_{n,j}}) \text{ corresponds to } E} \\
 &\quad f_{n,j,i}^E(E_{n,j,1}, \dots, E_{n,j,I_{n,j}-1}, E - \sum_{i=1}^{i=I_{n,j}-1} E_{n,j,i}) dE_{n,j,1} \dots dE_{n,j,I_{n,j}-1} \\
 &= \int_0^{E_{n,j,1}^{\max}} \int_0^{E_{n,j,2}^{\max}} \dots \int_0^{E_{n,j,I_{n,j}}^{\max}} \\
 &\quad \psi(E_{n,j,1}, \dots, E_{n,j,I_{n,j}}) \prod_{i=1}^{I_{n,j}} f_{n,j,i}^E(E) dE_{n,j,1} \dots dE_{n,j,I_{n,j}}, \tag{5.28}
 \end{aligned}$$

$$\psi(E_{n,j,1}, \dots, E_{n,j,I_{n,j}}) = \begin{cases} 1, & E = \sum_{i=1}^{i=I_{n,j}} E_{n,j,i}, \\ 0, & \text{else} \end{cases}, \tag{5.29}$$

where  $f_{n,j,i}^E$  is the joint probability function of energy consumption combination;  $\psi$  is a binary weight, which equals to one if (5.7) holds and zero otherwise. In this way, we can calculate the probability of specific EB energy consumption per journey according to the probability of inter-stop EB energy consumption combination  $(E_{n,j,1}, \dots, E_{n,j,I_{n,j}})$ .

### 5.3.2 Stochastic EBTC Energy Management Based on Modified Robust Optimization Over Time

As shown in Section II-A, the EBTC cost mainly consists of three parts: energy consumption cost, service charge for capacity, and power generation revenue. Since the power generation price  $p^r$  is typically much lower than the electricity cost  $p^e$  for EV applications [165], consuming all the PV generated power locally is preferred for EBTC energy management. Since the total energy consumption is not controllable as it is determined by the EB operation schedule set up by the public transit service, the energy consumption cost  $c^e$  is constant. Thus, the major component of the operation cost that can be reduced is the service charge for capacity, which mainly depends on the daily peak load. Here, we should notice that, this conclusion only holds when the energy consumption price is constant overtime. Otherwise, not only the peak load issue but also low energy consumption price period should be taken into account. Nevertheless, in this work, we consider the peak load reduction as a major issue since the cost reduction from time-variant price stays limited. So, the objective of the optimization problem can be transformed from cost minimization to peak load minimization, given by  $\min_{\substack{P_n^E(t), t \in \mathcal{T}_n^-, n \in [1, N] \\ P^S(t), t \in [1, T]}} \hat{P}$ . Generally, such problems can be solved with robust optimization so that the worst peak load can be avoided in advance [166]. However, this optimization problem is highly dynamic due to EB operation and the constraints can vary over time. As a result, optimization approaches based on expectation values are not applicable in this scenario. In order to solve this dynamic risk optimization problem, a modified ROOT approach is developed. As a novel approach to tackle the dynamic optimization, traditional ROOT is able to provide dynamic solutions according to specific time-variant fitness function [167]. However, for this optimization problem, the stochastic EB energy consumption is involved, and it is very difficult to find an explicit function to evaluate the solution fitness. Thus, we proposed a modified ROOT approach to solve this problem in two steps: In the first step, the known peak load in the past and the expected peak load in the future are compared. The higher one is selected as ideal peak load for the current time slot as it has stronger fitness. Mathematically, it can be calculated as follows:

$$\hat{P}_t = \max\{\hat{P}_{t-}, \hat{P}_{t+}\} \quad (5.30)$$

$$\hat{P}_{t+} = \max\{\hat{P}_{t+}^{OV}, \hat{P}_{t+}^{OVE}\} \quad (5.31)$$

$$\hat{P}_{t+}^{OV} = \arg \min_{\hat{P}_{t+}^{OV}} c^s + c^b, \quad (5.32)$$

where  $\hat{P}_t$  is the peak load expected in the current time slot,  $\hat{P}_{t-}$  is the known maximum load in the past,  $\hat{P}_{t+}$  is the expected peak load in the future,  $P_{t+}^{OV}$  is the expected peak load caused by the office load and PV generation in the future,  $P_{t+}^{OVE}$  is EBTC peak load considering the impact of EB, PV, and office load in the future. When the EB charging demand is not large,  $P_{t+}^{OV}$  depends on the worst-case office load and PV generation in

the future, which can be obtained from  $f_t^0(P)$  and  $f_t^V(P)$ , respectively. Otherwise, the office load, PV generation, and EB charging demand can all influence the expected peak load in the future, which can be formulated as an optimization problem, given by

$$\min_{\substack{P_n^E(\tau), \tau \in \mathcal{T}_n^- \cap [t, T], n \in [1, N] \\ P^S(\tau), \tau \in [t, T]}} \hat{P}_{t+}^{OVE}. \quad (5.33)$$

In the second step, based on  $\hat{P}_t$ , the feasible margins  $\pi(t)$  of the EB/ESS charging/discharging power in the current time slot can be determined, given by

$$\pi(t) = \{\pi(t) | \pi(t) = (P_1^E(t), \dots, P_N^E(t), P^S(t)), \hat{P}_t \geq \hat{P}_{(t+1)+}\}, \quad (5.34)$$

where  $\hat{P}_{(t+1)+}$  is the expected future peak load in the next time slot, if the EBs and ESS execute the strategy  $\pi(t)$ . Notice that, in this set, only the power of EBs in the EBTC can be controlled  $\{n | t \in \mathcal{T}_n^-\}$ . The power of other EBs depends on the actual energy consumption.

By now, we can find out that the strategy optimization mainly depends on the expected peak load. As long as the peak load is not increased, the charging strategies of EBs and ESS in the off-peak load period is flexible. Thus, given the value of expected peak load  $\hat{P}_t$ , the feasible EB/ESS charging/discharging margin can be obtained. The impact of the EBTC load on the distribution and local voltage quality will be explored in the next subsection. Accordingly, we can select the optimal EB/ESS charging/discharging power from the obtained margin and guarantee the local voltage quality.

### 5.3.3 Impact Analysis of EBTC Load on the Tap Selection in Voltage Regulation Process

Generally, the impact of the EBTC load on the local voltage quality depends on the real-time power for each bus in the distribution system. However, the robust optimization approach in the existing works used to ignore the impact of the voltage regulation process [166]. On one hand, the theoretical voltage drop problem discussed in these works might not happen because of the voltage regulation process. Thus, the OLTC tap selection in the voltage regulation process should be analyzed first, which can significantly improve the ROOT approach so that the local voltage quality can be guaranteed. According to (5.19) and (5.20), both objective functions are determined by the bus voltage magnitudes. To simplify the calculation process, linearization approach in [168] is applied. Assuming  $\theta_{kk'} \approx 0$  and  $V_k \approx 1$ , the power flow equation can be linearized, and the voltage magnitude can be calculated with a linear function of load and slack bus voltage magnitude. Mathematically, we can define the linearized power flow analysis function as  $V_k = \varphi_k V_1 + \epsilon_k$ , where  $\varphi_k$  and  $\epsilon_k$  are constant parameters determined by the line impedance and real-time load in the distribution system. Hence, the objective functions (5.19) and (5.20) can be converted

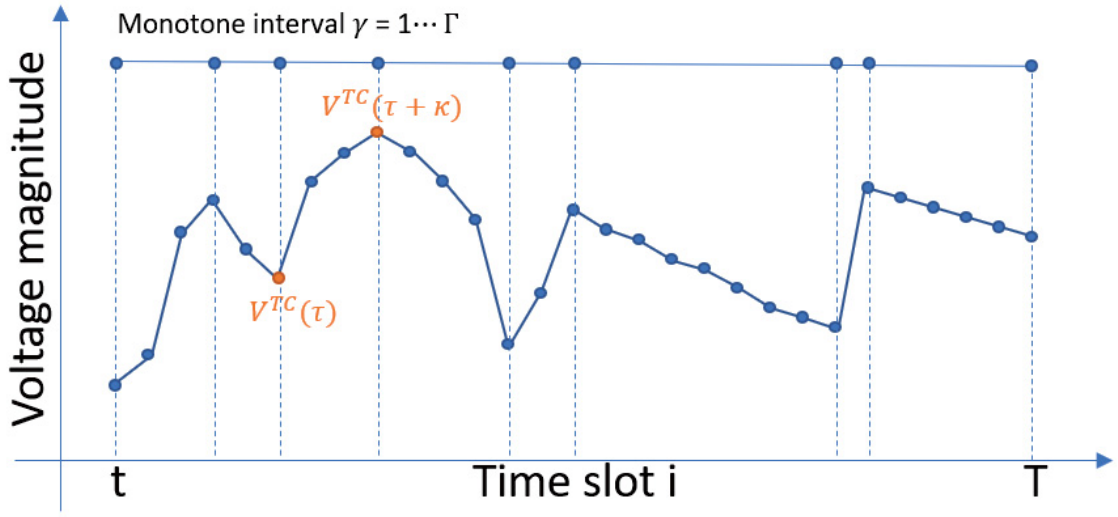


Figure 5.3: An illustration of greedy algorithm proof.

as follows:

$$\min_{\lambda} \frac{1}{K} \sum_{k=1}^K (V^{ref} - \varphi_k V_1 - \epsilon_k)^2 \quad (5.35)$$

$$\min_{\lambda} \sum_{k,k' \in \{1, \dots, K\}} \frac{(\varphi_k V_1 - \varphi_{k'} V_1)^2}{Z_{kk'}} \quad (5.36)$$

where  $Z_{kk'}$  is the impedance between nodes. Thereafter, both objective functions can be approximated as a quadratic function of slack bus voltage magnitude, which is a linear function of OLTC tap position, given by  $V_1 = \lambda V^{ref}$ . Then, both optimization problems can be converted into problems of finding a quadratic function's minimum value. With the optimal tap position  $\lambda^*$ , the local voltage magnitude  $V^{TC}(t)$  can be calculated.

### 5.3.4 Local Voltage Quality Optimization

Through the aforementioned derivation, we have obtained the proper EB/ESS charging/discharging margin as well as the relation between the EBTC load and local voltage magnitude. Then, the local voltage quality in (5.13) can be calculated. In the existing research [155], the voltage quality is usually optimized based on day ahead optimization. Yet, due to the inaccuracy of the estimation, the expected performance might not be satisfied. Besides, continuously modifying the established strategies according to information update can help to improve the performance of the approach. Thus, in this work, this problem is solved with dynamic programming based on a modified greedy algorithm. In this subsection, we prove that the optimal strategy obtained with the modified greedy algorithm is exactly the global optimum.

Because the total time slot  $T$  is a constant value, the voltage quality in (5.13) can be optimized as follows:

$$\min_{\pi(t) \in \boldsymbol{\pi}(t)} \sum_{i=t}^T |V^{TC}(i) - V^{TC}(i-1)|, \quad (5.37)$$

where  $V^{TC}(t-1)$  is the known local voltage magnitude in the previous time slot. Define  $V^{TC}(\tau), \dots, V^{TC}(\tau+\kappa)$  as a continuous increasing subsequence of  $V^{TC}(t-1), \dots, V^{TC}(T)$ . Thereafter, the elements in (5.37) can be simplified as follows.

$$\begin{aligned} \sum_{t=\tau+1}^{\tau+\kappa} |V^{TC}(t) - V^{TC}(t-1)| &= \sum_{t=\tau+1}^{\tau+\kappa} V^{TC}(t) - V^{TC}(t-1) \\ &= |V^{TC}(\tau+\kappa) - V^{TC}(\tau)|. \end{aligned} \quad (5.38)$$

For the continuous decreasing subsequence, the corresponding elements in (5.37) can also be simplified as one in a similar way. Assume that there are  $\Gamma$  such continuous increasing/decreasing subsequences. Then, the objective function (5.37) can be simplified as follows:

$$\min_{\pi(t) \in \boldsymbol{\pi}(t)} \sum_{\gamma=1}^{\Gamma} |V^{TC}(\kappa_{\gamma}) - V^{TC}(\kappa_{\gamma-1})|, \quad (5.39)$$

where  $\kappa_0 = t-1$  and  $\kappa_{\Gamma} = T$ , and for all  $\gamma$ , the following condition always holds.

$$(V^{TC}(\kappa_{\gamma}) - V^{TC}(\kappa_{\gamma-1}))(V^{TC}(\kappa_{\gamma}) - V^{TC}(\kappa_{\gamma+1})) > 0. \quad (5.40)$$

Without loss of generality, we assume that  $V^{TC}(\kappa_1) < V^{TC}(\kappa_0)$ . Then, the objective function is equivalent to:

$$\min_{\pi(t) \in \boldsymbol{\pi}(t)} V^{TC}(\kappa_0) + \sum_{\gamma=1}^{\Gamma-1} (-1)^{\gamma} 2V^{TC}(\kappa_{\gamma}) + (-1)^{\Gamma} V^{TC}(\kappa_{\Gamma}). \quad (5.41)$$

Thereafter, we can derive the partial derivative of PSVF with the respect to the EBTC volt-

age magnitude in the current time slot, given by  $\frac{\partial PSVF}{\partial V^{TC}(t)} = \begin{cases} 2, & \text{case 1} \\ -2, & \text{case 2} \\ 0, & \text{else} \end{cases}$ , where, com-

pared with the EBTC voltage magnitudes in both previous and after time slots,  $V^{TC}(t)$  is smaller in case 1 and larger in case 2. Thus,  $\frac{\partial PSVF}{\partial V^{TC}(t)} \leq 0$  holds when  $V^{TC}(t) \leq V^{TC}(t-1)$ , and  $\frac{\partial PSVF}{\partial V^{TC}(t)} \geq 0$  holds when  $V^{TC}(t) \geq V^{TC}(t-1)$ . Therefore, the original optimization problem can be simplified in the following optimal substructure, the optimal solution of which is included in the solution of the entire problem.

$$\pi^*(t) = \arg \min_{\pi(t)} |V^{TC}(t) - V^{TC}(t-1)|. \quad (5.42)$$

This conclusion is also intuitively shown in Fig. 5.3. In each monotone interval between extreme points, the internal voltage magnitude points do not influence the total PSVF value. Thus, as long as we can decrease the fluctuation between extreme values, the global PSVF minimization can be achieved. So, in the time slot  $t$ , no matter whether the voltage magnitude in the next time slot is an extreme value or not, as long as we minimize the difference between the voltage magnitude in the next and current time slots, we can achieve the global optimization. In other words, since the objective function of the optimal substructure is irrelevant to the charging/discharging strategies in future time slots, the solution obtained through the greedy algorithm is exactly the global optimal solution. Thereafter, based on the greedy algorithm, the optimal strategy  $\pi^*(t)$  can be selected in the obtained margin  $\pi(t)$ .

Discretizing the charging/discharging power of EBs/ESS into  $\beta^E$  and  $\beta^S$  levels [169, 170], respectively, we can find out the size of the original solution space obtained in the first layer optimization is  $[(\beta^E)^N \beta^S]^T$ , which is too large to solve. Based on the proof above, this problem can be solved with greedy algorithm, and the solution space size can be reduced to  $(\beta^E)^N \beta^S$  in each time slot. Thereafter, according to (42), all the strategies corresponding to the same EBTC voltage magnitude are equivalent. Thus, we can merge these equivalent strategies and further reduce the solution space size to  $N\beta^E + \beta^S$ . In this way, we can find out the optimal strategy through quicksort algorithm, whose time complexity is  $O(n \log n)$  [171],  $n = N\beta^E + \beta^S$ . For practical applications, to the best of our knowledge, the maximum number of EBs in one transit center is 155 in Los Angeles [172]. With the proposed optimization approach, the solution space size is less than 12500 even if we select 1 kW discretization interval<sup>2</sup> and there are 80 EB charging/discharging levels and 100 ESS charging/discharging levels. Thus, the proposed approach is practical for real-world EBTC applications.

## 5.4 Case Study

In the case study, we consider an EBTC with 10 EBs. The EB parameters are based on BYD K9 [173], which is the model used by St. Albert Transit, AB, Canada, for daily operation. The battery size of EB is 270 kWh, and the maximum charging/discharging power is 80 kW. The electricity rate from FortisAlberta, AB, Canada, is applied [147]. The office load, PV generation data, EB schedule, route, and energy consumption data are obtained from St. Albert Transit's daily operation statistics from Jun. 1 to Sep. 2 in 2018. The road slope data are obtained from the Google Map API. The battery size of ESS is 500 kWh, and the maximum charging/discharging power is 100 kW. As shown in Fig. 5.4, the IEEE 123-bus test feeder is applied and we assume that EBTC is connected on bus 10. The daily real-time

<sup>2</sup>In the existing works, the discretization interval can vary according to different accuracy requirement. In [169], the charging power is discretized into 3 levels, given by 100%, 50%, and 0% of maximum charging power, and the discretization interval in [170] is 2.5 kW.

Table 5.1: CONSTANT PARAMETERS IN SIMULATION.

Parameter	Value	Parameter	Value	Parameter	Value
$\rho$	1.18	$\varphi$	1.1	$\eta^r$	0.6
$C^a$	0.7	$\eta^g$	0.97	$m^p$	70
$A$	10	$\eta^{inv}$	0.95	$a^+$	1
$\zeta$	0.008	$\eta^e$	0.91	$a^-$	-1.5

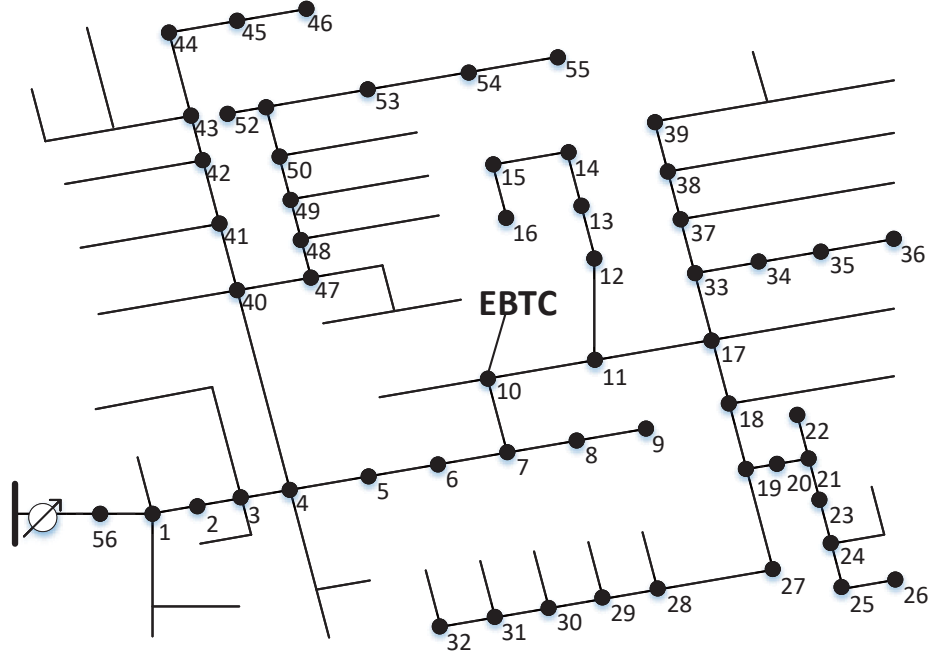


Figure 5.4: An illustration of the IEEE 123-bus test feeder with an EBTC.

load is generated according to the MAISY dataset [174]. The other constant parameters are listed in Table 5.1. Our case study is done in MATLAB 2018b on a desktop computer with Intel® Core™ i7-4770 CPU @3.40GHz. The average optimization time consumption for each time slot is 29.84 seconds.

The EB operation data are collected in St. Albert Transit, Canada, with an Android APP developed by ourselves, as shown in Fig. 5.5. Also, the data collection and distribution of estimated EB energy consumption per journey are compared with the distribution of actual values as shown in Fig. 5.6, where the coefficient of determination is 0.892, which indicates that the derived distribution  $f_{n,j}^E(E)$  provides a good approximation for the distribution of the statistic value [175].

In Fig. 5.7, the real-time total loads of the EBTC with four different EB/ESS charging/discharging strategies are shown. Notice that these strategies are all obtained from the first layer optimization. They have the same total energy consumption and the same peak load while satisfying the charging demand of all the EBs. Also, we can find out that through different optimal strategies, the daily peak load of the EBTC can be reduced from

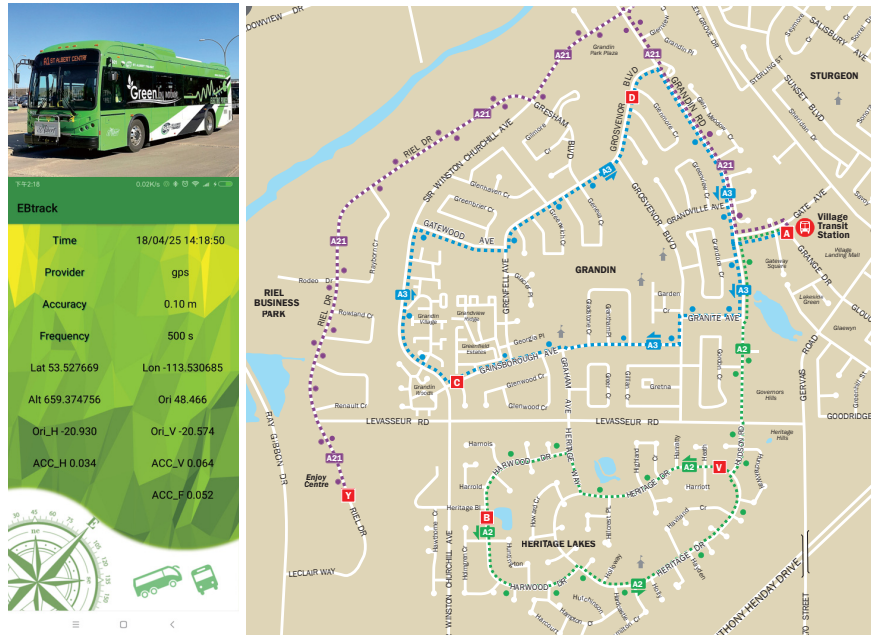


Figure 5.5: EB data collection APP and bus operation routes.

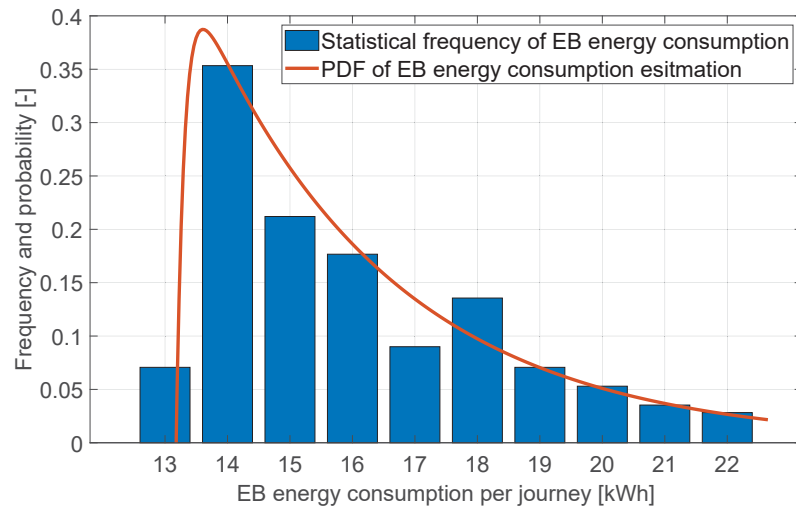


Figure 5.6: Comparison between the estimated energy consumption and the actual statistics.

276.5 kW to 173.4 kW. In the meantime, the power injection into the distribution system can always be avoided, which also reduces the operation cost. Since there are several optimal charging/discharging strategies with the same EBTC peak load, the corresponding impacts on the local voltage quality are\* compared in Table 5.2. We can find out that PSVF values corresponding to the four strategies are very different, which means that the voltage quality of the strategies with minimum cost can vary. Thus, it is necessary to find the optimal strategy with the best voltage quality. In this simulation, we discrete the EBTC load

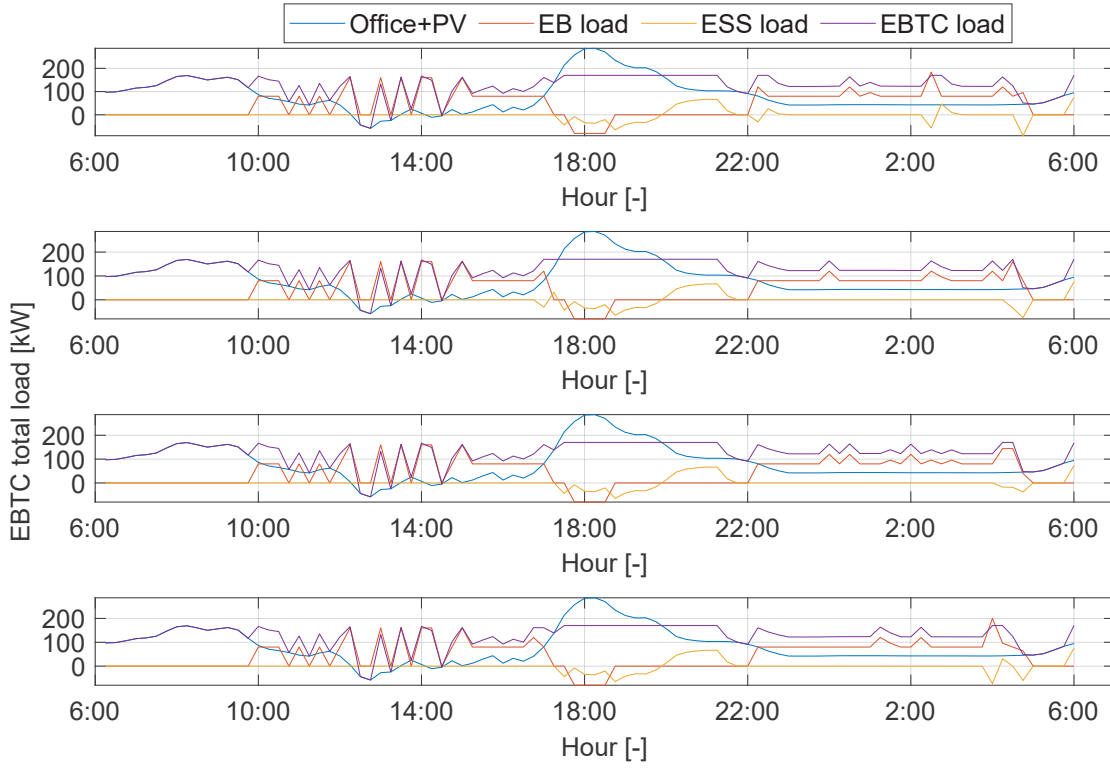


Figure 5.7: EBTC load profile comparison among different strategies.

Table 5.2: IMPACT OF CONSIDERING VOLTAGE REGULATION ON THE LOCAL VOLTAGE QUALITY.

Strategy Index	1	2	3	4
$V^{TC}$ w/o VR [p.u.]	0.9330	0.9330	0.9329	0.9330
$V^{TC}$ w/ VR [p.u.]	0.9847	0.9846	0.9846	0.9845
PSVF without VR [-]	0.0092	0.0086	0.0088	0.0088
PSVF with VR [-]	0.0094	0.0095	0.0086	0.0092

and EB/ESS charging/discharging power. Since the real-time available EBs, ESS state, office and PV load are all known, we can loop through all the possible strategies to find the optimal one. Also, we compare the daily local voltage magnitude profiles considering the impact of the voltage regulation process and the ones excluding the impact. According to the result, the actual voltage magnitude with voltage regulation process can be much higher than the theoretical value. In this way, the accuracy and practicality of the proposed approach can be improved.

At last, we compare the proposed three-layer stochastic energy management approach (TSEMA) with two benchmark approaches. The first one is the stochastic energy management approach (SEMA) developed in [92], where the charging/discharging strategies are optimized in day ahead based on the expected value of EB energy consumption, office

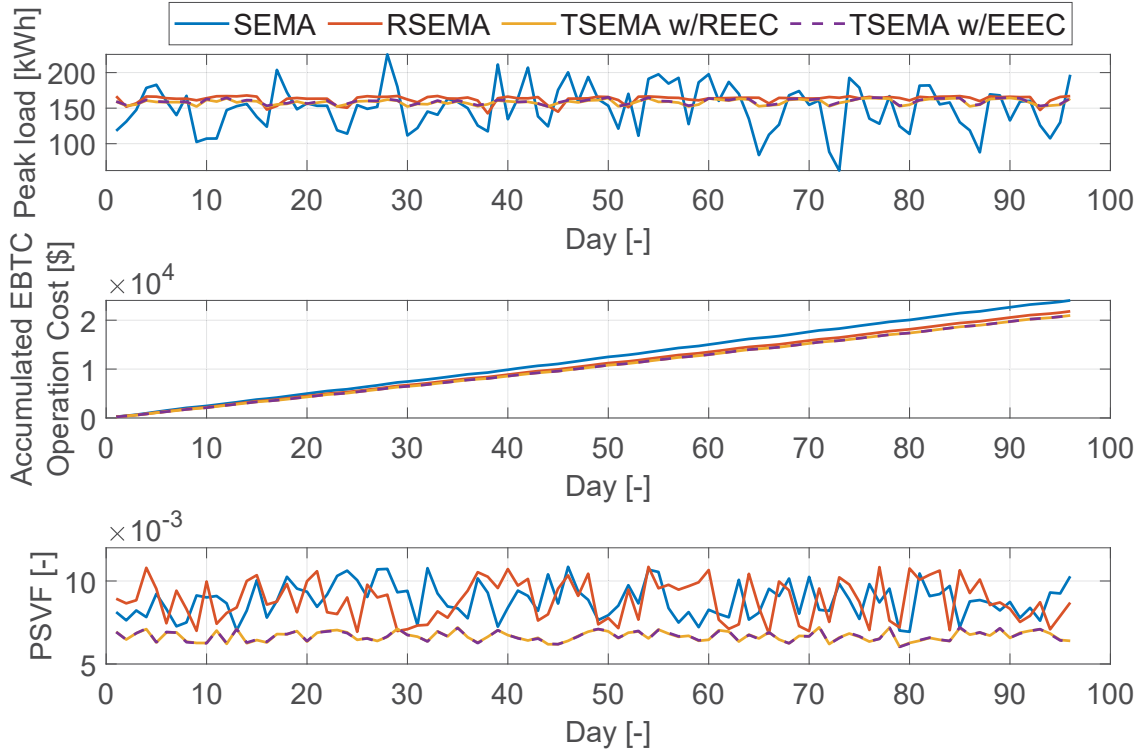


Figure 5.8: Performance comparison among SEMA, RSEMA, and TSEMA over time.

Table 5.3: PERFORMANCE COMPARISON AMONG SEMA, RSEMA, AND TSEMA.

	SEMA	RSEMA	TSEMA
Maximum peak load [kWh]	225.6	167.1	164.4
Accumulated operation cost [ $10^4$ \$]	2.412	2.182	2.127
Average PSVF [ $10^{-3}$ ]	9.105	8.877	6.791

load, PV generation, etc. Neither the robustness nor the local voltage quality is considered. The second approach is the robust stochastic energy management approach (RSEMA) developed in [166], where the charging/discharging strategies are optimized dynamically considering the worst case in the near future. Also, the impact on the local voltage quality is not considered in RSEMA. As shown in Fig. 5.8, the performance of these three approaches is compared in terms of peak load shaving, EBTC operation cost saving, and local voltage quality optimization. Also, the detailed values are given in Table 5.3. According to the result, we can find out that since the SEMA does not consider the robustness, the peak load in the extreme cases cannot be reduced. Besides, the peak load of the proposed TSEMA is lower than that of the RSEMA because we involve a more accurate approach to estimate the EB energy consumption, which enables us to forecast the charging/discharging capacity more accurately. Also, the accumulated EBTC operation cost of the proposed TSEMA is obviously lower than the other two approaches because we not only avoid injecting power into the distribution system but also achieve lower peak load.

Since the voltage quality is not considered in SEMA and RSEMA, the corresponding voltage quality is much lower than TSEMA. In addition, involving the impact of voltage regulation process and the load of other buses in the distribution system, the PSVF value can be maintained at a lower level with TSEMA. Finally, we also compare with the optimization results computed based on the real EB energy consumption (REEC) and the estimated EB energy consumption (EEEC). According to the results, we can find out that the maximum peak load relative error caused by the proposed EB energy consumption estimation approach is always less than 1%, and the relative error of accumulated operation cost is less than 0.05%. Also, the relative error of average PSVF is less than 0.01%, which shows the accuracy of the proposed estimation approach.

## **5.5 Summary**

In this chapter, a three-layer stochastic energy management approach is proposed for the EBTC with PV and ESS considering the operation cost minimization and local voltage quality optimization. In order to analyze the EBTC operation process, a stochastic model is built considering the randomness of the office load, PV generation, EB energy consumption, and practical electricity price. Based on synthetic driving profiles, a stochastic EB energy consumption estimation approach is developed, and a modified ROOT approach is applied to optimize the EB/ESS charging/discharging schedule. Also, the impact of voltage regulation process on the local voltage quality is taken into account. Through the case study, the performance of the proposed approach is evaluated, and the results indicate that it can not only minimize the EBTC operation cost, but also ensure the local voltage quality. In our future work, we will study how different probability distributions of on-bus passenger count affect the model accuracy and investigate the coordination among multiple EB/EV charging stations for optimal energy management in a distribution system. Also, a more detailed battery degradation cost model will be involved in the future work.

# 6

## Conclusions and Future Works

In the recent years, the popularity of EVs has provided a feasible option for the existing transportation systems to evolve towards a more economic and environmental-friendly future transportation systems. However, along with the ever-increasing EV penetration, the corresponding EV charging load may challenge the capability of the power systems. From the perspective of smart grid, V2G mechanism, ESS, and renewable energy sources can be involved to mitigate the impact of EVs on the distribution systems. Yet, the randomness of EV charging demands, EV mobility, renewable power generation, base load variation of the distribution system, and real-time pricing schemes should be considered in the EV energy management. In addition, the interactions among individual EV owners, EV AGGs, and DSOs need to be further investigated.

To achieve efficient EV integration in the future smart grid, stochastic models and the corresponding optimization problems have been investigated in this thesis. The stochastic optimization techniques utilized in this thesis involves MDP approach, repeated inverse Stackelberg game approach, DSMG approach, data-driven random decision forest approach, and ROOT approach. More specifically, the MDP approach is utilized to model the EV in-station charging process and the charging strategies are optimized with repeated inverse Stackelberg game approach. Based on the obtained optimal charging strategies, the pricing scheme of charging service provider is optimized. In the VR auction, the EV AGGs' auction strategies in the voltage regulation market are optimized with DSMG approach considering power system topology issue and practical auction mechanism. Considering the unique features of EBs, a data-driven EB energy consumption estimation approach is proposed to evaluate the impact of EB charging load on the distribution system based on modified KF and random decision forest approach. Also, an EB motion data collection APP is developed. Finally, a stochastic EBTC energy flow

model is developed, and a three-layer robust optimization approach is developed to minimize the EBTC operation cost and mitigate the impact on the distribution system.

## 6.1 Contributions of Thesis

The main contributions of this thesis can be summarized as follows:

- A stochastic game approach among DSO, charging stations, and EV owners is proposed, and the MDP is utilized to optimize the EV owners charging schedule. The corresponding algorithm for calculating the Nash equilibrium solution of the proposed game is developed. An RTP optimization approach for DSO is developed to improve the power grid condition.
- A new approach based on stochastic game model is proposed for VR auction considering the network topology impact. The problem is formulated as a DSMG, and the existence proof of stationary Markov perfect equilibrium is provided. The advantages of the proposed DSMG is demonstrated from the perspectives of network topology impact, VR capacity, regulated voltage magnitude, and accumulated revenue. Particularly, the proposed approach not only helps DSO to select the most efficient AGGs to be the VR sources but also decreases the total required VR capacity.
- A new EB energy consumption estimation approach is developed based on the known EB route, and a data preprocessing approach is proposed to mitigate the impact of the GPS signal noise on the energy consumption estimation. The acceleration of the EB is modeled as a control variable in the KF and the random decision forest algorithm is applied for estimation. A feature discarding approach is developed to reduce the error caused by the unimportant features. An Android APP is developed to collect the GPS data through smartphones.
- A three-layer stochastic energy management approach is proposed for the EBTC with PV and ESS considering the operation cost minimization and local voltage quality optimization in the VR process. A stochastic model is built considering the randomness of the office load, PV generation, EB energy consumption, and practical electricity price. Based on synthetic driving profiles, a stochastic EB energy consumption estimation approach is developed, and a modified ROOT approach is applied to optimize the EB/ESS charging/discharging schedule.

## 6.2 Directions for Future Work

In this thesis, several important issues related to stochastic energy management of EVs in smart grid are investigated. Although we have obtained some good results in these

works, there are still several open issues requiring future research, such as how to build stochastic EV model more accurately, how the EV AGGs manage the individual EVs through various pricing schemes, how the EV AGGs participate in other ancillary service markets besides voltage regulation, and how to achieve distributed EV charging optimization. In particular, the following topics will be investigated in our for future work:

- The charging stations in different regions provide service to EV owners with different charging demand in different periods. Thus, considering the impact of the traffic condition on the charging demand can improve the charging optimization revenue. Based on the historical traffic load data and individual EV trip data, we can extend the EV charging demand model with time attribute and location attribute. Then, the charging schedule can be optimized before the EV trip starts and additional optimization variables can be taken into account, including trip route and charging stations. In this way, the traffic segment model and power system model can be combined practically. For each selected trip route and charging station, a stochastic EV charging optimization problem needs to be solved. Accordingly, an efficient stochastic decision tree pruning algorithm should be developed.
- More efforts are needed to coordinate the EVs and AGGs in the distribution system to provide ancillary services in the transmission system. On one hand, the response times of EVs are shorter than the traditional thermal generators and the cost is lower. On the other hand, considering the topology issues, the efficiency of the ancillary service providers connected to different buses in the transmission system can vary. Thus, utilizing the stationary thermal generators to provide ancillary services might not always be the optimal solution, and the widely distributed EV sources can provide the transmission system operator with more flexible and effective strategies when selecting ancillary service providers. According to the structure of real-world transportation systems and power systems, there are a lot of charging stations closely related in the traffic network while belonging to different distribution systems. Thus, the interaction of these charging stations in the smart grid and their impact on the transmission system need to be further investigated. Besides, since the AGGs might not have the full knowledge of the power system in practice, a data-driven approach to help the AGGs to study the power system needs to be developed.
- To estimate the EB energy consumption more accurately, a time-varying stochastic model of on-board auxiliary device power is needed. Accordingly, we need to collect long-term data of weather conditions, traffic conditions, passenger trip profiles, and EB operation data. Then, we can further improve the accuracy of the EB

energy consumption model by involving the impacts of region, time, weather, and season. Based on the modified EB energy consumption model, the time-varying impact of the EB charging load on the distribution can be investigated. Thereafter, a real-time distributed EB charging schedule optimization problem can be developed. With the optimization result, we can evaluate the maximum EB numbers that the existing distribution system can support in a certain region.

- Corresponding to different power system conditions, the EB charging efficiency can vary. In other words, the real-time EB charging status in different nodes of a power system can affect the real-time actual power system state. Thus, by utilizing the EB charging status, we can improve power system state estimation against false data injection attacks. In particular, the large EB count and the stochastic charging schedule optimization enable us to generate more system observations. Based on the discussions in Chapter 5, there exist multiple optimal charging strategies for EBs. Accordingly, we can intentionally switch the charging schedule to change the observations of the distribution system. If the attacker is not aware of such charge, the measurement residual will increase, resulting in the detection of false data.

# Bibliography

- [1] International Energy Agency, "Global EV outlook 2017: Two million and counting," Jun. 2017.
- [2] TBRC, "Electric cars global market report 2020-30: COVID-19 growth and change," May 2020.
- [3] C. McKerracher, et al., "Electric vehicle outlook 2020," Mar. 2020.
- [4] M. Islam, N. Mithulananthan, and K. Lee, "Development of impact indices for performing charging of a large EV population," *IEEE Trans. Veh. Technol.*, vol. 67, no. 2, pp. 866-880, Feb. 2018.
- [5] A. Dube and S. Santoso, "Electric vehicle charging on residential distribution systems: impacts and mitigations," *IEEE Access*, vol. 3, pp. 1871-1893, Sept. 2015.
- [6] E. Veldman and R. Verzijlbergh, "Distribution grid impacts of smart electric vehicle charging from different perspectives," *IEEE Trans. Smart Grid*, vol. 6, no. 1, pp. 333-343, Jan. 2015.
- [7] N. Korolko and Z. Sahinoglu, "Robust optimization of EV charging schedules in unregulated electricity markets," *IEEE Trans. Smart Grid*, vol. 8, no. 1, pp. 149-157, Jan. 2017.
- [8] Q. Huang, Q. Jia, and X. Guan, "Robust scheduling of EV charging load with uncertain wind power integration," *IEEE Trans. Smart Grid*, vol. 9, no. 2, pp. 1043-1054, Mar. 2018.
- [9] H. Yang, S. Yang, Y. Xu, E. Cao, M. Lai, and Z. Dong, "Electric vehicle route optimization considering time-of-use electricity price by learnable Parthenon-genetic algorithm," *IEEE Trans. Smart Grid*, vol. 6, no. 2, pp. 657-666, Mar. 2015.
- [10] M. Ansari, A. Al-Awami, E. Sortomme, and M. Abido, "Coordinated bidding of ancillary service for vehicle-to-grid using fuzzy optimization," *IEEE Trans. Smart Grid*, vol. 6, no. 1, pp. 261-270, Jan. 2015.

- [11] J. Teng, S. Liao, and C. Wen, "Design of a fully decentralized controlled electric vehicle charger for mitigating charging impact on power grids," *IEEE Trans. Ind. Appl.*, vol. 53, no. 2, pp. 1497-1505, Apr. 2017.
- [12] Z. Liu, Q. Wu, S. Oren, S. Huang, R. Li, and L. Cheng, "Distribution locational marginal pricing for optimal electric vehicle charging through chance constrained mixed-integer programming," *IEEE Trans. Smart Grid*, vol. 9, no. 2, pp. 644-654, Mar. 2018.
- [13] C. Luo, Y. Huang, and V. Gupta, "Stochastic dynamic pricing for EV charging stations with renewable integration and energy storage," *IEEE Trans. Smart Grid*, vol. 9, no. 2, pp. 1494-1505, Mar. 2018.
- [14] Y. Zhang and L. Cai, "Dynamic charging scheduling for EV parking lots with photovoltaic power system," *IEEE Access*, vol. 6, pp. 56995-57005, Oct. 2018.
- [15] C. Mediwaththe and D. Smith, "Game-theoretic electric vehicle charging management resilient to no-idle user behavior," *IEEE Trans. Intell. Transp. Syst.*, vol. 19, no. 11, pp. 3486-3495, Nov. 2018.
- [16] Y. Xiong, J. Gan, B. An, C. Miao, and A. Bazzan, "Optimal electric vehicle fast charging station placement based on game theoretical frame working," *IEEE Trans. Intell. Transp. Syst.*, vol. 19, no. 8, pp. 2493-2504, Aug. 2018.
- [17] M. Mao, Y. Ding, L. Chang, N. Hatziaargyriou, Q. Chen, and T. Tao, "Multi-objective power management for EV fleet with MMC-based integration into smart grid," *IEEE Trans. Smart Grid*, vol. 10, no. 2, pp. 1428-1439, Mar. 2019.
- [18] J. Kim, J. Lee, S. Park, and J. Choi, "Battery wear model based energy trading in electric vehicles: a naive auction model and a market analysis," *IEEE Trans. Ind. Inform.*, vol. 15, no. 7, pp. 4140-4150, Jul. 2019.
- [19] Y. Zhang, Q. Yang, Q. Yang, W. Yu, D. An, D. Li, and W. Zhao, "An online continuous progressive second price auction for electric vehicle charging," *IEEE Internet Things J.*, vol. 6, no. 2, pp. 2907-2921, Apr. 2019.
- [20] M. Majidpour, C. Qiu, P. Chu, R. Gadh, and H. Pota, "Fast prediction for sparse time series: Demand forecast of EV charging stations for cell phone applications," *IEEE Trans. Ind. Inform.*, vol. 11, no. 1, pp. 242-250, Nov. 2014.
- [21] Q. Huang, Q. Jia, and X. Guan, "A multi-time scale and bilevel coordination approach for matching uncertain wind supply with EV charging demand," *IEEE Trans. Autom. Sci. Eng.*, vol. 14, no. 2, pp. 694-704, Apr. 2017.

- [22] J. Dong, C. Liu, and Z. Lin, "Charging infrastructure planning for promoting battery electric vehicles: An activity-based approach using multiday travel data," *Transp. Res. C, Emerging Technol.*, vol. 38, pp. 44-55, Jan. 2014.
- [23] X. Xi, R. Sioshansi, and V. Marano, "Simulation-optimization model for location of a public electric vehicle charging infrastructure," *Transp. Res. D, Transp. Environ.*, vol. 22, pp. 60-69, Jul. 2013.
- [24] I. Frade, A. Ribeiro, G. Goncalves, and A. Antunes, "Optimal location of charging stations for electric vehicles in a neighborhood in Lisbon," *Transp. Res. Rec.*, vol. 2252, pp. 91-98, 2011.
- [25] H. Ding, Z. Hu, and Y. Song, "Value of energy storage system in an electric bus fast charging station," *Appl. Energy*, vol. 157, no. 1, pp. 630-639, Nov. 2015.
- [26] Y. He, Z. Song, and Z. Liu, "Fast-charging station deployment for battery electric bus systems considering electricity demand charges," *Sust. Cities Soc.*, vol. 48, Jul. 2019.
- [27] H. Wang, J. Jiang, M. Huang, W. Zhang, and Y. Bao, "Hierarchical energy storage configuration method for pure electric vehicle fast charging station," in *Proc. IEEE ITECAP'17*, pp. 1-6, Aug. 2017.
- [28] H. Fathabadi, "Novel solar powered electric vehicle charging station with the capability of vehicle-to-grid," *Sol. Energy*, vol. 142, no. 15, pp. 136-143, Jan. 2017.
- [29] J. Torreglosa, P. Garacía-Triviño, L. Fernández-Ramirez, and F. Jurado, "Decentralized energy management strategy based on predictive controllers for a medium voltage direct current photovoltaic electric vehicle charging station," *Energy Conv. Manag.*, vol. 108, no. 15, pp. 1-13, Jan. 2016.
- [30] Y. Cheng and J. Tao, "Optimization of a micro energy network integrated with electric bus battery swapping station and distributed PV," in *Proc. IEEE EI2'18*, pp. 1-6, Oct. 2018.
- [31] V. Tran, M. Islam, K. Muttaqi, D. Sutanto, "An efficient energy management approach for a solar-powered EV battery charging facility to support distribution grids," *IEEE Trans. Ind. Appl.*, vol. 55, no. 6, pp. 6517-6526 Nov. 2019.
- [32] K. Hu, P. Yi, and C. Liaw, "An EV SRM drive powered by battery/supercapacitor with G2V and V2H/V2G capabilities," *IEEE Trans. Ind. Inform.*, vol. 62, no. 8, pp. 4714-4727, Aug. 2015.

- [33] N. Rahbari-Asr, M. Chow, J. Chen, and R. Deng, "Distributed real-time pricing control for large-scale unidirectional V2G with multiple energy suppliers," *IEEE Trans. Ind. Inform.*, vol. 12, no. 5, pp. 1953-1962, Oct. 2016.
- [34] X. Bai and W. Qiao, "Robust optimization for bidirectional dispatch coordination of large-scale V2G," *IEEE Trans. Smart Grid*, vol. 6, no. 4, pp. 1944-1954, Jul. 2015.
- [35] W. Zhong, K. Xie, Y. Liu, C. Yang, and S. Xie, "Topology-aware vehicle-to-grid energy trading for active distribution systems," *IEEE Trans. Smart Grid*, vol. 10, no. 2, pp. 2137-2147, Mar. 2019.
- [36] W. He and Y. Sun, "Stationary Markov perfect equilibria in discounted stochastic games," *J. Econ. Theory*, vol. 169, pp. 35-61, Jan. 2017.
- [37] J. Tan and L. Wang, "A game-theoretic framework for vehicle-to-grid frequency regulation considering smart charging mechanism," *IEEE Trans. Smart Grid*, vol. 8, no. 5, pp. 2358-2369, Sept. 2017.
- [38] A. Paul, D. Mukherjee, P. Das, A. Gangopadhyay, A. Chintla, and S. Kundu, "Improved random forest for classification," *IEEE Trans. Image Process*, vol. 27, no. 8, pp. 4012-4024, Aug. 2018.
- [39] N. Y. Soltani, S. J. Kim, and G. B. Giannakis, "Real-time load elasticity tracking and pricing for electric vehicle charging," *IEEE Trans. Smart Grid*, vol. 6, no. 3, pp. 1303-1313, May. 2015.
- [40] C. Vivekananthan, Y. Mishra, and F. Li, "Real-time price based home energy management scheduler," *IEEE Trans. Power Syst.*, vol. 30, no. 4, pp. 2149-2159, Jul. 2015.
- [41] K. Zhou, J. Pan, and L. Cai, "Indirect load shaping for CHP systems through real-time price signals," *IEEE Trans. Smart Grid*, vol. 7, no. 1, pp. 282-290, Jan. 2016.
- [42] R. Deng, Z. Yang, M. Y. Chow, and J. Chen, "A survey on demand response in smart grids: Mathematical models and approaches," *IEEE Trans. Ind. Inform.*, vol. 11, no. 3, pp. 570-582, Jun 2015.
- [43] T. Theodoropoulos, I. Damousis, and A. Amditis, "Demand-side management ICT for dynamic wireless EV charging," *IEEE Trans. Ind. Electron.*, vol. 63, no. 10, pp. 6623-6630, Oct. 2016.
- [44] M. Kisacikoglu, F. Erden, and N. Erdogan, "Distributed control of EV charging based on energy demand forecast," *IEEE Trans. Ind. Inform.*, vol. 14, no. 1, pp. 117-126, Jan. 2018.

- [45] P. You, Z. Yang, M. Chow, and Y. Sun, "Optimal cooperative charging strategy for a smart charging station of electric vehicles" *IEEE Trans. Power Syst.*, vol. 31, no. 4, pp. 2946-2956, Jul. 2016.
- [46] Y. Mou, H. Xing, Z. Lin and M. Fu, "Decentralized optimal demand-side management for PHEV charging in a smart grid," *IEEE Trans. Smart Grid*, vol. 6, no. 2, pp. 726-736, Mar. 2015.
- [47] A. Kulvanitchaiyanunt, V. C. P. Chen, J. Rosenberger, P. Sarikprueck and W. J. Lee, "A linear program for system-Level control of regional PHEV charging stations," *IEEE Trans. Ind. Appl.*, vol. 52, no. 3, pp. 2046-2052, Jun. 2016.
- [48] C. Kong, I. S. Bayram and M. Devetsikiotis, "Revenue optimization frameworks for multi-class PEV charging stations," *IEEE Trans. Smart Grid*, vol. 3, pp. 2140-2150, Nov. 2015.
- [49] X. Tan, G. Qu, B. Sun, N. Li, and D. Tsang, "Optimal scheduling of battery charging stations serving electric vehicle based on battery swapping," *IEEE Trans. Smart Grid*, vol. 10, no. 2, pp. 1372-1384, Mar. 2019.
- [50] B. Sun, Z. Huang, X. Tan, and D. Tsang, "Optimal scheduling for electric vehicle charging with discrete charging levels in distribution grid," *IEEE Trans. Smart Grid*, vol. 9, no. 2, pp. 624-634, Mar. 2018.
- [51] L. Zhang and Y. Li, "A game-theoretic approach to optimal scheduling of parking-lot electric vehicle charging," *IEEE Trans. Veh. Technol.*, vol. 65, no. 6, pp. 4068-4078, Jun. 2016.
- [52] S. Bahrami and M. Parniani, "Game theoretic based charging strategy for plug-in hybrid electric vehicles," *IEEE Trans. Smart Grid*, vol. 5, no. 5, pp. 2368-2375, Sept. 2014.
- [53] R. Yu, J. Ding, W. Zhong, Y. Liu and S. Xie, "PHEV charging and discharging cooperation in V2G networks: a coalition game approach," *IEEE Internet Things*, vol. 1, no. 6, pp. 578-589, Dec. 2014.
- [54] S. Yoon, Y. Choi, J. Park et al., "Stackelberg-game-based demand response for at-home electric vehicle charging," *IEEE Trans. Veh. Technol.*, vol. 65, no. 6, pp. 4172-4184, Jun. 2016.
- [55] H. Yang, X. Xie and A. V. Vasilakos, "Noncooperative and cooperative optimization of electric vehicle charging under demand uncertainty: a robust Stackelberg game," *IEEE Trans. Veh. Technol.*, vol. 65, no. 3, pp. 1043-1058, Mar. 2016.

- [56] Y. Yang, Q. Jia, X. Guan, X. Zhang, Z. Qiu, and G. Deconinck, "Decentralized EV-based charging optimization with building integrated wind energy," *IEEE Trans. Autom. Sci. Eng.*, vol. 16, no. 3, pp. 1002-1017, Jul. 2019.
- [57] R. Leou, J. Teng and C. Su, "Modelling and verifying the load behaviour of electric vehicle charging stations based on field measurements," *IET Gener. Transm. Distrib.*, vol. 9, no. 11, pp. 1112-1119, Aug. 2015.
- [58] I. S. Bayram, G. Michailidis, M. Devetsikiotis and F. Granelli, "Electric power allocation in a network of fast charging stations," *IEEE J. Sel. Areas Commun.*, vol. 31, no. 7, pp. 1235-1246, Jul. 2013.
- [59] H. Liang, I. Sharma, W. Zhuang, and K. Bhattacharya, "Plug-in electric vehicle charging demand estimation based on queueing network analysis," in *Proc. IEEE PES GM'14*, Jul. 2014.
- [60] C. H. Ou, H. Liang and W. Zhuang, "Investigating wireless charging and mobility of electric vehicles on electricity market," *IEEE Trans. Ind. Electron.*, vol. 62, no. 5, pp. 3123-3133, May 2015.
- [61] C. Wang, Y. Chen, H. Y. Wei, and K. J. R. Liu, "Scalable video multicasting: a stochastic game approach with optimal pricing," *IEEE Trans. Wirel. Commun.*, vol. 14, no. 5, pp. 2353-2367, May 2015.
- [62] J. Li, C. Li, Y. Xu, Z. Dong, K. Wong, and T. Huang, "Noncooperative game-based distributed charging control for plug-in electric vehicles in distribution networks," *IEEE Trans. on Ind. Inform.*, vol. 14, no. 1, pp. 301-310, Jan. 2108.
- [63] S. Bhattacharya, K. Kar, J. Chow, and A. Gupta, "Extended second price auctions with elastic supply for PEV charging in the smart grid," *IEEE Trans. Smart Grid*, vol. 7, no. 4, pp. 2082-2093, Oct. 2016.
- [64] J. Donadee and M. Ilic, "Stochastic optimization of grid to vehicle frequency regulation capacity auctions," *IEEE Trans. Smart Grid*, vol. 5, no. 2, pp. 1061-1069, Mar. 2014.
- [65] M. Zeng, S. Leng, S. Maharjan, S. Gjessing, and J. He, "An incentivized auction-based group-selling approach for demand response management in V2G systems," *IEEE Trans. Ind. Inf.*, vol. 11, no. 6, pp. 1554-1563, 2015.
- [66] S. Vagropoulos and A. Bakirtzis, "Optimal auction strategy for electric vehicle aggregators in electricity markets," *IEEE Trans. Power Syst.*, vol. 28, no. 4, pp. 4031-4041, Nov. 2013.

- [67] H. Yang, S. Zhang, J. Qiu, D. Qiu, M. Lai, and Z. Dong, "CVar-constrained optimal auction of electric vehicle aggregators in day-ahead and real-time markets," *IEEE Trans. Ind. Inf.*, vol. 13, no. 5, pp. 2555-2565, Oct. 2017.
- [68] M. Ansari, A. Al-Awami, E. Sortomme, and M. Aautiono, "Coordinated auction of ancillary services for vehicle-to-grid using fuzzy optimization," *IEEE Trans. Smart Grid*, vol. 6, no. 1, pp. 261-270, Aug. 2014.
- [69] H. Wu, M. Shahidehpour, A. Alabdulwahab, and A. Abusorrah, "A game theoretic approach to risk-based optimal auction strategies for electric vehicle aggregators in electricity market with variable wind energy resources," *IEEE Trans. Sustain. Energy*, vol. 7, no. 1, pp. 374-385, Jan. 2016.
- [70] E. Karfopoulos and N. Hatziargyriou, "Distributed coordination of electric vehicles providing V2G services," *IEEE Trans. Power Syst.*, vol. 31, no. 1, pp. 329-338, Jan. 2016.
- [71] W. Zhong, R. Yu, X. Shengli, Y. Zhang, and D. Yau, "On stability and robustness of demand response in V2G mobile energy networks," *IEEE Trans. Smart Grid*, vol. 9, no. 4, pp. 3203-3212, Jul. 2016.
- [72] U. Michael, "Stochastic multiplayer games: theory and algorithms," Amsterdam University Press, 2010.
- [73] L. Alfaro, T. Henzinger, and O. Kupferman, "Concurrent reachability games," *Theor. Comput. Sci.*, vol. 386, no. 3, pp. 188-217, Nov. 2007.
- [74] O. Hafez and K. Bhattacharya, "Queuing analysis based on PEV load modeling considering battery charging behavior and their impact on distribution system operation," *IEEE Trans. Smart Grid*, vol. 9, no. 1, pp. 261-273, Jan. 2018.
- [75] C. Liberto, G. Valenti, S. Orchi, M. Lelli, M. Nigro, and M. Ferrara, "The impact of electric mobility scenarios in large urban areas: the Rome case study," *IEEE Trans. Intell. Transp. Syst.*, vol. 19, no. 11, pp. 3540-3549, Nov. 2018.
- [76] K. Kivekas, J. Vepsalainen, and K. Tammi, "Stochastic driving cycle synthesis for analyzing the energy consumption of a battery electric bus," *IEEE Access*, vol. 6, pp. 55586-55598, Oct. 2018.
- [77] S. Khan and M. Kushler, "Plug-in electric vehicles: challenges and opportunities," *American Council for an Energy-Efficient Economy*, Jun. 2013. [Online]. Available: <http://aceee.org/sites/default/files/publications/researchreports/t133.pdf>.
- [78] BYD eBus Tech. Spec., [Online]. Available: <http://www.byd.com/la/auto/ebus.html>.

- [79] D. Stroe, V. Knap, M. Swierczynski, A. Stroe, and R. Teodorescu, "Operation of a grid-connected lithium-ion battery energy storage system for primary frequency regulation: a battery lifetime perspective," *IEEE Trans. Ind. Appl.*, vol. 53, no. 1, pp. 430-438, Jan. 2017.
- [80] R. Basso, B. Kulcsar, B. Egardt, P. Lindroth, and I. Sanchez-Diaz, "Energy consumption estimation integrated into the electric vehicle routing problem," *Transportation Research Part D*, vol. 69, pp. 141-167, Apr. 2019.
- [81] M. Sebastiani, R. Lüders, and Keiko, "Evaluating electric bus operation for a real-world BRT public transportation using simulation optimization," *IEEE Trans. Intell. Transp. Syst.*, vol. 17, no. 10, pp. 2777-2786, Oct. 2016.
- [82] A. Lajunen, "Energy consumption and cost-benefit analysis of hybrid and electric city buses," *Transp. Res. C, Emerging Technol.*, vol. 38, pp. 1-15, Jan. 2014.
- [83] P. Sinhubera, W. Rohlfsa, and D. Sauera, "Study on power and energy demand for sizing the energy storage systems for electrified local public transport buses," in *Proc. IEEE Veh. Power Propulsion Conf.*, pp. 315-320, Feb. 2013.
- [84] R. Beekman and R. Hoed, "Operational demands as determining factor for electric bus charging infrastructure," in *Proc. CPE-POWERENG 10th*, Aug. 2016.
- [85] Y. Jang, E. Suh, and J. Kim, "System architecture and mathematical models of electric transit bus system utilizing wireless power transfer technology," *IEEE Syst. J.*, vol. 10, no. 2, pp. 495-506, Jan. 2015.
- [86] S. Taghvaeeyan and R. Rajamani, "Portable roadside sensors for vehicle counting, classification, and speed measurement," *IEEE Trans. Intell. Transp. Syst.*, vol. 15, no. 1, pp. 73-83, Feb. 2014.
- [87] R. Zhang, W. Liu, Y. Jia, G. Jiang, J. Xing, H. Jiang, and J. Liu, "Wifi sensing-based real-time bus tracking and arrival time prediction in urban environments," *IEEE Sens. J.*, vol. 18, no. 11, pp. 4746-4760, Jun. 2018.
- [88] A. Perez, M. Garcia, M. Nieto, J. Pedraza, S. Rodriguez, and J. Zamorano, "Argos: an advanced in-vehicle data recorder on a massively sensorized vehicle for car driver behavior experimentation," *IEEE Trans. Intell. Transp. Syst.*, vol. 11, no. 2, pp. 463-473, Jun. 2010.
- [89] M. Islam, U. Vandebona, V. Dixit, and A. Sharma, "A bulk queue model for the evaluation of impact of headway variations and passenger waiting behavior on public transit performance," *IEEE Trans. Intell. Transp. Syst.*, vol. 15, no. 6, pp. 2432-2442, Dec. 2014.

- [90] K. Kivekas, J. Vepsalainen, and K. Tammi, "Stochastic driving cycle synthesis for analyzing the energy consumption of a battery electric bus," *IEEE Access*, vol. 6, Oct. 2018.
- [91] X. Gong, J. Zhang, and J. Fang, "A modified nonlinear two-filter smoothing for high-precision airborne integrated GPS and inertial navigation," *IEEE Trans. Instrum. Meas.*, vol. 64, no. 12, pp. 3315-3322, Dec. 2015.
- [92] Q. Yan, B. Zhang, and M. Kezunovic, "Optimized operational cost reduction for an EV charging station integrated with battery energy storage and PV generation," *IEEE Trans. Smart Grid*, vol. 10, no. 2, pp. 2096-2106, Jan. 2018.
- [93] M. Shin, D. Choi, and J. Kim, "Cooperative management for PV/ESS-Enabled vehicle charging stations: a multiagent deep reinforcement learning approach," *IEEE Trans. Ind. Inform.*, vol. 16, no. 5, pp. 3493-3503, May. 2020.
- [94] I. Lymperopoulos, F. Qureshi, A. Bitlislioglu, J. Poland, A. Zandarini, M. Mercangoez, and C. Jones, "Ancillary services provision utilizing a network of fast-charging stations for electrical buses," *IEEE Trans. Smart Grid*, vol. 11, no. 1, pp. 665-672, Jan. 2020.
- [95] Y. Cheng, W. Wang, Z. Ding, and Z. He, "Electric bus fast charging station resource planning considering load aggregation and renewable integration," *IET Renew. Power Gener.*, vol. 13, no. 7, pp. 1132-1141, May. 2019.
- [96] C. Yang, W. Lou, J. Yao, and S. Xie, "On charging scheduling optimization for a wirelessly charged electric bus system," *IEEE Trans. Intell. Transp. Syst.*, vol. 19, no. 6, pp. 1814-1826, Jun. 2018.
- [97] H. Ramadan, M. Becherif, and F. Claude, "Energy management improvement of hybrid electric vehicles via combined GPS/Rule-based methodology," *IEEE Trans. Autom. Sci. Eng.*, vol. 14, no. 2, pp. 586-597, Apr. 2017.
- [98] M. Gallet, T. Massier, and T. Hamacher, "Estimation of the energy demand of electric buses based on real-world data for larger-scale public transport networks," *Appl. Energy*, vol. 230, pp. 344-356, Nov. 2018.
- [99] K. Kivekäs, J. Vepsäläinen, and K. Tammi, "Stochastic driving cycle synthesis for analyzing the energy consumption of a battery electric bus," *IEEE Access*, vol. 6, pp. 55586-55598, Sept. 2018.
- [100] T. Boonraksa, A. Paudel, P. Dawan, and B. Marungsri, "Impact of electric bus charging on the power distribution a case study IEEE 33 bus test system," in *Proc. IEEE PES GTD Asia'19*, pp. 819-823, Mar. 2019.

- [101] N. El-Taweel, H. Farag, and M. Mohamed, "Integrated utility-transit model for optimal configuration of battery electric bus systems," *IEEE Systems Journal*, vol. 14, no. 1, pp. 738-748, Mar. 2020.
- [102] X. Cheng et al., "Electrified vehicles and the smart grid: the ITS perspective," *IEEE Trans. Intell. Transp. Syst.*, vol. 15, no. 4, pp. 1388-1404, Aug. 2014.
- [103] D. P. Bertsekas. *Dynamic Programming and Optimal Control, vols. 1 and 2*. Athena Scientific, 2007.
- [104] Y. Mu, "Inverse Stackelberg public goods Game with multiple hierarchies under global and local information structures," *J. Optim. Theory Appl.*, vol. 163, no. 1, pp. 332-350, Oct. 2014.
- [105] N. Forouzandehmehr, Z. Han and R. Zheng, "Stochastic dynamic game between hydropower plant and thermal power plant in smart grid networks," *IEEE Syst. J.*, vol. 10, no. 1, pp. 88-96, Mar. 2016.
- [106] Ontario Energy Board, "Your electricity bill on an energy contract," [Online]. Available: <http://www.ontarioenergyboard.ca/>.
- [107] Alberta Energy, "Electricity rates and prices," [Online]. Available: <http://energy.alberta.ca/>.
- [108] M. F. Shaaban, Y. M. Atwa and E. F. El-Saadany, "PEVs modeling and impacts mitigation in distribution networks," *IEEE Trans. Power Syst.*, vol. 28, no. 2, pp. 1122-1131, May 2013.
- [109] H. Bessembinder and M. L. Lemmon, "Equilibrium pricing and optimal hedging in electricity forward markets," *J. Finance*, vol. 57, no. 3, pp. 1347-1382, Jun. 2002.
- [110] K. R. C. Mamandur and R. D. Chenoweth, "Optimal control of reactive power flow for improvements in voltage profiles and for real power loss minimization," *IEEE Trans. Power App. & Syst.*, vol. 100, pp. 3185-3194, Jul. 1981.
- [111] B. Hu, C. A. Caizares and M. Liu, "Secondary and tertiary voltage regulation based on optimal power flows," in *Proc. IEEE IREP'10*, Aug. 2010.
- [112] S. Bolognani and S. Zampieri, "On the existence and linear approximation of the power flow solution in power distribution networks," *IEEE Trans. Power Syst.*, vol. 31, no. 1, pp. 163-172, Dec. 2015.
- [113] OpenEI dataset. [Online]. Available: <http://en.openei.org/datasets/files/961/pub/>.
- [114] 2009 National Household Travel Survey (NHTS). [Online]. Available: <http://nhts.ornl.gov/>.

- [115] 2010 National Travel Survey (NTS). [Online]. Available: <https://www.gov.uk/government/statistics/national-travel-survey-2010>.
- [116] W. Kempton, V. Udo, K. Huber, K. Komara, S. Letendre, S. Baker, D. Brunner, and N. Pearre, "A test of Vehicle-to grid(V2G) for energy storage and frequency regulation in the PJM system," Jan. 2009. [Online]. Available: <http://www1.udel.edu/V2G/resources/test-v2g-in-pjm-jan09.pdf>.
- [117] H. Yuan, F. Li, Y. Wei, and J. Zhu, "Novel linearized power flow and linearized OPF models for active distribution networks with application in distribution LMP," *IEEE Trans. Smart Grid*, vol. 9, no. 1, pp. 438-448, Jan. 2018.
- [118] PJM Manual 03: Transmission Operations, Revision 58, Nov. 2020. [Online]. Available: <https://www.pjm.com/-/media/documents/manuals/m03.ashx>.
- [119] PJM Manual 12: Balancing operations Services Market Operations, Revision 79, Feb. 2017. [Online]. Available: <http://www.pjm.com/~media/documents/manuals/m11.ashx>.
- [120] R. Yu, W. Zhong, S. Xie, C. Yuen, S. Gjessing, and Y. Zhang, "Balancing power demand through EV mobility in vehicle-to-grid mobile energy networks," *IEEE Trans. Ind. Inform.*, vol. 12, no. 1, pp. 79-90, Feb. 2016.
- [121] D. Wang, K. Meng, X. Gao, J. Qiu, L. Lai, and Z. Dong, "Coordinated dispatch of virtual energy storage systems in LV-grids for voltage regulation," *IEEE Trans. Ind. Inform.*, vol. 14, no. 6, pp. 2452-2462, Jun. 2018.
- [122] H. Zhang, Z. Hu, Z. Xu, and Y. Song, "Evaluation of achievable vehicle-to-grid capacity using aggregate PEV model," *IEEE Trans. Power Syst.*, vol. 32, no. 1, pp. 784-794, Jan. 2017.
- [123] J. Tan and L. Wang, "Real-time charging navigation of electric vehicles of fast charging stations: a hierarchical game approach," *IEEE Trans. Smart Grid*, vol. 8, no. 2, pp. 846-856, Mar. 2017.
- [124] P. Fan, B. Sainbayar, and S. Ren, "Operation analysis of fast charging stations with energy demand control electric vehicles," *IEEE Trans. Smart Grid*, vol. 6, no. 4, pp. 1819-1827, Jul. 2015.
- [125] A. Lam, K. Leung, and V. Li, "Capacity estimation for vehicle-to-grid frequency regulation services with smart charging mechanism," *IEEE Trans. Smart Grid*, vol. 7, no. 1, pp. 156-166, Jan. 2018.

- [126] J. Ren, J. Hu, R. Deng, D. Zhang, Y. Zhang, and X. Shen, "Joint load scheduling and voltage regulation in the distribution system with renewable generators," *IEEE Trans. Ind. Inform.*, vol. 14, no. 4, pp. 1564-1574, Apr. 2018.
- [127] T. Zhang, S. Chen, H. Gooi, and J. Maciejowski, "A hierarchical EMS for aggregated BESSs in energy and performance-based regulation market," *IEEE Trans. Power Syst.*, vol. 32, no. 3, pp. 1751-1760, May. 2017.
- [128] K. Ko, S. Han, and D. Sung, "A new mileage payment for EV aggregators with varying delays in frequency regulation service," *IEEE Trans. Smart Grid*, vol. 9, no. 4, pp. 2616-2624, Jul. 2018.
- [129] D. John, "Noisy stochastic games," *Econometrica*, vol. 88, no. 5, pp. 2017-2045, Sept. 2012.
- [130] Y. Levy, "A discounted stochastic game with no stationary Nash equilibrium: two examples," *Econometrica*, vol. 81, no. 5, pp. 1973-2007, Sept. 2013.
- [131] M. Baran and F. Wu, "Network reconfiguration in distribution systems for loss reduction and load balancing," *IEEE Trans. Power Deliv.*, vol. 4, no. 2, pp. 1401-1407, Apr. 1989.
- [132] PVWatts Calculator, [Online]. Available: <https://pvwatts.nrel.gov/index.php>.
- [133] Market Analysis and Information System, [Online]. Available: <http://www.maisy.com/hourly.htm>.
- [134] C. Zhou, K. Qian, M. Allan, and W. Zhou, "Modeling of the cost of EV battery wear due to V2G application in power systems," *IEEE Trans. Energy Convers.*, vol. 26, no. 4, pp. 1041-1049, Dec. 2011.
- [135] J. Ferreira, J. Almeida, and A. Silva, "The impact of driving styles on fuel consumption: A data-warehouse-and-data-mining based discovery process," *IEEE Trans. Intell. Transp. Syst.*, vol. 16, no. 5, pp. 2653-2662, Oct. 2015.
- [136] Travel Survey of Residents of Canada: Public Use Microdata File, *Statistics Canada*, Jul. 2018. [Online]. Available: <https://www150.statcan.gc.ca/n1/en/catalogue/87M0016X2018001>.
- [137] St. Albert Travel Demand Model- Calibration Report (Appendix B), *Associated Engineering Albert Ltd*, [Online]. Available: <https://stalbert.ca/uploads/PDF-reports/City-of-StAlbert-Transportation-Master-Plan-Appendices.pdf>.
- [138] K. Kivekas, J. Vepsalainen, and K. Tammi, "Stochastic driving cycle synthesis for analyzing the energy consumption of a battery electric bus," *IEEE Access*, vol. 6, pp. 55586-55598, Oct. 2018.

- [139] X. Xiang, K. Zhou, W. Zhang, W. Qin, and Q. Mao, "A closed-loop speed advisory model with driver's behavior adaptability for eco-driving," *IEEE Trans. Intell. Transp. Syst.*, vol. 16, no. 6, pp. 3313-3324, Dec. 2015.
- [140] R. Satzoda and M. Trivedi, "Drive analysis using vehicle dynamics and vision-based lane semantics," *IEEE Trans. Intell. Transp. Syst.*, vol. 16, no. 1, pp. 9-18, Feb. 2015.
- [141] M. Bartłomiejczyk, "Driving performance indicators of electric bus driving technique: naturalistic driving data multicriterial analysis," *IEEE Trans. Intell. Transp. Syst.*, vol. 20, no. 4, pp. 1442-1451, Apr. 2019.
- [142] Y. Wang, S. Xia, Q. Tang, J. W, and X. Zhu, "A novel consistent random forest framework: Bernoulli random forests," *IEEE Trans. Neural Netw. Learn.*, vol. 29, no. 8, pp. 3510-3523, Aug. 2018.
- [143] X. Zhao, Y. Wu, D. Lee, and W. Cui, "iForest: Interpreting random forests via visual analytics," *IEEE Trans. Vis. Comput. Graph.*, vol. 25, no. 1, pp. 407-416, Jan. 2019.
- [144] Y. Liu and H. Liang, "An MHO approach for electric bus charging scheme optimization based on energy consumption estimation," in *Proc. IEEE PES GM'18*, Aug. 2018.
- [145] *RideGuide-A1-A2-A3-A21*, St. Albert. [Online]. Available: <https://stalbert.ca/uploads/PDF-infosheets/RideGuide-A1-A2-A3-A21.pdf>.
- [146] Y. Zhang, W. Yuan, R. FU, and C. Wang, "Design of an energy-saving driving strategy for electric buses," *IEEE Access*, vol. 7, pp. 157693 - 157706, Oct. 2019.
- [147] FortisAlberta Inc., "2019 Annual performance-based regulation rate adjustment filing," Nov. 2018. [Online]. Available: <http://www.auc.ab.ca/Shared%20Documents/Fortis-RateSchedule.pdf>.
- [148] A. Lajunen, K. Kivekaes, F. Baldi, J. Vepsaelaeninen, and K. Tammi, "Different approaches to improve energy consumption of battery electric buses," in *Proc. IEEE VPPC'18*, pp. 1-6, Aug. 2018.
- [149] B. Hu, S. Feng, J. Li, and H. Zhao, "Statistical analysis of passenger-crowding in bus transport network of Harbin," *Physica A*, vol. 490, pp. 426-438, Jun. 2018.
- [150] H. Gong, X. Chen, L. Yu, and L. Wu, "An application-oriented model of passenger waiting time based on bus departure time intervals," *Transp. Plan. Technol.*, vol. 39, no. 4, pp. 424-437, Jan. 2016.

- [151] P. Wirasanti, W. Srirattanawichaikul, S. Premrudeepreechacham, "Online Soc and battery life estimation: results from field test of electric bus transit," in *PROC. ICEMS'21*, pp. 854-858, Oct. 2018.
- [152] D. Nicolaides, A. Madhusudhanan, X. Na, J. Miles, and D. Cebon, "Technoeconomic analysis of charging and heating options for an electric bus service in London," *IEEE Trans. Transp. Electrif.*, vol. 5, no. 3, pp. 769-781, Sept. 2019.
- [153] A. Khan, S. Menmon, and T. Sattar, "Analyzing integrated renewable energy and smart-grid systems to improve voltage quality and harmonic distortion losses at electric-vehicle charging stations," *IEEE Access*, vol. 6, pp. 26404-26415, Apr. 2018.
- [154] S. Amamra and J. Marco, "Vehicle-to-grid aggregator to support power grid and reduce electric vehicle charging cost," *IEEE Access*, vol. 7, pp. 178528-178538, Dec. 2019.
- [155] K. Mehmood, S. Khan, S. Lee, Z. Haider, M. Rafique, and C. Kim, "A real-time optimal coordination scheme for the voltage regulation of a distribution network including an OLTC, capacitor banks, and multiple distributed energy resources," *Int. J. Electr. Power Energy Syst.*, vol. 94, pp. 1-14, Jan. 2018.
- [156] F. Viawan and D. Karlsson, "Combined local and remote voltage and reactive power control in the presence of induction machine distributed generation," *IEEE Trans. Power, Syst.*, vol. 22, no. 4, pp. 2003-2012, Nov. 2007.
- [157] A. Humayd and K. Bhattacharya, "Design of optimal incentives for smart charging considering utility-customer interactions and distribution systems impacts," *IEEE Trans. Smart Grid*, vol. 10, no. 2, pp. 1521-1531, Mar. 2019.
- [158] R. Leou, J. Teng, H. Lu, B. Lan, H. Chen, T. Hsieh, and C. Su, "Stochastic analysis of electric transportation charging impacts on power quality of distribution systems," *IET Gener. Transm. Distrib.*, vol. 12, no. 11, pp. 2725-2734, Jun. 2018.
- [159] S. Sun, Q. Yang, and W. Yan, "A novel Markov-based temporal-SoC analysis for characterizing PEV charging demand," *IEEE Trans. Ind. Inform.*, vol. 14, no. 1, pp. 156-166, Jan. 2018.
- [160] B. Zhang, A. Lam, A. Domínguez-García, and D. Tse, "An optimal and distribution method for voltage regulation in power distribution systems," *IEEE Trans. Power Deliv.*, vol. 30, no. 4, pp. 1714-1726, Jul. 2015.
- [161] B. Ke, T. Ku, Y. Ke, C. Chung, and H. Chen, "Sizing the battery energy storage system on a university campus with prediction of load and photovoltaic generation," *IEEE Trans. Ind. Appl.*, vol. 52, no. 2, pp. 1136-1147, Mar. 2016.

- [162] H. Kikusato, K. Mori, S. Yoshizawa, Y. Fujimoto, H. Asano, Y. Hayashi, A. Kawashima, S. Inagaki, and T. Suzuki, "Electric vehicle charge-discharge management for utilization of photovoltaic by coordination between home and grid energy management systems," *IEEE Trans. Smart Grid*, vol. 10, no. 3, pp. 3186-3197, May. 2019.
- [163] B. Chen, W. Lam, A. Sumalee, Q. Li, and M. Tam, "Reliable shortest path problems in stochastic time-dependent networks," *J. Intell. Transport. Syst.*, vol. 18, no. 2, pp. 177-189, Apr. 2014.
- [164] Y. Zheng, Y. Zhang, and L. Li, "Reliable path planning for bus networks considering travel time uncertainty," *IEEE Intell. Transp. Syst. Mag.*, vol. 8, no. 1, pp. 35-50, Jan. 2016.
- [165] H. Li, M. Alsolami, S. Yang, Y. Alsmadi, and J. Wang, "Lifetime test design for second-use electric vehicle batteries in residential applications," *IEEE Trans. Sustain. Energy*, vol. 8, no. 4, pp. 1736-1746, Oct. 2017.
- [166] H. Yang, X. Xie, and A. Vasilakos, "Noncooperative and cooperative optimization of electric vehicle under demand uncertainty: A robust Stackelberg game," *IEEE Trans. Veh. Technol.*, vol. 65, no. 3, pp. 1043-1058, Mar. 2016.
- [167] D. Yazdani, T. Nguyen, and J. Branke, "Robust optimization over time by learning problem space characteristics," *IEEE Trans. Evol. Comput.*, vol. 23, no. 1, pp. 143-155, Feb. 2019.
- [168] H. Yuan, F. Li, Y. Wei, and J. Zhu, "Novel linearized power flow and linearized OPF models for active distribution networks with application in distribution LMP," *IEEE Trans. Smart Grid*, vol. 9, no. 1, pp. 438-448, Jan. 2018.
- [169] A. Dubey and S. Santoso, "Electric vehicle charging on residential distribution systems: impacts and mitigations," *IEEE Access*, vol. 3, pp. 1871-1893, Sept. 2015.
- [170] C. Ziras, A. Prostejovsky, H. Binder, and M. Marinelli, "Decentralized and distributed control for storage systems offering primary frequency control," *Electr. Power Syst. Res.*, vol. 177, pp. 1-10, Dec. 2019.
- [171] C. A. R. Hoare, "Algorithm 64: quicksort," *Commun. ACM*, vol. 4, no. 7, pp. 321-321, 1960.
- [172] S. Wray, "LA orders 155 electric buses," *SmartCitiesWorld*, Feb. 2020. [Online]. Available: <https://www.smartcitiesworld.net/news/news/la-orders-155-electric-buses-5053#:~:text=The%20Los%20Angeles%20Department%20of,city%20a%20fleet%20of%20159>.

- 
- [173] BYD eBus Tech. Spec., [Online]. Available: <http://www.byd.com/la/auto/ebus.html>.
- [174] Market Analysis and Information System, [Online]. Available: <http://www.maisy.com/hourly.htm>.
- [175] S. Glantz, B. Slinker, and T. Neilands, *Primer of Applied Regression and Analysis of Variance 3rd*, New York: McGraw-Hill, 1990.